

FUNDAMENTAL AND APPLIED STUDIES ON CYANIDE

FORMATION IN THE CARBON LINER OF AN

INDUSTRIAL ALUMINIUM ELECTROLYTIC CELL

by

Bin Kiat YAP

A dissertation submitted in fulfilment
of the requirements for the degree of
Master of Science (Chemistry)

THE UNIVERSITY OF TASMANIA

HOBART, AUSTRALIA

*graduating
1986*

Date: July 1985

ACKNOWLEDGEMENTS

My appreciation to my supervisor, Dr. Peter Smith, and to Dr. Barry O'Grady for their suggestions and encouragement during the course of this project.

Acknowledgement is also due to Tony Feest, John Osborne and other members of staff of Development Services (Comalco Ltd., Bell Bay) for their interest and help in my work. Grateful acknowledgement must also go to Comalco Aluminium (Bell Bay) Limited and Comalco Research Centre (Thomastown) for the facilities that enabled this project to be carried out.

In addition, I would like to extend my thanks to Professor Barry Welch (University of Auckland, New Zealand) for the many suggestions and interest in my research.

Sincere thanks are extended to Margaret Pakura for her care and application in the typing of this thesis.

Special thanks go to my wife, Edna, for her encouragement and understanding.

DECLARATION OF ORIGINALITY

This is to certify that the work presented in this thesis has not been submitted previously to any other university or institution for a degree or award.



BIN KIAT YAP

ABSTRACT

The objective of this study was to investigate the presence of cyanide in the industrial aluminium electrolytic cell. Therefore, it was an aim of this investigation to identify the favoured regions of cyanide formation in potlining, and conduct parallel laboratory studies to determine some of the chemical factors likely to influence cyanide formation.

The study was conducted in three stages. The first stage involved autopsies of cells of various ages, design and construction in detail. This was followed by extensive sampling of sections of the trenched sidewalls and cathode combined with chemical analyses of the specimens, to enable mapping of the cyanide distribution profiles. Examination of these profiles revealed that major amounts of cyanide were generally concentrated in the carbon sidewall region near the collector bars and to a lesser extent in the cathode near the mid-section of the pot. In particular, carbon that was heavily impregnated with metallic sodium and easily accessible to air ingress, was found to contain high concentrations of cyanide. Thus, from the cyanide profiles it was evident that air ingress through the collector bar seals of the cathode, and sodium penetration of the carbon governed the favoured region for cyanide formation during normal pot operation.

In the second stage, an examination of the kinetics of sodium cyanide formation in carbon-mix was performed in the laboratory. Metallic sodium was reacted with carbon and gaseous nitrogen over a range of temperatures. Rate plots derived from a combination of thermogravimetric and integral analysis techniques indicated that there was increasing reactivity with increase in sodium content during the initial stages of reaction. Furthermore, rate data obtained appeared to fit a second-order reaction relative to reactant sodium after the initial burst of reaction.

Further laboratory investigations were conducted to establish the temperatures required for cyanide formation, and determine the susceptibility of different forms of carbon to cyanide generation. The carbon types ranged from plant derived carbon-mix through commercial preformed cathode material to high purity graphite. Whilst cyanide formation was found to readily occur in the temperature range of 500-600°C in all the carbons tested, the less ordered carbon-mix was significantly more vulnerable. However, highly graphitised carbon was the least susceptible to cyanide formation within its structure.

Moreover, the reaction was accelerated by the presence of small amounts of iron impurity. Laboratory tests also indicated that the predominant cyanide-containing species formed in potlinings was most likely uncomplexed sodium cyanide.

The overall results obtained from laboratory studies were consistent with plant measurements and observations derived from the complex industrial situation. Conclusions drawn from this work may have implications in terms of future cell design, and the ultimate impact of spent potlinings on the surrounding environment.

TABLE OF CONTENTS

	<u>Page</u>
ACKNOWLEDGEMENTS	i
ABSTRACT	iii
TABLE OF CONTENTS	v
LIST OF TABLES	vii
LIST OF FIGURES	viii
1. Introduction	1
1.1 Glossary	3
2. The Problem	4
2.1 Cyanide Presence in Potlining	4
2.2 Cyanide Distribution Profile in Potlinings	5
2.2.1 Introduction	5
2.3 Industrial Background	6
2.3.1 Pot Construction	6
2.3.2 Cathode Failure	7
2.4 Pot Autopsies	11
2.4.1 Autopsy Procedure	12
2.4.2 Mapping Procedure	17
2.4.3 Chemical Analysis	17
2.5 Autopsy Examination of Potlining	17
3. Laboratory Studies of Sodium Cyanide Formation	28
3.1 Introduction	28
3.1.1 Rate of Sodium Cyanide Formation	30
3.1.2 The Importance of Carbon Quality	30
3.2 Experimental	31
3.2.1 Reaction Cell and Furnace	31
3.2.2 Gas Cover and Flowmeter	32
3.2.3 Carbon Types	37
3.2.4 Thermogravimetric Analysis	42
3.2.5 Cyanide Synthesis in Experimental Specimens	43
3.2.6 Sample Analysis	44

TABLE OF CONTENTS (cont'd)

	<u>Page</u>
3.3 Results and Discussion	44
3.3.1 Rate of Sodium Cyanide Formation	44
3.3.2 Effect of Temperature	59
3.3.3 Effect of Graphite Content	64
3.3.4 Effect of Iron (as Fe_2O_3) Impurity	70
3.3.5 Predominant Cyanide - Containing Species	74
4. Conclusions	77
References	83
Appendix 1	87
Appendix 2	122
Appendix 3	124
Appendix 4	141

LIST OF TABLES

<u>Table No.</u>		<u>Page</u>
1	Characteristic Fluorescences	16
2	Failed Pots Selected for Autopsy	20
3	Typical Formulation of Monolithic Carbon-Mix	40
4	Chemical Analyses of Carbon Specimens	41
5	Rate Data Derived from Integral Analyses with 5 wt.% Initial Sodium Charge	45
6	Rate Data Derived from Integral Analysis with 10 wt.% Initial Sodium Charge	45
7	Rate Data Derived from Thermogravimetric Analysis with 5 wt.% Initial Sodium Charge	46
8	Rate Data Derived from Thermogravimetric Analysis with 10 wt.% Initial Sodium Charge	47
9(i)	Cyanide Synthesis - Plant Derived Carbon-Mix	61
9(ii)	Cyanide Synthesis - Commercial Prebaked Block Cathode	61
9(iii)	Cyanide Synthesis - Graphite AGSX	62
10	Graphite Content in Prebaked Block Cathode and Monolithic Carbon	66
11	Effect of Graphite Content on Cyanide Formation	67
12	Effect of Graphite Content of Spent Potlinings on Total Cyanide Concentration	69
13	Effect of Iron (as Fe_2O_3) Addition on Cyanide Production in Plant Derived Carbon-Mix	72
14	Comparison of Total and Free Cyanide Content in Spent Potlining Specimens	76

LIST OF FIGURES

<u>Figure No.</u>		<u>Page</u>
1	Cross-section of a Modern Aluminium Reduction Cell	8
2	Transverse Section of Autopsied Lining	9
3	Transverse half-section of block cathode showing perpendicular crack formation	9
4	Transverse section of inverted failed block cathode pot	10
5	Close-up of a cathode surface which has been cleaned and prepared for autopsy examination	13
6	Autopsied section of block cathode and sidewall encased within potshell	14
7	Close-up of trenched sidewall section	15
8	Generalised Cyanide Distribution Profile Bell Bay Pot 1/92	21
9	Generalised Cyanide Distribution Profile Bell Bay Pot 2/137	22
10	Generalised Cyanide Distribution Profile Bell Bay Pot 2/65	23
11	Generalised Cyanide Distribution Profile Bell Bay Pot 4/201	24
12	Generalised Cyanide Distribution Profile Bell Bay Pot 4/57	25
13	Generalised Cyanide Distribution Profile 150 kA Cell (Age: 1347 days)	26
14	Generalised Cyanide Distribution Profile 150 kA Cell (Age: 2382 days)	27
15	General Layout of Reaction Cell and Furnace	33
16	Section of Crucible and Lid Arrangement used in Reaction Cell	34
17	Close-up of Reaction Cell located in Furnace	35
18	The System used in the Study	36
19	Schematic Representation of Mould and Specimen	39

LIST OF FIGURES (cont'd)

<u>Figure No.</u>		<u>Page</u>
20	Rate Plot for Reactant Sodium at 550°C Derived from Integral Analysis	48
21	Rate Plot for Reactant Sodium at 550°C Derived from Thermogravimetric Analysis	49
22	Second-order Reaction Plot for 5 wt.% Sodium at 550°C derived from Integral Analyses	50
23	Second-order Reaction Plot for 10 wt.% Sodium at 550°C derived from Integral Analyses	51
24	Second-order Reaction Plot for 5 wt.% Sodium at 550°C derived from Thermo- gravimetric Analysis	52
25	Second-order Reaction Plot for 10 wt.% Sodium at 550°C derived from Thermo- gravimetric Analysis	53
26	Typical Isotherms in Transverse Centre Half-section of an Aluminium Reduction Cell	63
27(i)	Cyanide Formation in Different Carbon Types	68
27(ii)	Cyanide Formation in Graphite	68
28	Effect of Iron Impurity on Cyanide Formation in Carbon-Mix	73

Chapter 1

1. Introduction

During normal pot operation the movement of various reactive bath constituents through the potlining at operating temperatures of approximately 970°C initiates a wide range of chemical reactions which lead to the formation of by-products. Some of the components identified include compounds such as β -alumina ($\text{Na}_2\text{O} \cdot 11\text{Al}_2\text{O}_3$), aluminium carbide (Al_4C_3) and sodium cyanide (NaCN) ⁽¹⁾. Other by-products such as sodium carbide (Na_2C_2) ⁽²⁻⁴⁾ and aluminium nitride (AlN) ^(2,3) have also been reported.

Amongst the products generated, cyanide compounds command particular attention. The toxicity and harmful effects of cyanides as well as the potential environmental impact that they can produce have caused considerable concern in the aluminium industry ⁽⁵⁾. Because of the need to continue developing strategies for treating cyanide-contaminated wastes generated from pot operation, a greater understanding of cyanide formation in the potlining is desirable.

It is an aim of this investigation, therefore, to identify the favoured regions of cyanide generation in the potlining, and to evaluate some of the chemical factors likely to influence cyanide formation.

Essentially, the investigation comprised three stages. In the first stage, autopsies of failed electrolytic cells followed by extensive mapping of the cyanide distribution profiles in the potlinings were conducted in detail. Pots of different ages, design and construction were selected for autopsy and examination.

A fundamental approach was applied in the investigation in the following stages. The kinetics of the reaction of metallic sodium with pure nitrogen gas and carbon to form sodium cyanide was examined in the second stage. This was accomplished by continuous monitoring of the reaction process at thermal equilibrium involving the application of thermogravimetric and integral analysis techniques. Attention was focussed on the effect of sodium content on the rate of cyanide formation. The data derived were subsequently graphed, and an attempt was made to discuss the physical and chemical processes affecting the reaction rate.

In the third stage, attempts were made to establish the range of temperatures required for the formation of sodium cyanide. This was carried out by reacting small size sodium-impregnated carbon specimens with nitrogen in a reaction cell over a range of temperatures.

The susceptibility of carbon, containing varying amounts of graphite, to cyanide formation was similarly studied. Three forms of carbon material, comprising plant derived monolithic carbon-mix, commercial preformed cathode material and high purity graphite were used.

Finally, the influence of iron impurity in carbon on cyanide generation was investigated. Laboratory trials with moulded monolithic carbon specimens, doped with various concentrations of iron oxide and reacted over a range of temperatures, were performed.

Results derived from the above fundamental studies were subsequently correlated with plant measurements to enable an understanding of the presence of cyanide, and its chemical relationship with the thermal environment in the industrial operating cell.

A more detailed description of procedures and techniques is presented in the following chapters.

1.1 Glossary

A glossary of some of the common expressions used is given here:

Bath/Pot Bath	The liquid electrolyte used in the electrolytic cell; basically a solution of alumina in molten cryolite.
Isothermal Freeze Zones	Narrow freezing zones of certain bath components, at locations within the cathode, that correspond to particular isotherms at the time of solidification.
Pot	An expression used for an operating electrolytic cell.
Free Cyanide	A term referring to the summation of molecular HCN and the cyanide ion in aqueous solution.
Total Cyanide	The term refers to all the different forms of cyanide that exist in an aqueous solution. It includes free cyanide and all the simple and complex cyanides.
Cathodic Bath	Product of chemical reaction between certain bath components and metallic sodium formed within the cathode mass.

Chapter 2

2. The Problem

2.1 Cyanide Presence in Potlining

Cyanide in potlining may exist as two forms, simple salts and complex iron cyanide. During wet weather, spent potlinings stored in open heaps are very vulnerable to leaching of cyanide compounds by rain. Leachate emanating from the heap can, if not controlled, seep into the soil and flow into effluent streams leaving the plant. If left undetoxified, the cyanide-bearing wastes can prove acutely toxic to fauna and flora living in the immediate vicinity of the effluent discharge point.

The harmful effects of the wastes are mainly attributed to both free cyanide salts and hydrogen cyanide (HCN). Under most surface water conditions tested in the laboratory, the toxicity of free and complex cyanide solutions to fish has been shown to be directly related to the concentration of molecular HCN generated from the dissociation of cyanide salts⁽⁵⁾. Moreover, the unbound cyanide ion (CN^-) contributes to toxicity under alkaline conditions. Although complex iron cyanides are extremely stable, they are also prone to photolytic decomposition under certain conditions and serve as a delayed source of free cyanide⁽⁵⁾.

The quantity of cyanide in effluents varies from one plant to another. Farrier and Patterson⁽⁶⁾ state that up to 17.5 g CN^- /litre can be found in the rain water run-off from the spent cathode site. Another report⁽⁷⁾ suggests a free cyanide concentration range of 150 - 600 mg/litre in leachate collected in a moat adjacent to the cathode heap. According to Mitchell⁽⁸⁾, analyses of crushed potlining reveal

0.35 wt.% of ferrocyanide complex and 0.10 wt.% NaCN, whilst earlier, Holo⁽⁹⁾ indicated a total cyanide concentration of 4 wt.% of the entire cathode.

Nearly all the findings presented reflect the very real impact on the environment that cyanide emission can cause, if not responsibly contained and treated. In fact, the environmental problem created is of sufficient importance and concern to have generated a number of processes for detoxification of cyanide in spent potlinings^(10,11).

2.2 Cyanide Distribution Profile in Potlinings

The evidence described in Section 2.1 highlights the importance of the presence of cyanide in potlinings. The continuing concern by the aluminium industry over the build-up of cyanides in spent cathode heaps has led to the present stage of investigations which involve pot autopsies and mapping of the cyanide distribution profiles in the linings.

2.2.1 Introduction

All the information gathered confirms that cyanide is a by-product generated in the potlining during normal pot operation. However, a survey of existing literature shows that there is limited information on the distribution of cyanide and its formation in potlinings. Most of the information published is of a general nature related to the presence of cyanide in crushed potlining samples. Although Mitchell⁽⁸⁾ claims that the location of cyanides in the cathode is most probably zoned due to the presence of temperature gradients in the lining, no data has been presented to support the claim.

To date, available data on the presence of cyanide and its formation within the carbon linings is inconclusive. Therefore, to obtain an overall picture of the distribution of cyanide and a greater insight into its formation in potlinings, it is important that the location of the species is pinpointed. This was accomplished through a series of autopsies of 48 kA and 88 kA failed reduction cells of various ages and construction from the Bell Bay, Tasmania, plant of Comalco Limited, followed by extensive mapping of the cyanide distribution profiles in the linings. The investigation was also extended to include larger cells of 150 kA.

So that the philosophy behind pot autopsies can be clarified, a brief account of pot construction and factors leading to pot failure is given below.

2.3 Industrial Background

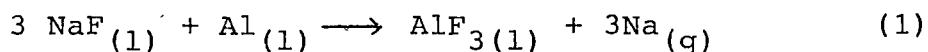
2.3.1 Pot Construction

Essentially, the aluminium electrolytic cell consists of a carbon cathode encased within a steel shell and a superstructure for supporting the carbon anodes. The shell is normally lined with a layer of bricks or powdered alumina which acts as thermal insulation for the cell.

Packed against the layer of insulation is a layer of carbon lining which acts as the sidewall of the cell. The base lining comprises a layer of cathode carbon surrounding a set of iron collector bars which conduct the current during electrolysis. Immediately below the cathode is another layer of insulation which may be either powdered alumina or refractory brickwork. The cross-section of a cell fitted with pre-baked anodes is depicted in Figure 1.

2.3.2 Cathode Failure

During normal pot operation, bath and free sodium species, permeate the lining and initiate a host of chemical reactions within the carbon mass. Generation of the sodium species can occur via the chemical pathway⁽¹²⁾:



Sodium atoms accumulating at the metal-cathode interface can diffuse into the cathode by either a vapour diffusion⁽¹³⁾ or, grain boundary mechanism^(2,14) or a combination of both.

As the sodium permeates the lining, swelling of the carbon occurs. The sites of swelling ultimately advance downward through the cathode and towards the sidewalls. The advancing sodium front is subsequently followed by an infiltrating wave of bath from the cathode surface (Figure 2). As the bath occupies the carbon pores and capillary channels constituting the porosity of the carbon, chemical interaction between bath components and reactant sodium intercalated in the cathode commences.

Some of the reactions initiate the formation of by-products which are believed to produce volume expansion in the pores⁽¹⁴⁾. Moreover, as bath seeps further down the cathode, it encounters a decreasing temperature gradient and undergoes a gradual process of fractional crystallization which also expands the carbon lattice. Consequently, the expansion could generate sufficient stresses which may overcome the tensile strength of the carbon and ultimately initiate crack formation within the carbon mass (Figure 3). Similarly, the lining undergoes a growth and disruption which eventually results in its failure (Figure 4).

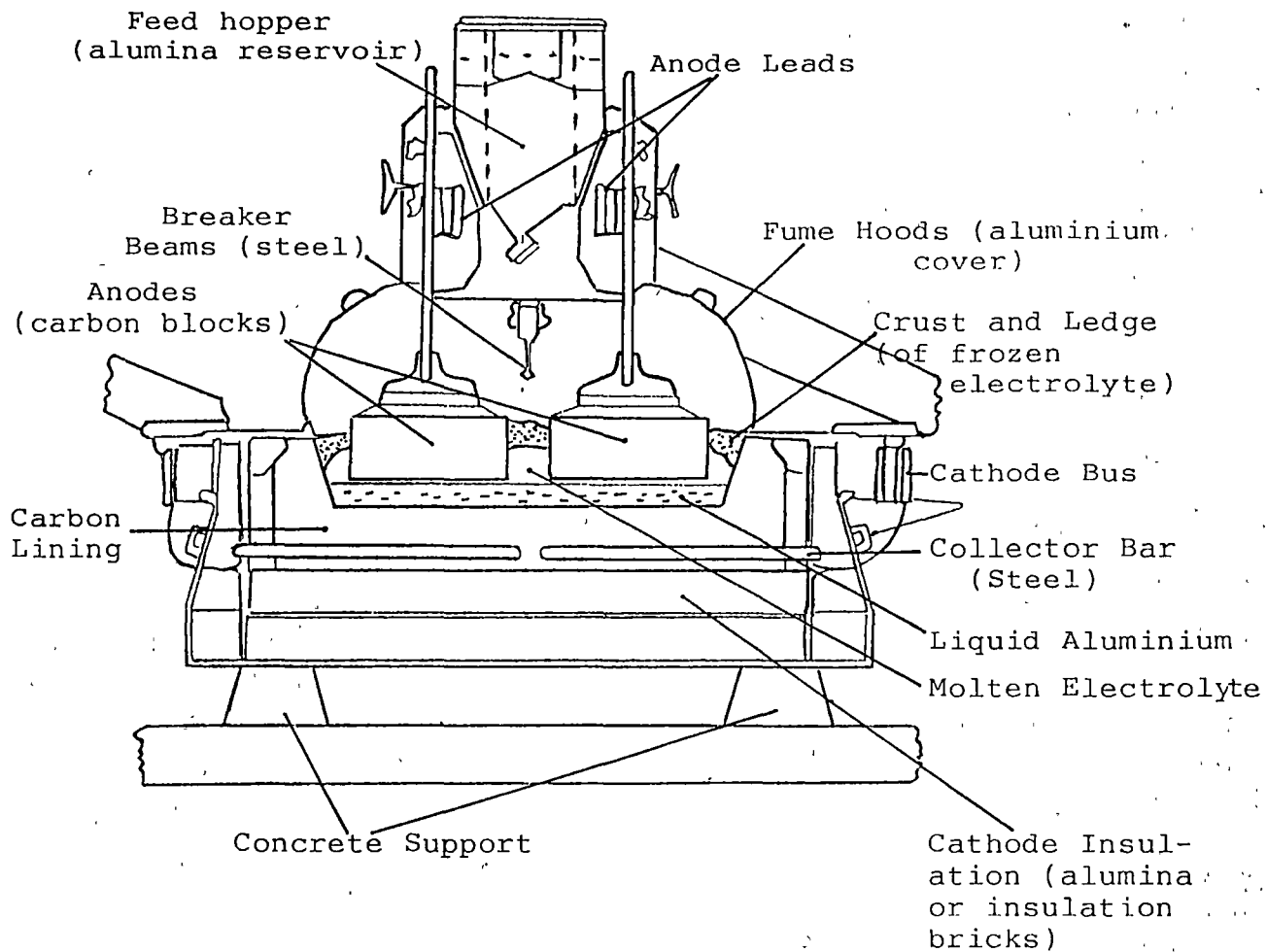


Figure 1: Cross-section of a Modern Aluminium
Reduction Cell ⁽¹⁵⁾



FIGURE 2: Transverse section of the autopsied lining showing the presence of a mixture of solidified electrolyte and metallic aluminium(1) outlining a dish-shaped crack(2) in the carbon.

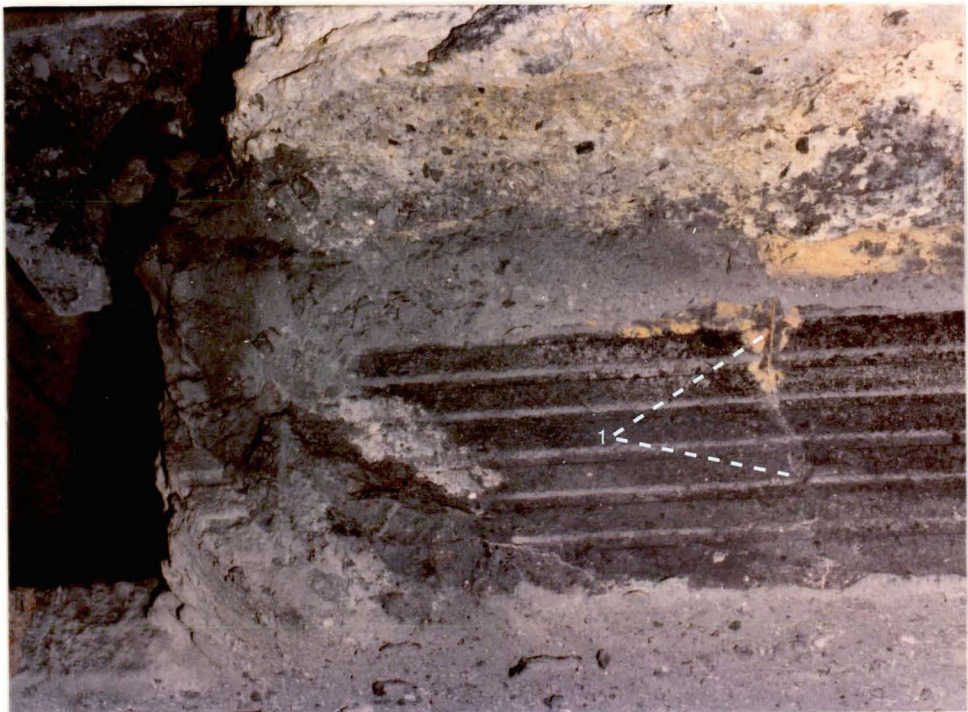


FIGURE 3: Transverse half-section of block cathode showing perpendicular crack formation(1) in the carbon probably due to differential expansion between expanded sodium-impregnated layer and unexpanded lower section of cathode.



FIGURE 4: Transverse section of inverted failed block cathode pot, showing arching of the collector bar(1) due to the tension generated by a combination of sodium swelling of and crystallization pressure on the cathode.

Owing to the disruptive effect of some of the chemical reactions within the carbon mass, the potlining exhibits a decline in useful life-span over a period of time. Hence, one of the principal objectives of the autopsy effort is to identify the potlining deterioration and failure mechanism as rapidly and conclusively as possible. The autopsy would not only facilitate the diagnosis of the cause of failure of a prematurely failed cell, but would also enable the evaluation of the effectiveness of the design, construction or operation of the cell.

Pot autopsies also provide the opportunity for locating and determining some of the chemical components in the lining. Owing to the cyclical nature of thermal isotherms in the cell, a number of distribution profiles of chemical species is created within the lining. Therefore, comprehensive mapping of these profiles followed by chemical analyses of the specimens extracted would present an insight into some of the chemistry in the potlining.

2.4 Pot Autopsies

Several failed Bell Bay cells were selected for autopsy. A .47 kA cell with a fully monolithic cathode and four 87 kA prebaked cathode cells were autopsied, and specimens from larger cells of 150 kA were also obtained for examination.

Essentially, the autopsy was performed in two main stages so that detailed examination of the cathode integrity and general condition of the pot could be made. A brief description of the autopsy procedure is given below.

2.4.1 Autopsy Procedure

After removal from the process line, the pot was positioned upright so that the cathode cavity was accessible from the top of the pot. The first stage of autopsy involved the systematic removal of debris from the cavity. This was accomplished by cutting the frozen bath and residual solidified aluminium pad on the surface of the cathode with air-powered jack-hammers fitted with silicon carbide tipped steel blades. The operation was performed in a manner so that chipping of the cathode carbon was minimised. After the removal of large pieces of debris, the cathode surface was subsequently cleaned with an industrial vacuum cleaner and its condition thoroughly examined. Figure 5 illustrates the state of a block cathode cavity which had been cleaned and prepared for examination.

In the second stage of autopsy, transverse sections of the sidewall and cathode were sliced and removed while the pot-shell was still intact. Initially, a cathode block was removed from the mid-section of the pot by sectioning the cathode through the cathode-slots to form a trench. Formation of the trench, therefore, allowed direct access to the cross-section and facilitated examination of the potlining. An autopsied section of a block cathode and sidewall still encased within the shell is shown in Figure 6.

Following examination of the cathode for significant crack formation and propagation, the positions of bath isothermal freeze zones and sodium condensation bands in the carbon mass were located. This was accomplished by beaming ultra-violet light at the trenched surface with a prospector's portable hand lamp⁽¹⁶⁾, and simultaneously using coloured chalks to trace the fluorescent bands. The various chemical

compounds and their corresponding fluorescence colours are listed in Table 1. Figure 7 shows a photograph of a trenched sidewall exhibiting a band of cathodic bath isothermal freeze zone marked with red coloured chalk. Immediately adjacent to the edge of the sidewall is a separate band of sodium carbonate deposit outlining the position of the sodium condensation zone.



FIGURE 5: Close-up of a cathode surface which has been cleaned and prepared for autopsy examination. Residual bath and metal are visible as white-opaque patches against a greyish-black background of cathode carbon.



FIGURE 6: Autopsied section of block cathode (A) and sidewall (B) encased within potshell (C)



FIGURE 7: Close-up of trenched sidewall section pinpointing the bath isothermal freeze zone(1) and the location of the zone of maximum sodium condensation(2).

Table 1: Characteristic Fluorescences⁽¹⁴⁾

Phase	Natural Colour	Fluorescent Colour
Na_3AlF_6 (pure)	white	none
NaF	white	none
CaF_2	white	rusty-orange
Pot bath	white	pink
Cathodic bath	white	pale blue
$\text{Na}_2\text{O} \cdot 11 \text{ Al}_2\text{O}_3$	white	yellow-green
Eutectic	white	bluish-white
Sodium vapour zone	not applicable	deep black

2.4.2 Mapping Procedure

Mapping of the cyanide profile was achieved by carefully extracting specimens from various selected regions of the trenched sidewalls and cathodes with a hand-pick. The location of the sampling points was measured from a reference position, such as the potshell, and marked for identification. Sample extraction was conducted over a 50 mm diameter area of each sampling point. The samples were subsequently sealed in marked plastic bags and stored over granular silica gel in desiccators.

During the mapping process, particular attention was focussed on the condition of the sampling regions and their locations relative to special features such as bath isothermal freeze zones, crack formation areas and failure zone in the lining. These observations would facilitate the understanding of the cyanide presence within the potlining.

2.4.3 Chemical Analysis

The specimen was ground to -200 mesh in a ring-mill, a portion taken for acidic cuprous chloride distillation, and the distillate collected in 2.5N NaOH solution (Appendix 2). The distillate was subsequently analysed for total cyanide with an Orion Cyanide - Ion Selective Electrode connected to an Orion Research Microprocessor Ionalyser - 901 unit.

2.5 Autopsy Examination of Potlining

The results of all cyanide analyses are detailed in Tables 1.1 to 1.16 in Appendix 1, and sampling locations are indicated on associated diagrams. An attempt to explain the cyanide distribution profile in the potlining is made in this section, and a

generalised picture of all the results is presented in Figures 8 to 14. Particulars related to the autopsied pots of various construction and type are summarised in Table 2.

Autopsy examination of the trenched linings clearly reveals that carbon which is heavily impregnated with sodium is more susceptible to cyanide formation in areas which are easily accessible to air ingress. This is particularly evident in regions which are immediately adjacent to the points of air ingress such as the collector bar seals, and other areas which allow direct entry of air such as cracks in the carbon lining.

However, the cyanide concentration is relatively low in cathode regions near the mid-section of the pot. A number of factors may limit the generation of cyanide in these regions, but it seems that restricted access to air ingress may have been a major contributor. Accordingly, severe crack formation and propagation in the cathode carbon must also facilitate direct entry of air into the sodium-impregnated carbon mass and enhance cyanide formation. A typical example is reflected in the cyanide-profile illustrated in Figure 11 which shows abnormally high cyanide content in the mid-section of the cathode. Autopsy examination of the pot revealed the presence of massive crack formation in and bath flooding of the entire mid-section of the cathode. Crack formation of this nature would most likely enable direct entry of air into the heavily sodium-impregnated carbon and ultimately intensify cyanide generation in this region.

The isolated pocket of high cyanide content in the alumina insulation was probably due to the permeation of cyanide from the cathode region. As the operating temperature in many regions of the cathode was above the melting point of most cyanides (e.g. NaCN m.pt: 563°C) during its formation, it was not unlikely for a portion of the melt to permeate downwards into the insulation. On the basis of this reasoning, it would appear that cyanide accumulation in the alumina occurred via the above mode of transport.

In general, medium (2.0 - 4.0 wt.%) to high (>4.0 wt.%) concentrations of cyanide are located in the sidewall region and adjoining areas around the collector bars, whilst smaller amounts of cyanide are distributed in the cathode carbon. In particular, regions of maximum sodium condensation are potential chemically reactive sites for cyanide formation.

Thus, as sodium penetration and deterioration of the carbon lining progresses, air ingress into the carbon mass is likely to increase. Eventually, this will lead to a build-up of cyanide in the lining.

Table 2: Failed Pots Selected For Autopsy

CURRENT RATING	AGE AT FAILURE (Days)	DESIGN TYPE	NATURE OF FAILURE	CAUSE OF FAILURE
Bell Bay 47 kA	1920	Monolithic	Not Applicable	Cut out - line closure
Bell Bay 87 kA	1060	GLCC Block Cathode SiC - Type III (Borgestad bricks)	Corner tap-out	Failure of bolted corner joints leading to severe carbon airburn and subsequent bath flood into areas adjacent to corner section
Bell Bay 87 kA	823	Sers Block Cathode SiC - Type III (Skamol and Vulcan bricks)	Tap-out through collector bar	Re-opening of previously formed crack at surface of block following cradle breakage
Bell Bay 88 kA	432	Nippon Block Cathode SiC - Type IV	Tap-out through collector bar	Excessive bath leaks via inter- face of block-end and sidewall into alumina insulation leading to insulation deterioration
Bell Bay 88 kA	850	Nippon Block Cathode SiC - Type IV	Tap-out through collector bar	Excessive bath leaks via inter- face of block-end and sidewall into alumina insulation leading to insulation deterioration
150 kA	1347	Great Lakes Carbon Block Cathode	Not Applicable	Cut-out for reconstruction
150 kA	2382	Great Lakes Carbon Block Cathode	Tap-out through collector bar	Excessive bath erosion of side- wall region

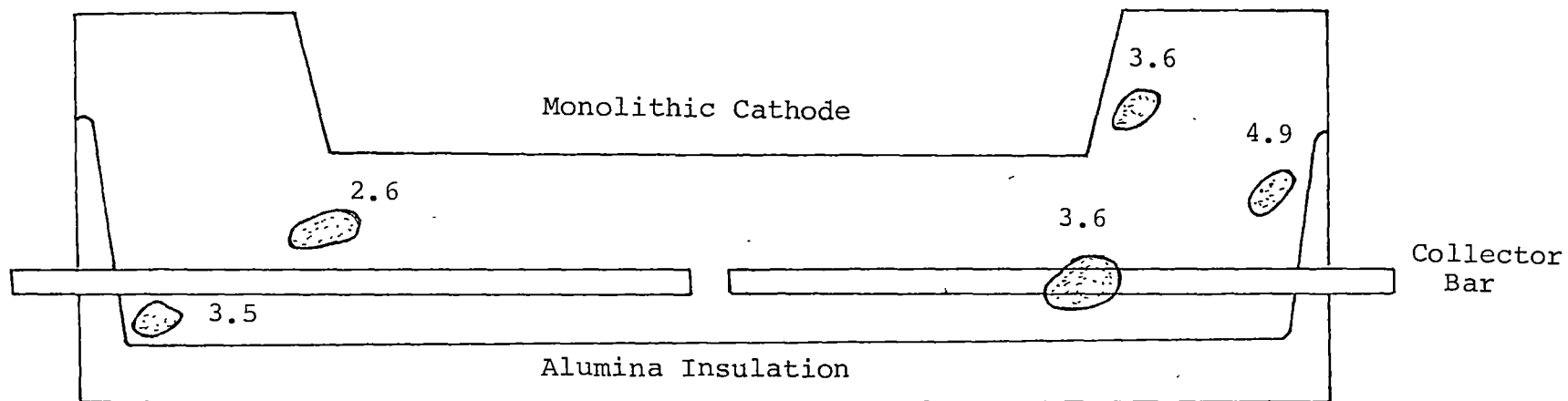
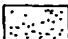


Figure 8: Generalised Cyanide Distribution Profile

Bell Bay Pot 1/92 Age: 1920 days

Transverse Section - Monolithic Construction

Legend:  Location of Cyanide Species - Concentration*

* All concentrations expressed as wt.% CN^-

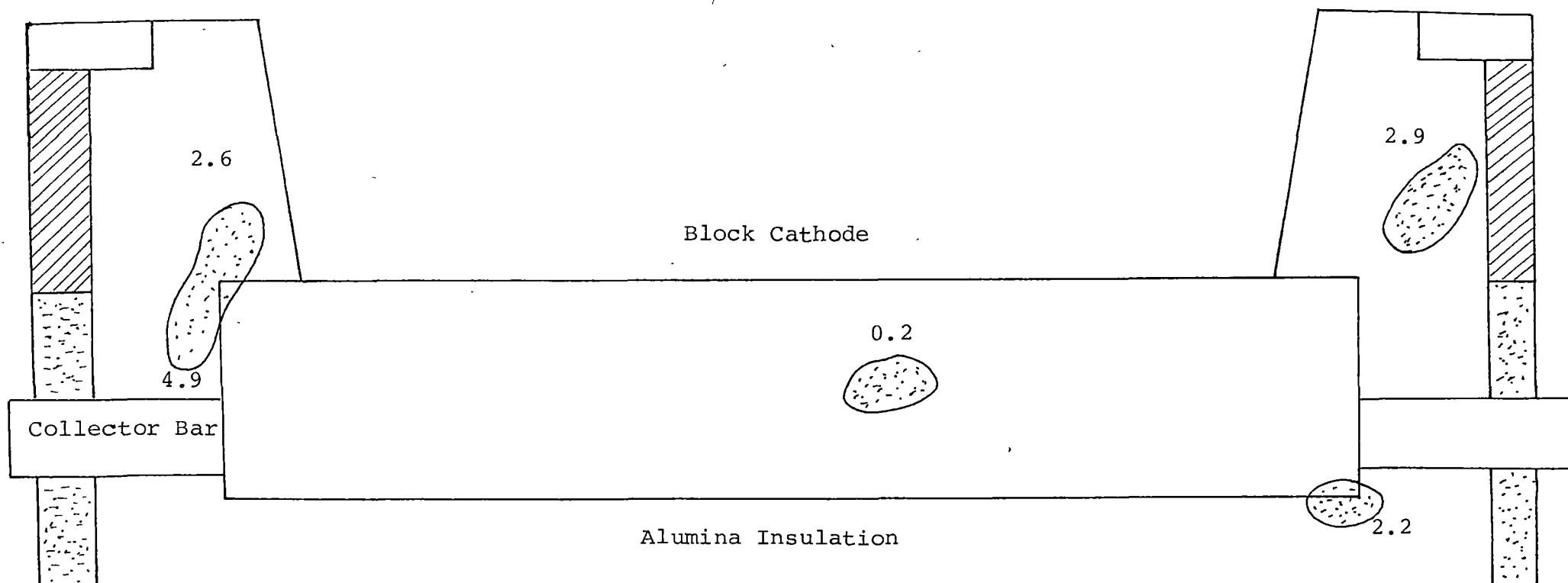



Figure 9: Generalised Cyanide Distribution Profile
Bell Bay Pot 2/137 Age: 1060 days
Transverse Section - Block Cathode Construction

Legend:  Location of Cyanide Species - Concentration*

* All concentrations expressed as wt % CN^-

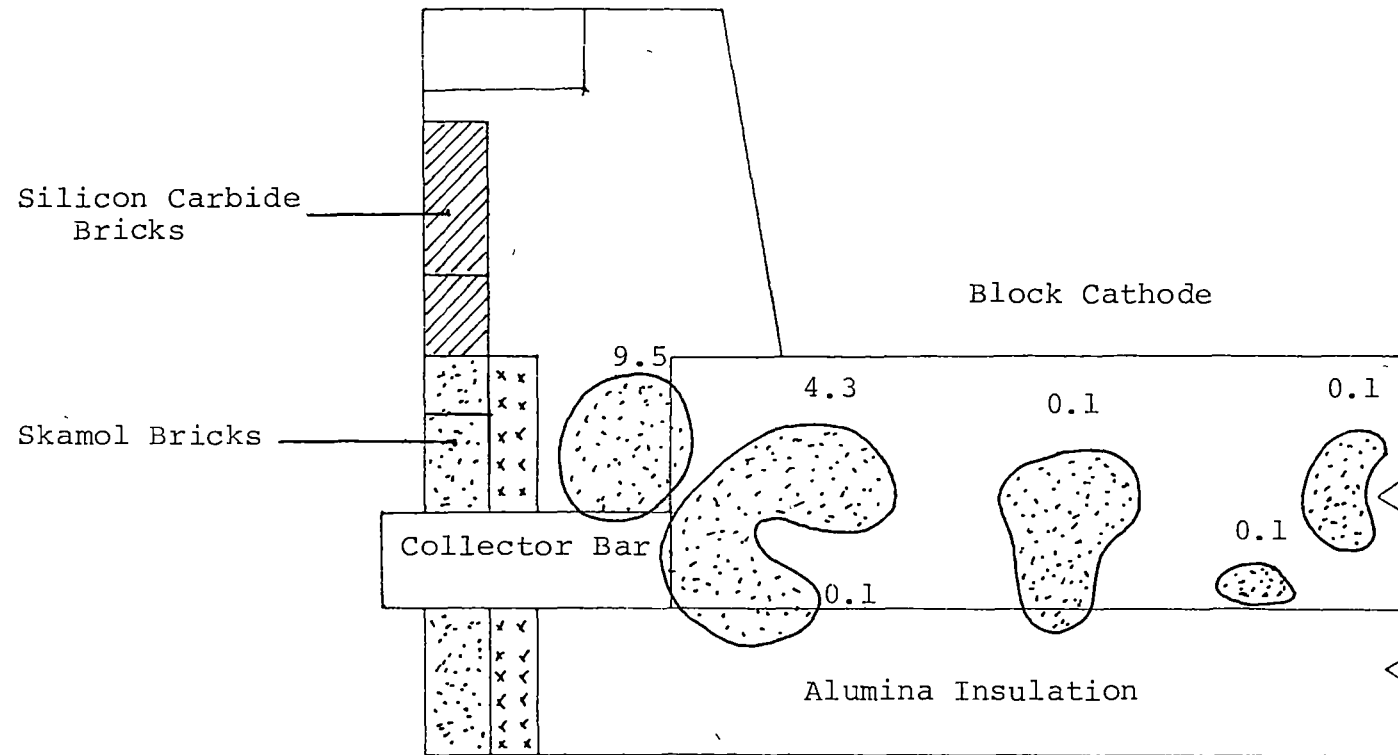
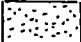


Figure 10: Generalised Cyanide Distribution Profile
Bell Bay Pot 2/65 Age: 823 days
Transverse Half-Section of Block Cathode

Legend:  Location of Cyanide Species - Concentration Range*

* All concentrations expressed as wt % CN^-

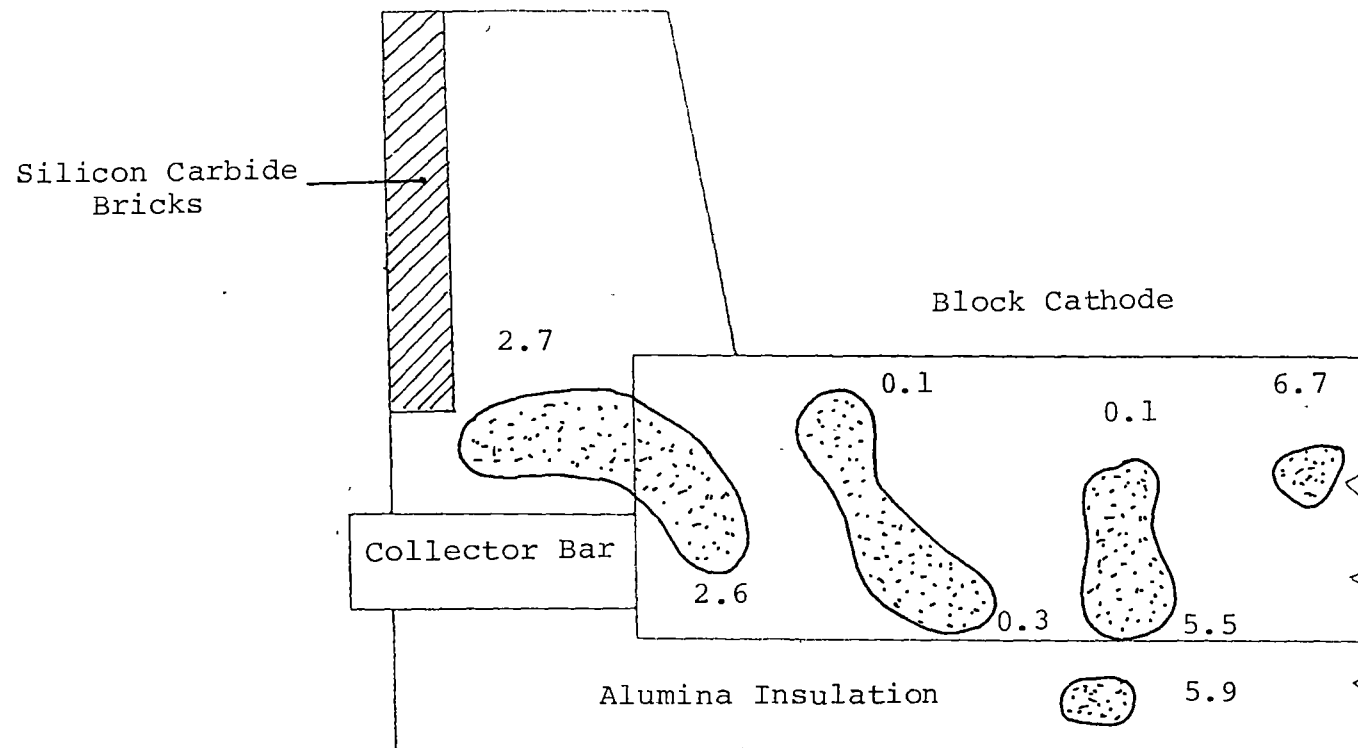



Figure 11: Generalised Cyanide Distribution Profile
Bell Bay Pot 4/201 Age: 432 days
Transverse Half-Section of Block Cathode

Legend:  Location of Cyanide Species - Concentration Range*

* All concentrations expressed as wt % CN^-

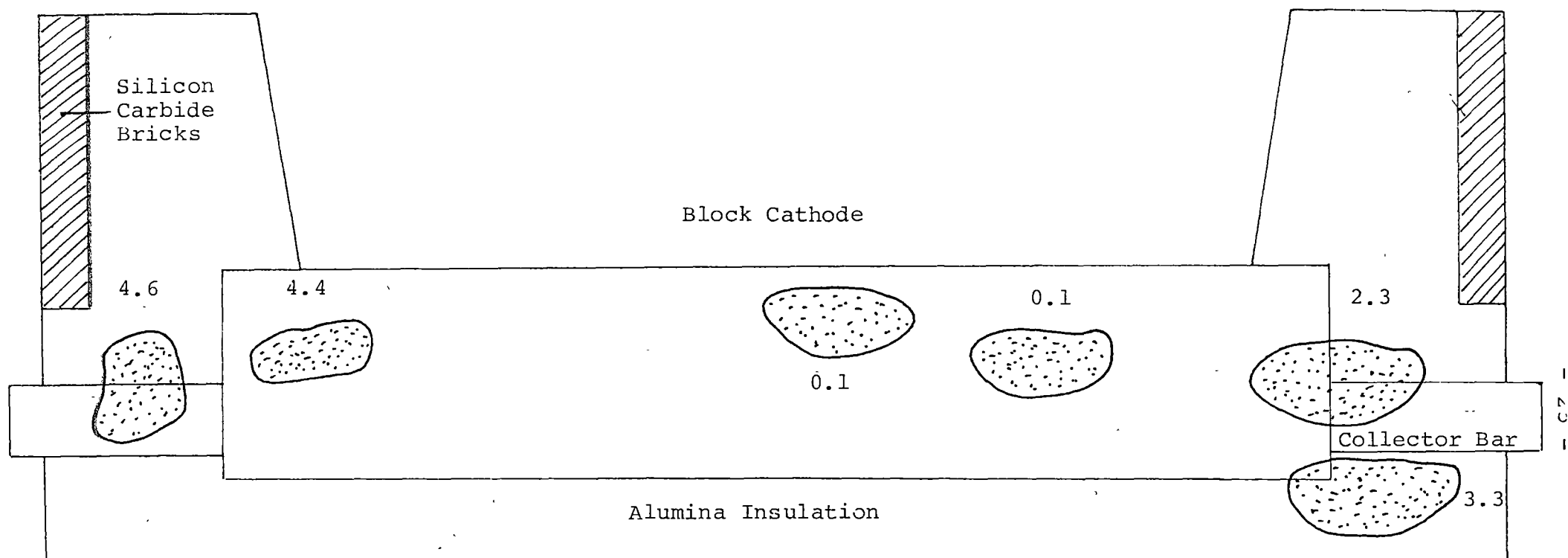
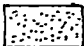


Figure 12: Generalised Cyanide Distribution Profile

Bell Bay Pot 4/57 Age: 850 days

Transverse Section of Block Cathode

Legend:  Location of Cyanide Species - Concentration*

* All concentrations expressed as wt % CN^-

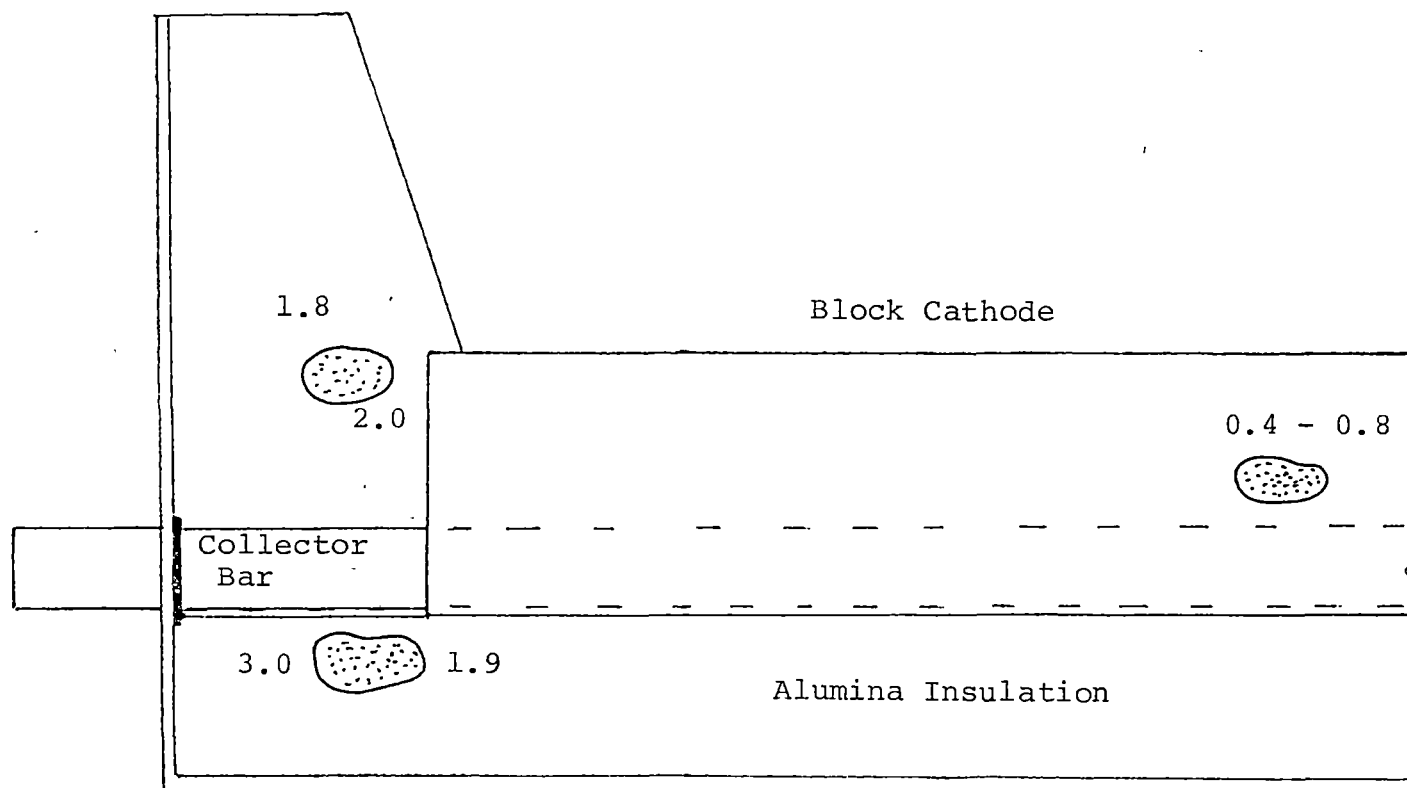
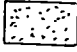


Figure 13: Generalised Cyanide Distribution Profile
150 kA Cell Age: 1347 days
Transverse Half-Section of Cathode

Legend:  Location of Cyanide Species - Concentration Range*

* All concentrations expressed as wt % CN^-

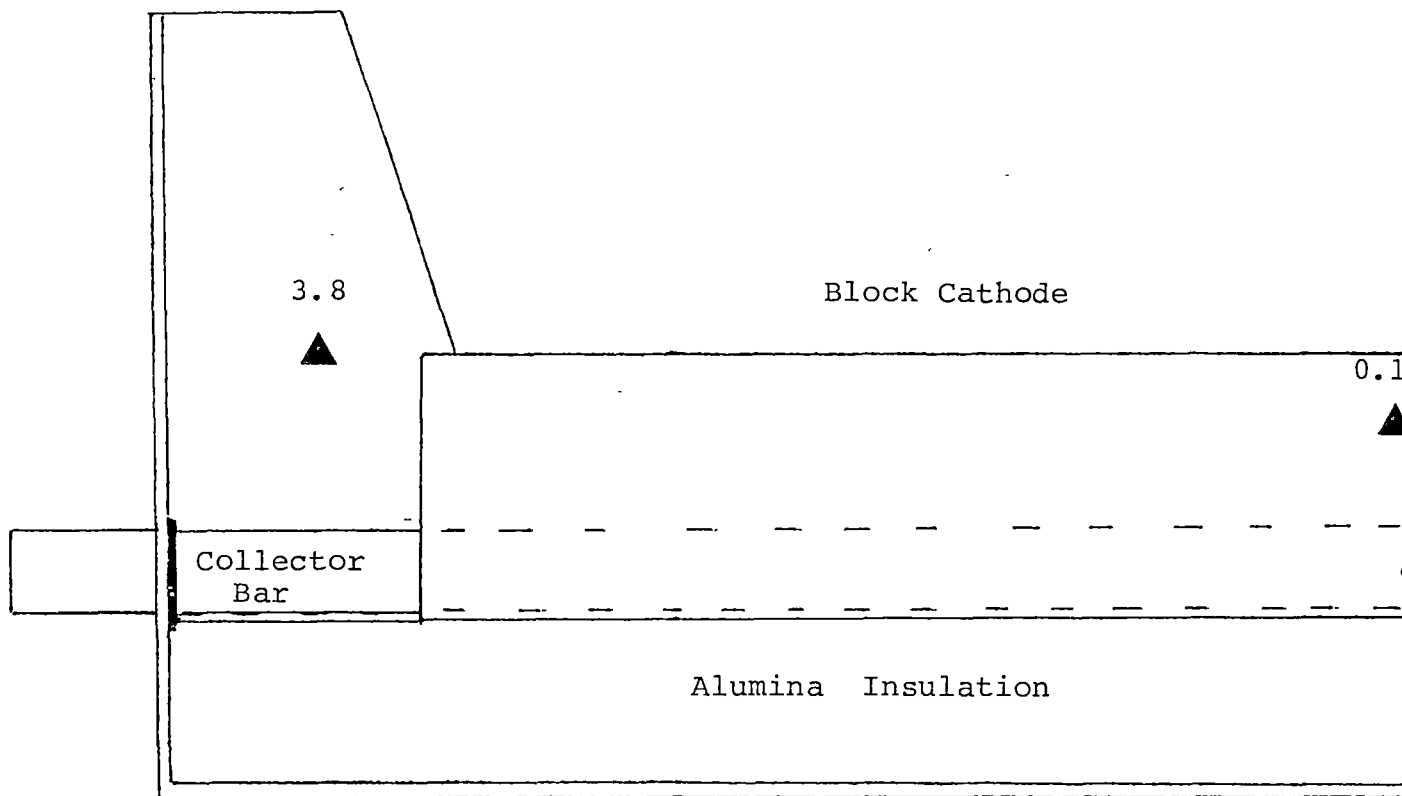


Figure 14: Generalised Cyanide Distribution Profile

150 kA Cell Age: 2382 days

Transverse Half-Section of Block Cathode

Legend: ▲ Location of Cyanide Species - Concentration*

* All concentrations expressed as wt % CN^-

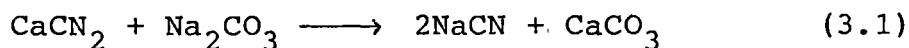
Chapter 3

3. Laboratory Studies of Sodium Cyanide Formation

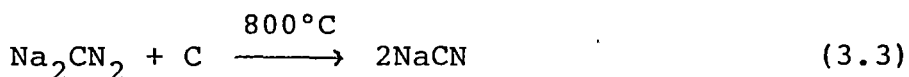
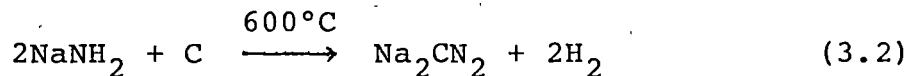
3.1 Introduction

A search of the literature reveals that several pathways are known for the formation of sodium cyanide⁽¹⁷⁻²⁰⁾. These processes are summarised as follows:

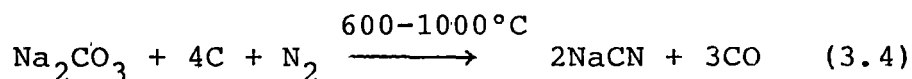
- (a) Reaction of calcium cyanamide with sodium carbonate and carbon⁽¹⁷⁾:



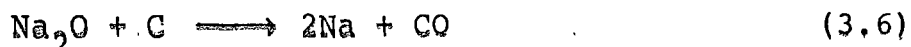
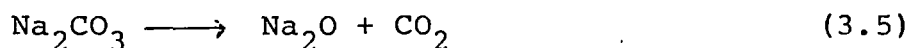
- (b) Castner process⁽¹⁷⁾:



- (c) Bucher process⁽¹⁸⁻²⁰⁾:



As the formation of sodium amide is unlikely under the reaction conditions involving interaction between gaseous nitrogen, metallic sodium and carbon used in this study, the route to cyanide formation that appears most likely is the Bucher process. In this process, reaction (3.4) has been reported to proceed via several intermediate pathways at temperatures ranging from 600°C to 1000°C⁽¹⁹⁾:





The above sequence shows that several combinations of compounds will eventually yield sodium cyanide. The interesting point to note from these intermediate compounds is that the occurrence of both sodium carbide and sodium cyanide in spent potlinings of industrial cells have been reported previously^(2,4). Therefore, it appears that the mechanism of cyanide formation in the pot may be similar to the reactions quoted above.

In addition, the formation of sodium cyanide is thermochemically favoured over a range of temperatures^(1,18,21). For instance, the Bucher process has been found to be endothermic with an enthalpy of formation value of ~~46.2~~ kcal./mole at about 1000°C⁽¹⁸⁾. Similarly, recent thermodynamic feasibility studies reveal that cyanide formation from its elements is thermochemically favoured in the range of temperature 630 - 1000°C in the lining of industrial cells⁽¹⁾. Moreover, a survey of thermochemical tables shows that cyanide formation from its elements is also favoured in the lower temperature range of 527°C to 627°C ($\Delta H^\circ_f = -21.27$ to -21.18 kcal./mole)⁽²¹⁾. On the basis of the above data gathered, it is evident that sodium cyanide formation can occur over a wide range of temperatures.

From the discussion above, it is clear that further laboratory studies to complement recent findings from autopsy examinations of failed industrial cells presented earlier in Section 2.5, can only lead to a better understanding of the cyanide presence in the industrial cell. Consequently, the following study plan was drawn up to investigate some of the factors

influencing cyanide formation using a system relevant to the complex situation in the industrial environment.

3.1.1 Rate of Sodium Cyanide Formation

A survey of literature reveals that very little information on the reaction kinetics of the formation of sodium cyanide, relevant to the system being studied, is documented. Nearly all the early laboratory studies⁽¹⁷⁻²⁰⁾ were focussed mainly on the production of sodium cyanide from its elements under different reaction conditions, where mixtures of sodium carbonate and carbon were reacted with gaseous nitrogen in an iron tube at temperatures above 900°C.

Nevertheless, Bucher⁽¹⁸⁾ observed that the rate of sodium cyanide formation was affected by the amount of reactant sodium in the reaction at 950 - 1000°C. An increase in reaction rate was noted when the concentration of sodium carbonate was decreased. No explanation nor kinetic data was given to support the observation. Evidently, further laboratory investigation of the reaction kinetics can only lead to a greater understanding of the chemical and physical processes that are related to the rate of cyanide formation within the carbon lining of the industrial cell.

A discussion of the above processes affecting the rate of cyanide formation is given later in Section 3.3.1.

3.1.2 The Importance of Carbon Quality

Pertinent data derived from the pot autopsy examinations reported earlier in Section 2.5 imply that cyanide generation is affected by the form of carbon used as potlining. It seems that carbon that

is graphitic in nature tends to be less susceptible to cyanide generation. Therefore, in view of the application of different carbon types as industrial cell linings, the vulnerability of different forms of carbon to cyanide formation is an important factor for close study.

Likewise, the quality of carbon with respect to the level of iron impurity is another factor worth noting. Experimental results recorded by earlier workers^(18,20) revealed that large quantities of particulate iron (Fe) could accelerate cyanide formation at temperatures over 900°C. For instance, mixtures of carbon, iron powder and sodium carbonate reacted with nitrogen at 950 - 1000°C were found to generate large quantities of sodium cyanide compared to those without iron addition. Therefore, as small amounts of iron compounds are present in the carbonaceous materials used for lining the industrial cell, any catalytic effect they may have on cyanide formation in the thermal environment of the operating cell needs further evaluation.

Clearly, a close examination of the influence that some of the above factors may have on cyanide formation can only be achieved by systematic laboratory investigations. In this respect, a fundamental approach has been adopted to enable the generation of pertinent data for analysis.

3.2 Experimental

3.2.1 Reaction Cell and Furnace

A general layout of the reaction cell and furnace is illustrated in Figure 15. The reaction cell comprises a recrystallized alumina crucible of 27 mm diameter and 28 mm height with a lid of boron nitride

material, and a silica reaction tube attached to a Cahn RH Electrobalance. A cross-section of the crucible and lid arrangement is depicted in Figure 16. The base of the tube holds two ports, one for the monitor thermocouple and the other serves as a gas outlet. The crucible is suspended by a length of nichrome wire from a hook at the end of the Electrobalance ribbon. The reaction cell arrangement is heated by a non-inductive electrical resistance furnace which can be motor-driven along a vertical axis. In the mid-section of the furnace is a port for the control thermocouple. A close-up of the equipment is shown in Figure 17. Temperature control of the system is effected via the set-point control facility in a Trendtrak Unit. Figure 18 shows the entire system used in this study.

3.2.2 Gas Cover and Flowmeter

Ultra-high purity grade argon gas was used as the gas cover and the same grade of nitrogen gas was used as one of the reactants in this study. Removal of moisture and carbon dioxide from the gas was conducted in two stages:

- (i) Initial dry-scrubbing with granular silica gel (analytical grade).
- (ii) Final removal of moisture and carbon dioxide with analytical grade granular "Sodasorb" and magnesium perchlorate.

A constant gas pressure of $1 \times 10^5 \text{ Nm}^{-2}$ absolute and a flow rate of 0.2 litres per minute was maintained during the reaction process.

A Ficher and Porter Precision Bore Flowrator calibrated for the argon and nitrogen gas at 25°C was used to regulate the gas flowrate.

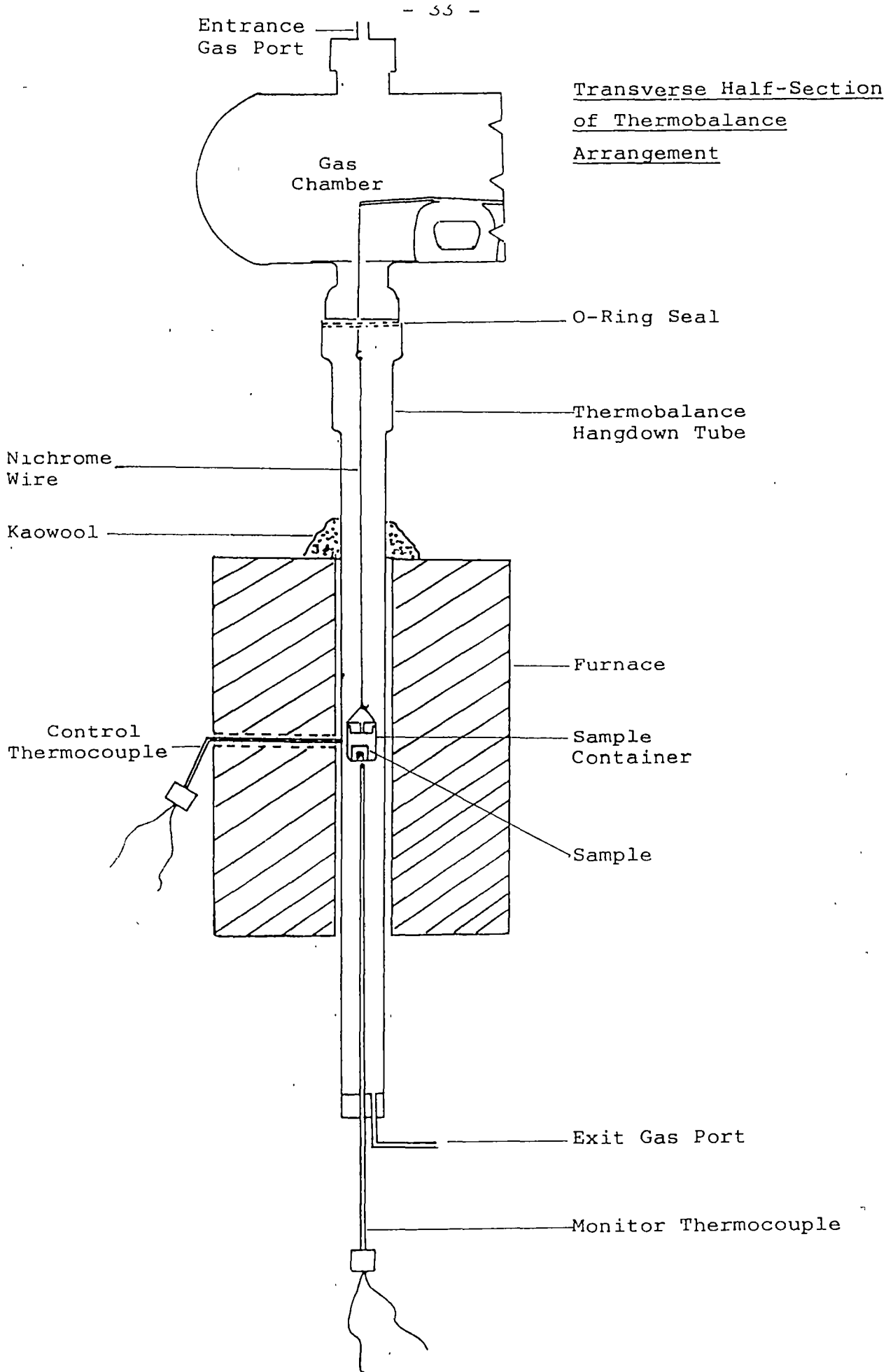
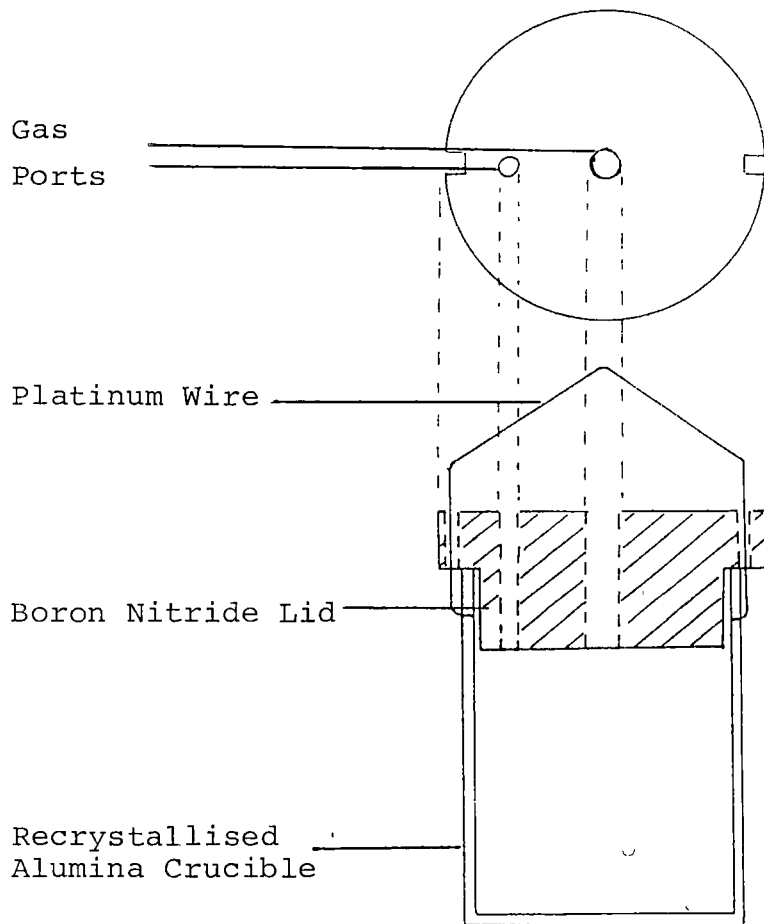


Figure 15: General Layout of Reaction Cell and
Furnace

Plan View of Lid



X-Section View of
Crucible and Lid

Figure 16: Section of Crucible and
Lid Arrangement used in
Reaction Cell



FIGURE 17: Close-up of Reaction Cell located in Furnace



FIGURE 18: The System used in the Study

3.2.3 Carbon Types

Three types of carbonaceous materials were used in the investigation.

Sidewall Carbon-Mix (ex Bell Bay Green Carbon Plant)

Green monolithic carbon-mix, used in pot-sidewall construction, was obtained directly from a batch of cathode paste manufactured at the Bell Bay Green Carbon Plant. A typical formulation⁽²²⁾ of the mix is listed in Table 3. The mix was initially heated to a temperature of 150°C in an air-oven and stirred thoroughly to obtain uniform mixing. A small portion (approximately 8 g) of the mix was subsequently added to a stainless steel mould (Figure 19) and hot pressed at a pressure of approximately $2 \times 10^7 \text{ Nm}^{-2}$.

Where additions of Fe_2O_3 (analytical grade) were required in the carbon specimens, a weighed amount of the carbon-mix was uniformly mixed with a calculated amount of anhydrous Fe_2O_3 before specimen manufacture. Specimens produced were approximately 15 mm in length and 20 mm in diameter. A hole of approximately 9 mm in diameter was similarly formed in the centre of the specimen (Figure 19) for later insertion of metallic sodium.

After manufacture, the specimens were covered with fine fluid coke in an electrical resistance furnace and baked to a maximum temperature of 1000°C over 24 hours. After a cooling period of 48 hours, the specimens were removed from the furnace and stored over granular silica gel in a glass desiccator.

Commercial Preformed Block Cathode Carbon

Two block cathodes were obtained for examination. A cylindrical plug of sample was cored out from each block of unused preformed block cathode with a motor-driven silicon carbide tipped core-drill. The plug was sawn into smaller pieces and machined to physical dimensions similar to those of the carbon-mix specimen.

High Purity Graphite (ex Union Carbide)

Commercial extruded graphite rods of 20 mm diameter and AGSX grade were supplied by Union Carbide Pty Ltd. The rods were machined to similar physical dimensions as those of the other carbon specimens.

A sample from each type of carbon was analysed for trace metals. Some of the impurity levels are listed in Table 4. All the carbon specimens were packed in marked plastic bags for identification and stored over granular silica gel in glass desiccators until they were used.

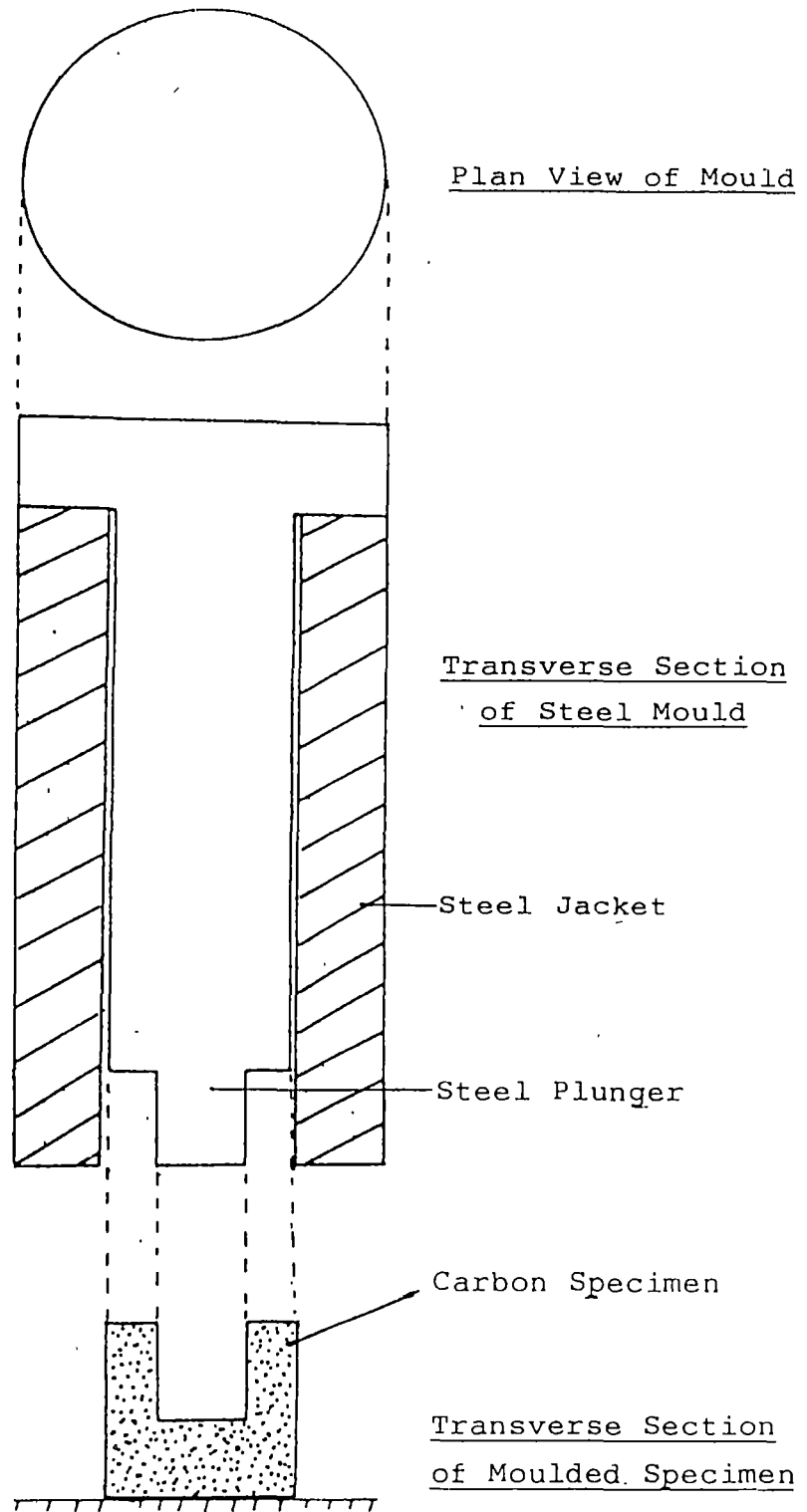


Figure 19: Schematic Representation of
Mould and Specimen

Table 3: Typical Formulation of Monolithic Carbon Mix⁽²²⁾
(ex Bell Bay Green Carbon Plant)

COMPONENT	WT. %
Anthracite Size Fractions (+4 to -200 mesh)	
Coarse	25
Intermediate	20
Fines	55
Pitch	7
Pitch Oil	3

Table 4
Chemical Analyses of Carbon Specimens

IDENTITY	Ash (wt.%)	Na (wt.%)	Fe (wt.%)	S (wt.%)	Ca (wt.%)	Si (wt.%)	V (wt.%)	Cd (wt.%)
Showa-Savoie preformed carbon	4.44	0.08	0.64	0.36	<0.05	1.75	n.d.*	n.d.
Nippon preformed carbon	5.95	0.12	0.70	0.38	<0.10	n.d.	n.d.	n.d.
Graphite AGSX Grade ⁽²³⁾	0.13	n.d.	0.047	0.12	n.d.	n.d.	0.006	0.012
Monolithic carbon-mix	9.42	0.20	0.49	0.72	<0.10	1.50	n.d.	n.d.

* not determined

3.2.4 Thermogravimetric Analysis

When studying the reaction kinetics of a system it is necessary to use a technique for continuous monitoring of the reaction process throughout the reaction period. In this way, changes in the rate of reaction with time may be followed closely.

In this instance, thermogravimetric analysis was used for measuring the rate of sodium cyanide formation. The system used to accomplish this was the Cahn RH Electrobalance with a controlled automatic recording facility and 20 gram maximum recording range (Figure 18). The fundamental principles of its operation and the method utilised for calibration have been discussed in the Manual⁽²⁴⁾.

Essentially, a weighed amount of -200 mesh predried carbon-mix was packed with a calculated amount (based on carbon weight) of metallic sodium followed by chemical interaction with gaseous nitrogen in the reaction cell at 550°C. The weight change due to the reaction was continuously plotted by an X-Y chart recorder over 2 hours. Data derived from this process were corrected for blank determinations and used in calculations. Refer also Appendix 4, p. 141.

The rate graphs derived from the above technique were subsequently compared with similar graphs attributed to the alternative method of integral analyses. In this method, individual samples were reacted over selected time periods and subsequently removed for analysis for cyanide according to the method described in Section 3.2.6.

While thermogravimetric analysis enables a close study of the overall reaction, integral analysis provides a means for verifying the rate data obtained. Thus, a combination of both techniques is a useful tool for monitoring the reaction process.

3.2.5 Cyanide Synthesis in Experimental Specimens

The baked carbon specimen was dried at 110°C in an air-oven for 20 hours to remove adsorbed surface moisture. An amount of freshly cut analytical grade metallic sodium equivalent to 10 wt.% of the specimen weight was inserted in the hole in the centre of the specimen to form a sodium plug. The prepared sample was placed in an inverted position in the crucible, so that the exposed surface of the plug was sitting on the crucible base. Positioning of the sample in this manner minimises sodium loss and facilitates sodium-impregnation of the carbon mass during heating.

This arrangement was immediately placed in the reaction chamber containing an argon atmosphere. A chromel-alumel thermocouple for monitoring the sample temperature was positioned so that its tip was approximately 5 mm from the base of the crucible. When the thermal environment was stabilised at the selected reaction temperature, the argon atmosphere was replaced with nitrogen and the reaction conditions maintained for 3 hours.

At the end of this period, the nitrogen gas was replaced with argon gas. The reaction cell was disconnected from the electrobalance gas chamber, and the sample was removed from the cell and allowed to cool over silica gel in a desiccator under vacuum.

The sample was crushed to -200 mesh in a ring-mill and stored under a protective argon atmosphere in a sealed plastic container in a desiccator while awaiting chemical analysis.

3.2.6 Sample Analysis

Following removal of the prepared sample from its container, a weighed portion was taken for hydrochloric acid distillation. The distillate was collected in 2.5N NaOH solution and the cyanide content was determined with a cyanide ion-selective electrode.

3.3 Results and Discussion

3.3.1 Rate of Sodium Cyanide Formation

The reaction rate was studied at 5 wt.% and 10 wt.% metallic sodium relative to the weight of the carbon specimen. In order that meaningful measurements could be made, a reaction temperature of 550°C was selected to enable a rapid uptake of sodium by carbon. This phase of the reaction proceeded under argon gas cover until the temperature was stabilised at $550 \pm 1^\circ\text{C}$, when gaseous nitrogen displaced the argon in the reaction cell to initiate cyanide formation.

Rate data derived from integral and thermogravimetric analysis are compiled in Tables 5-8, while rate graphs of $[\text{Na}]_t$ versus time are depicted in Figures 20 and 21. Similarly, graphs reflecting the reaction-order of the process are illustrated in Figures 22-25.

Table 5: Rate Data Derived from Integral Analyses with
5 wt.% Initial Sodium Charge

Time t (min)	Na charge based on final reacted sample (wt.%)	NaCN as Na (wt.%)	[Na] _t (wt.%)	$\frac{1}{[\text{Na}]_t}$ (wt.%)
15	4.74	0.030	4.71	0.212
30	4.73	0.060	4.67	0.214
45	4.72	0.063	4.66	0.215
60	4.75	0.19	4.56	0.219
90	4.76	0.25	4.51	0.222
120	4.73	0.28	4.45	0.225

Table 6: Rate Data Derived from Integral Analyses with
10 wt.% Initial Sodium Charge

Time t (min)	Na charge based on final reacted sample (wt.%)	NaCN as Na (wt.%)	[Na] _t (wt.%)	$\frac{1}{[\text{Na}]_t}$ (wt.%)
15	9.11	0.067	9.04	0.1106
30	9.06	0.20	8.86	0.1128
45	9.03	0.19	8.84	0.1131
60	8.96	0.30	8.66	0.1155
90	9.00	0.45	8.55	0.1170
120	8.95	0.50	8.45	0.1183

Table 7: Rate Data Derived from Thermogravimetric
Analysis with 5 wt.% Initial Sodium Charge

TIME t (min.)	$[\text{Na}]_t$ (wt.%)	$\frac{1}{[\text{Na}]_t}$ (wt.%)
6	4.74	0.211
12	4.72	0.212
18	4.67	0.214
24	4.65	0.215
30	4.59	0.218
36	4.55	0.220
42	4.50	0.222
48	4.48	0.223
54	4.46	0.224
60	4.44	0.225
66	4.41	0.227
72	4.39	0.228
78	4.37	0.229
84	4.35	0.230
90	4.35	0.230
96	4.33	0.231
102	4.31	0.232
108	4.29	0.233
114	4.29	0.233
120	4.29	0.233

Table 8: Rate Data Derived from Thermogravimetric
Analysis with 10 wt.% Initial Sodium Charge

TIME t (min.)	$[\text{Na}]_t$ (wt.%)	$\frac{1}{[\text{Na}]_t}$ (wt.%)
6	9.01	0.111
12	8.77	0.114
18	8.62	0.116
24	8.47	0.118
30	8.40	0.119
36	8.33	0.120
42	8.26	0.121
48	8.20	0.122
54	8.13	0.123
60	8.13	0.123
66	8.06	0.124
72	8.06	0.124
78	8.00	0.125
84	8.00	0.125
90	7.94	0.126
96	7.94	0.126
102	7.94	0.126
108	7.87	0.127
114	7.87	0.127

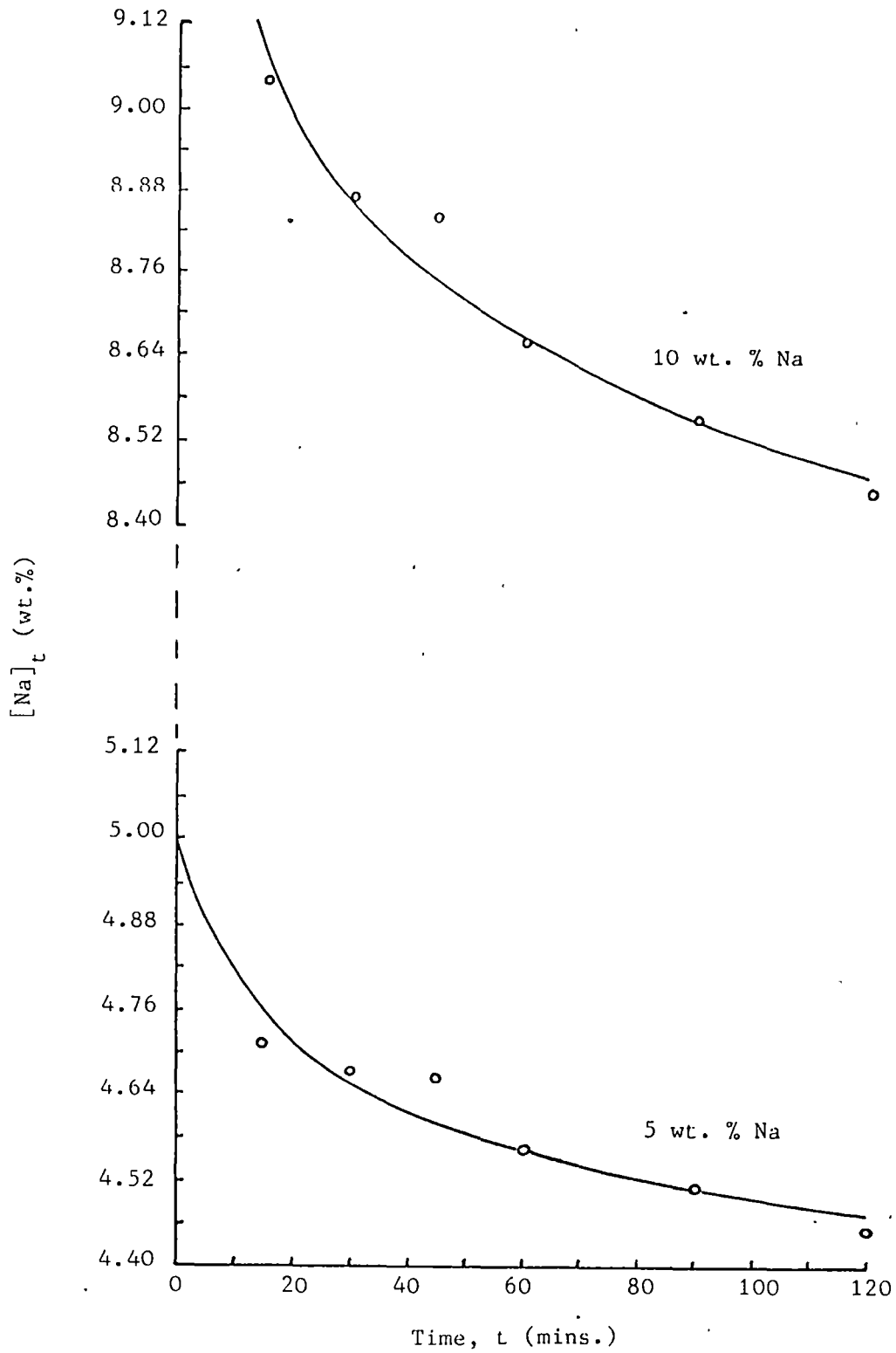


Figure 20 Rate Plot for Reactant Sodium at 550°C
Derived from Integral Analysis

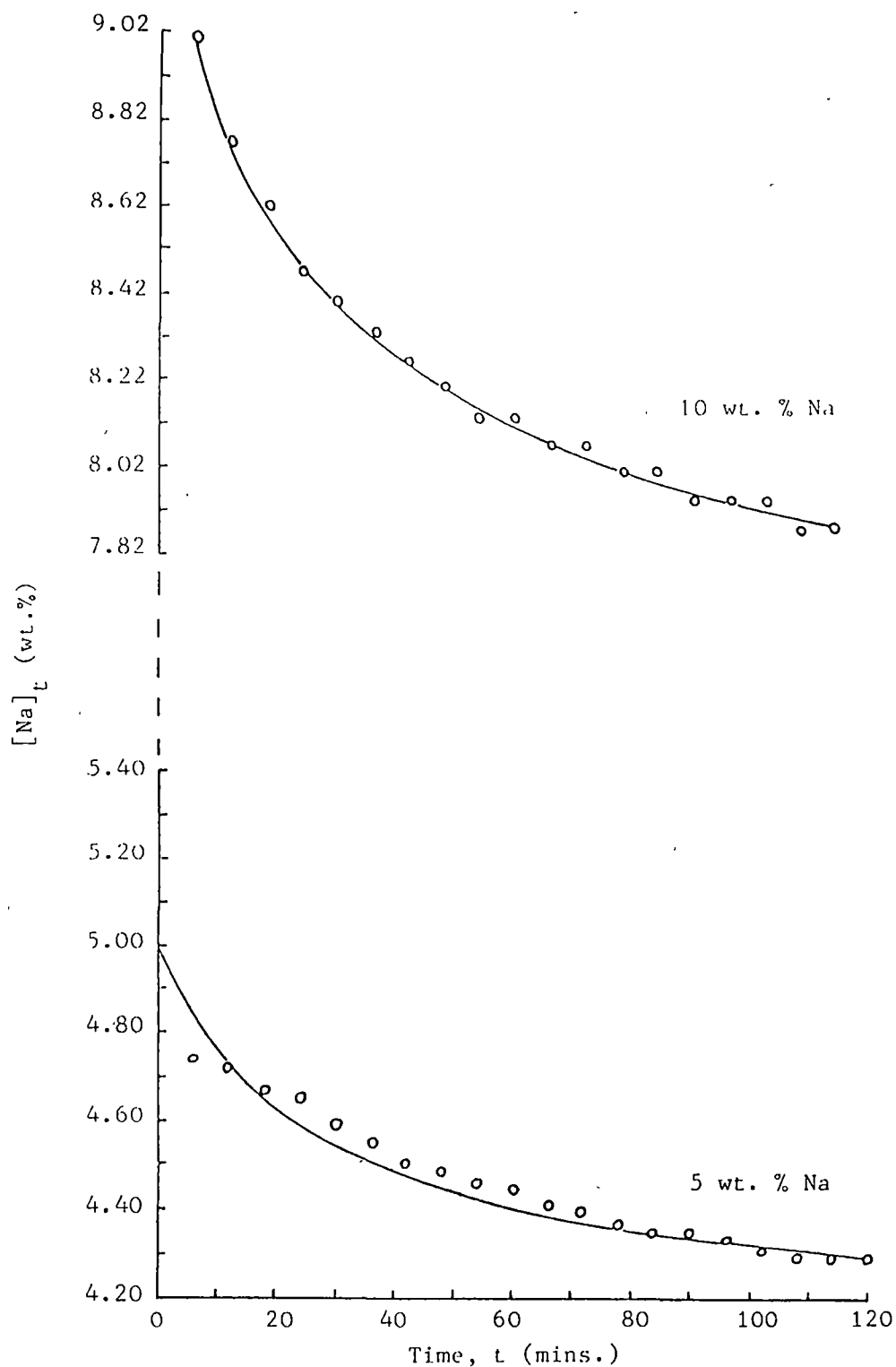


Figure 21 Rate Plot for Reactant Sodium at 550°C
Derived from Thermogravimetric Analysis

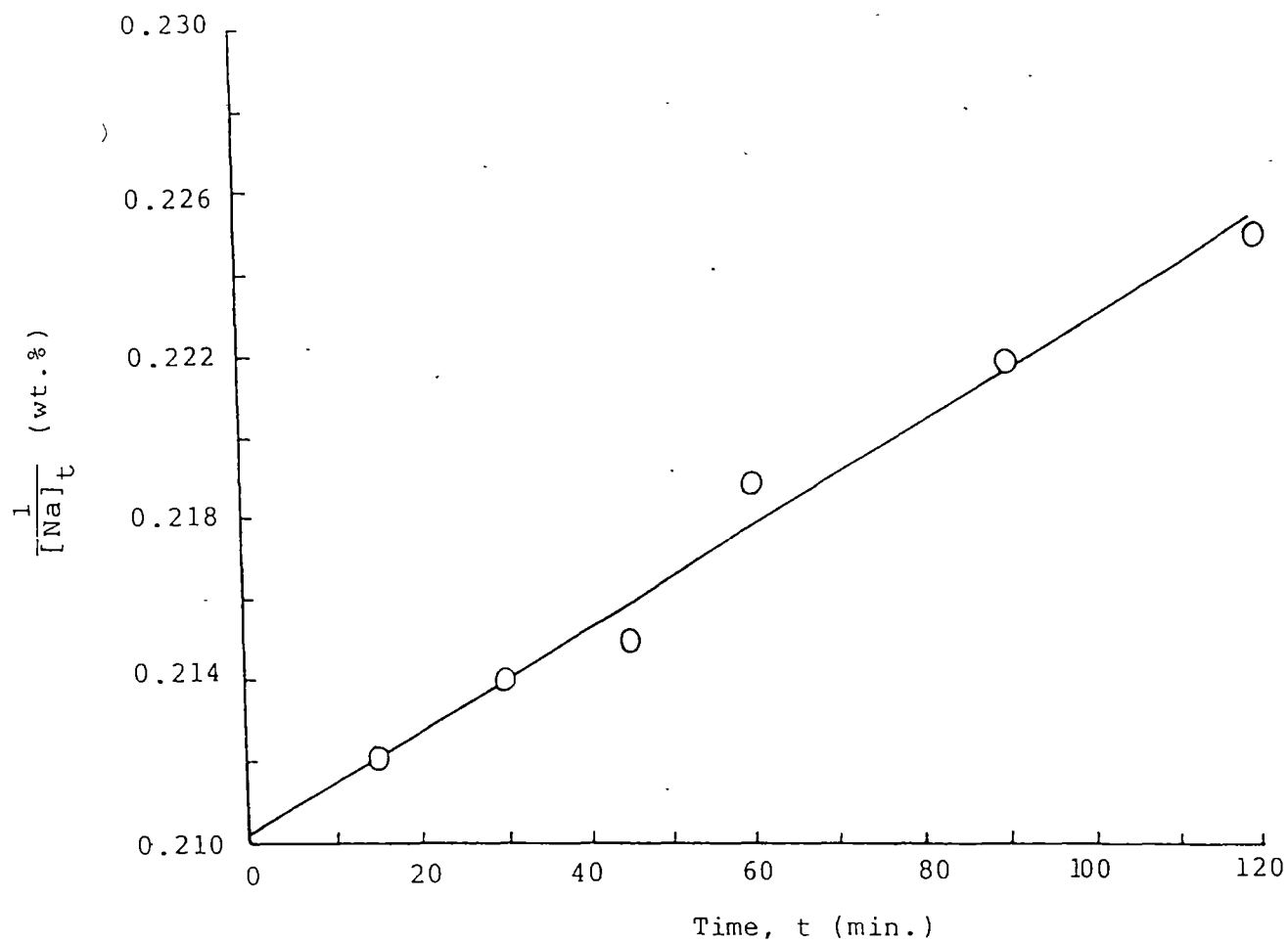


Figure 22: Second-order Reaction Plot for 5 wt.% Sodium at 550°C derived from Integral Analyses

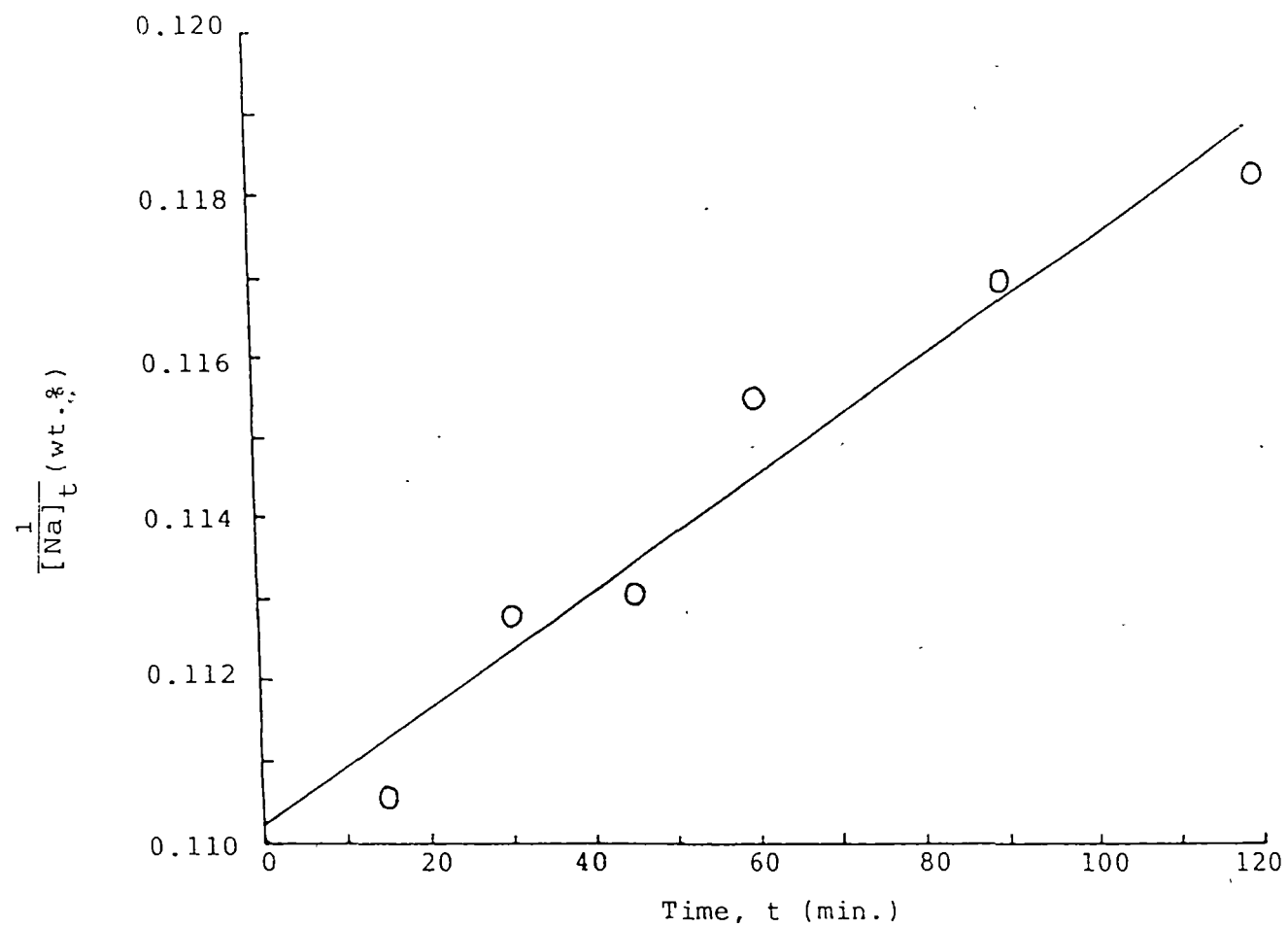


Figure 23: Second-order Reaction Plot for
10 wt.% Sodium at 550°C derived
from Integral Analyses

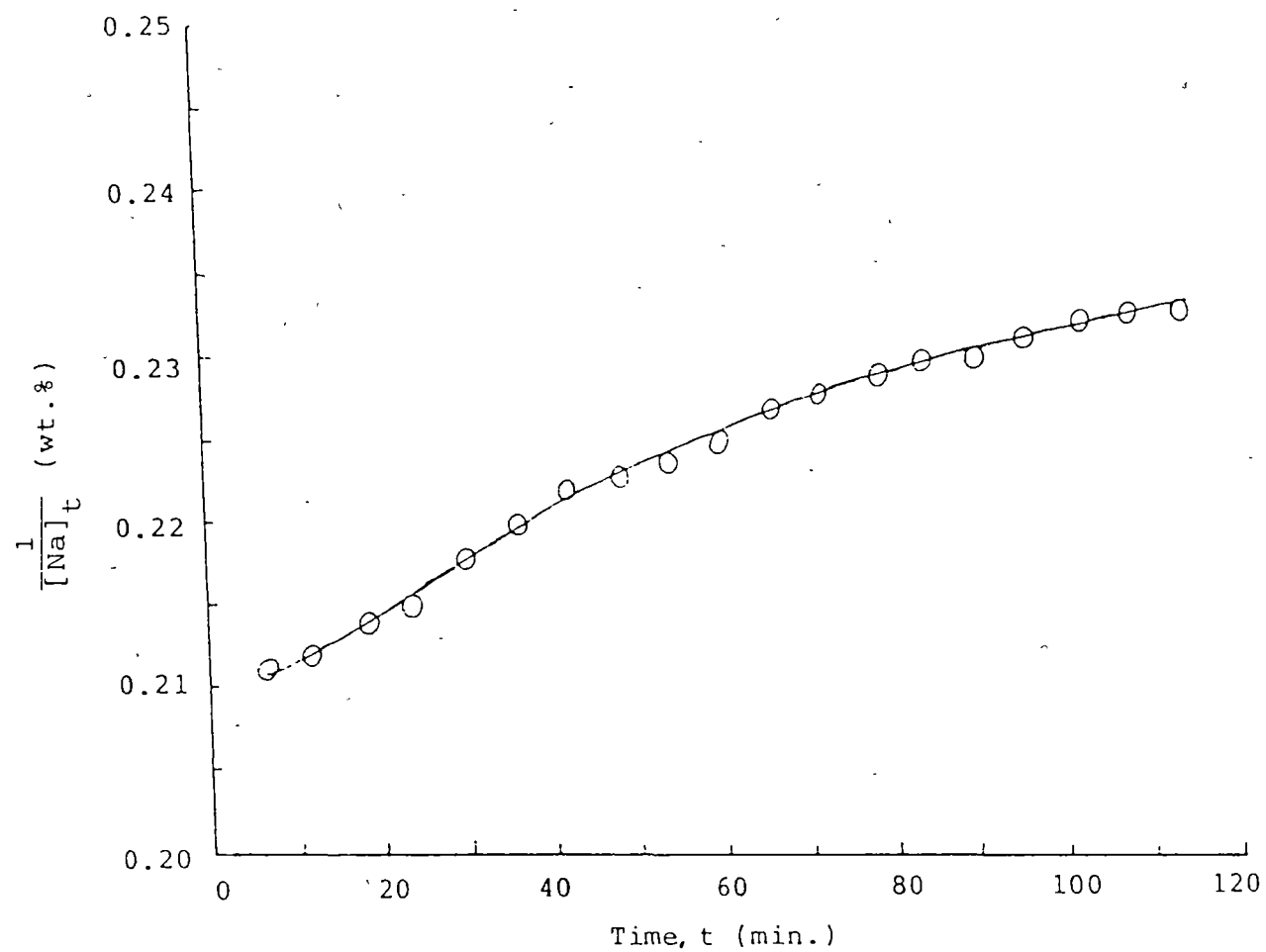


Figure 24 : Second-order Reaction Plot for
5 wt.% Sodium at 550°C derived
from Thermogravimetric Analysis

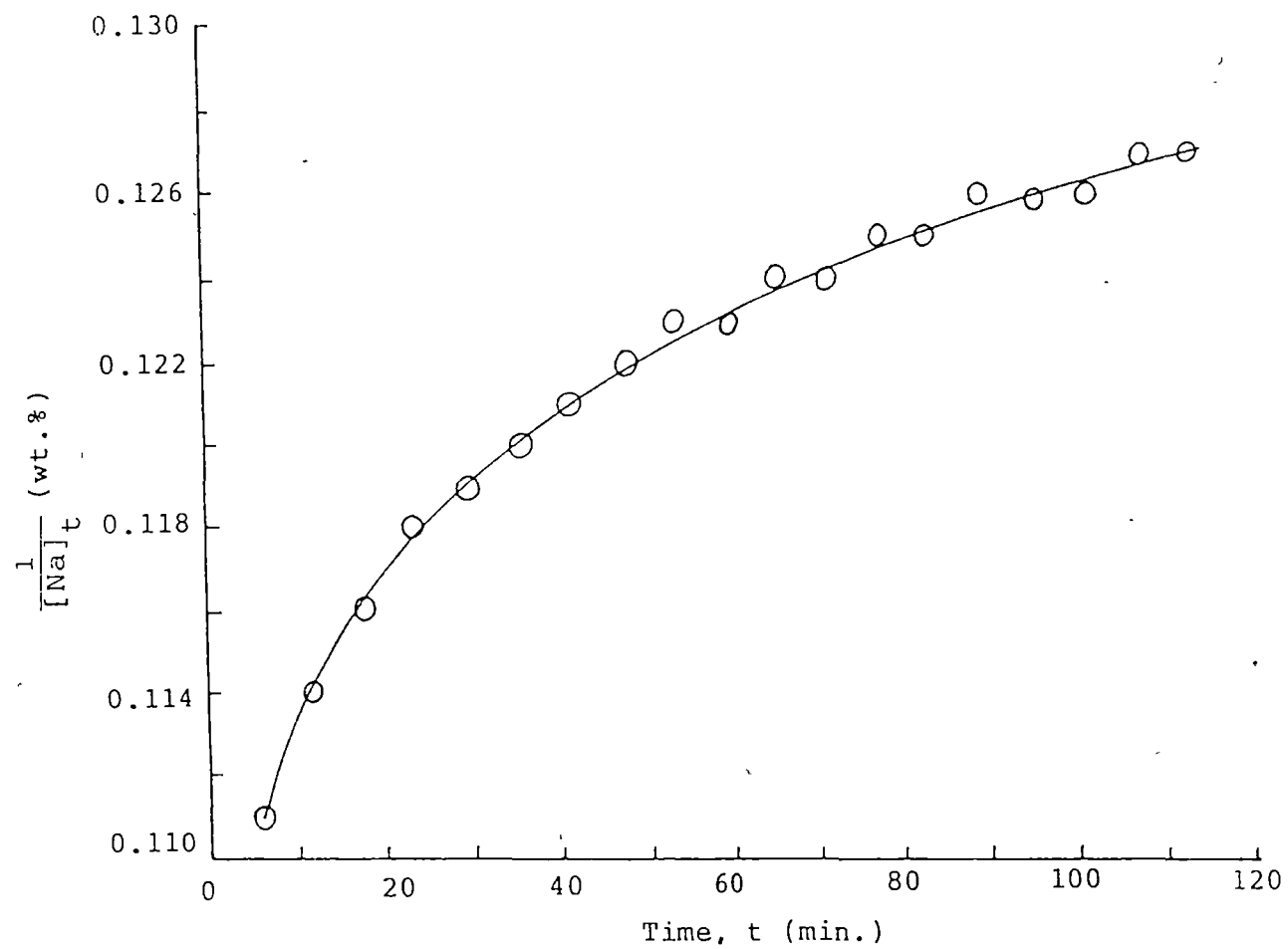


Figure 25 : Second-order Reaction Plot for
10 wt.% Sodium at 550°C derived
from Thermogravimetric Analysis

Further to this, an attempt has been made to explain the rate graphs derived. Because there may be numerous factors contributing to the complexities of the reaction, it would be realistic to discuss the progress of the reaction on the basis of some of the chemical and physical processes that may effect the reaction rate. Consequently, rate graphs of reactant sodium concentration are plotted against reaction time to enable a discussion of significant processes that operate at different stages of cyanide formation.

Generally, in studies related to gas-solid reactions, four basic phenomena such as external mass transfer, pore diffusion, adsorption/desorption and chemical reaction are involved⁽²⁵⁾. Therefore, a common feature of the system under study is that the overall reaction process may involve several intermediate steps:

- (i) Gaseous diffusion (mass transfer) of reactant from the bulk of the gas phase to the internal surface of the reacting solid particle.
- (ii) Diffusion of gaseous reactant through the pores of a partially reacted solid or through the pores of a solid reaction product.
- (iii) Adsorption of the gaseous reactant on and desorption of reaction product from the solid surfaces.
- (iv) The actual chemical reaction between the adsorbed gas and the solid.

The general manner in which the sodium concentration varies with reaction time is shown by the rate curves in Figures 20 and 21. Both approaches show that

there is a consistent trend of increasing reactivity with increase in sodium content. Furthermore, the results indicate that the overall rate of change in sodium concentration is faster at the higher sodium content by a factor of approximately two.

Subsequently, a discussion of some of the chemical and physical processes affecting the progress of the reaction is given below.

Formation of Sodium Carbide

Initially, at the reaction temperature of 550°C, the uptake of sodium by carbon is sufficiently rapid to enable both permeation and diffusion of the carbon matrix by metallic sodium. This process soon leads to the enlargement of the carbon pore structure and resultant swelling of the matrix. Moreover, owing to the porous nature of the carbon used, diffusion and chemical reaction are likely to occur simultaneously throughout the carbon matrix.

Therefore, the possible chemical reaction between sodium and carbon or nitrogen leading to the formation of intermediate compounds has to be considered. In this respect, two possible compounds immediately come to mind; reaction between sodium and nitrogen to form sodium nitride (Na_3N), and the reaction between sodium and carbon to form sodium carbide (Na_2C_2).

A survey of literature reveals that formation of nitride is unlikely under the reaction conditions of the system used in this study^(19,26,27). For example, direct reaction between sodium and nitrogen to form nitride occurs under more rigorous conditions such as an electrical discharge^(26,27). Various attempts to generate sodium nitride in reactions at

800 - 1000°C using nitrogen and metallic sodium have also been unsuccessful⁽¹⁹⁾, confirming the unlikelihood of nitride formation in the system.

However, efforts to form sodium carbide via the direct reaction between carbon and sodium have not been disappointing. Earlier experiments, using an evacuated iron tube maintained at 800 - 900°C, have been found to produce a condensate containing sodium carbide at the cooler end of the tube, indicating the formation of gaseous carbide at the above temperatures⁽¹⁹⁾. In addition, calculated thermodynamic data rule out the formation of sodium carbide solid from a direct reaction between the reactants over the temperature range of 127 - 827°C⁽²⁸⁾. In fact, a direct reaction process is more likely to form a solution of sodium carbide in liquid sodium at the above temperature range, on thermodynamic grounds⁽²⁸⁾.

Further to this, observations derived from this work involving direct reaction between plant manufactured carbon specimens and metallic sodium under an argon atmosphere at 550 - 600°C, confirm the evolution of gaseous acetylene when the sample is moistened with water. As hydrolysis of sodium carbide yields acetylene at ambient temperature⁽²⁹⁾, it is evident that sodium carbide has been formed under the reaction conditions used.

Accordingly, at the reaction temperature of 550°C, direct chemical reaction between sodium and carbon leads to the formation of a solution of sodium carbide in liquid sodium via the pathway⁽²⁸⁾:



Once sodium carbide has been generated in the reaction, it is essential to establish whether it is the precursor for sodium cyanide synthesis in the presence of gaseous nitrogen. In fact, a series of experiments conducted by Guernsey and Sherman⁽¹⁹⁾ soon reveal that nitrification of sodium carbide is feasible in the range of temperature 500 - 1000°C.

Formation of Sodium Cyanide

Basically, several intermediate steps leading to the formation of sodium cyanide may operate when nitrogen gas is introduced into the system. Initially, there is gas phase mass transfer of reactant nitrogen from the bulk of the gas stream to the external surface of the carbon specimen.

Subsequently, nitrogen diffuses through the pores of the carbon matrix comprising a mixture of unreacted metallic sodium and a solution of sodium carbide in liquid sodium. This is followed by physical adsorption of nitrogen on the surface of the carbon matrix, whilst chemical reaction between nitrogen and sodium carbide results in the formation of sodium cyanide. The conversion of carbide to cyanide is rapid at this stage, as reflected by the steep gradient in the initial segments of the rate plots.

As more sodium cyanide forms, densification of the carbon matrix occurs and this results in the formation of finer pores which may inhibit the progress of reaction. A layer of sodium cyanide is formed which may also cover the remaining reactive sites, and lead to lower effective diffusion of nitrogen throughout the carbon matrix. This behaviour may be represented by the gradual decrease in the gradient of the curve after the first 30 minutes of the reaction process.

Similarly, desorption of sodium cyanide from the carbon surface to the bulk of the gas stream may also take place. However, the reaction conditions used do not favour the generation of gaseous sodium cyanide. Therefore, loss of product cyanide from the system would be negligible.

Of note, the closeness of the reaction temperature to the melting point of sodium cyanide ($\Delta t = 130^{\circ}\text{C}$) may also contribute to the complexity of the reaction. However, whether the temperature difference may initiate a process of transition from a solid to liquid state and significantly affect the reaction progress is uncertain.

In general, experimental data gathered at this stage are not very clear. The rate data obtained, from both approaches used, appear to fit a second-order reaction relative to reactant sodium after the initial burst of reaction, as illustrated in Figures 22-25. However, interpretation of the overall results at this point is not very clear as the system studied is complex and affected by numerous factors. Consequently, future studies of the effect of nitrogen partial pressure and different nitrogen concentration on the rate of sodium cyanide formation, may clarify the general behaviour of the reaction.

The above findings suggest that when the carbon sidewalls of industrial cells are impregnated with large amounts of metallic sodium in the early stages of pot operation, a parallel production of cyanide at an accelerating rate occurs in the potlining. As the pot ages and the carbon liner is impregnated with increasing amounts of metallic sodium, the rate of cyanide generation is gradually reduced. Nevertheless, formation of sodium cyanide would continue

until all reactant sodium is consumed or diffusion of air via the collector bar seals to the chemically reactive sites is restricted.

3.3.2 Effect of Temperature

The effects of temperature, ranging from 500-600°C, on cyanide generation in the three carbon types, outlined in Section 3.2.3, were investigated. The cyanide concentration determined was calculated as the amount of free cyanide based on the weight of the reacted sample. Results of the analyses are listed in Tables 9(i) - 9(iii).

Tables 9(i) and 9(ii) show that increasing the temperature from 500 to 600°C result in a significant increase in the amount of cyanide formed in the fixed time, while the data in Table 9(iii) show a smaller increase in cyanide content. Therefore, irrespective of the type of carbonaceous material, there is a consistent trend of greater cyanide generation with increase in temperature.

In the industrial operating cells, the sidewall carbon temperatures can vary from 450-700°C (Figure 26), while recent plant autopsy examination of failed cathodes confirm that massive amounts of sodium (Figure 7) and cyanide are predominantly located in these regions of the pot. On the basis of these data, it is now evident that reactive sites for the production of cyanide are continuously generated in the thermal environment of the sidewalls during pot operation.

Similarly, cyanide species originating from higher temperature zones are also likely to condense in the sidewall region. Earlier experiments^(18,19) have shown that formation of gaseous NaCN can occur at

temperatures above 850°C. Thus, it seems that cathode regions in this temperature range may also serve as potential chemically reactive sites for cyanide generation.

Table 9(i): Cyanide Synthesis - Plant Derived
Carbon-Mix

RUN NO.	TEMPERATURE (°C)	SODIUM CHARGE BASED ON CARBON wt (wt.%)	FREE CYANIDE CONTENT BASED ON SAMPLE wt.	
			(wt.% CN ⁻)	(Av.wt.% CN ⁻)
1	500	10.0	0.23	0.17
2	500	10.0	0.10	
3	550	9.99	0.74	0.82
4	550	10.0	0.89	
5	600	10.0	1.3	1.9
6	600	9.97	2.5	

Table 9(ii): Cyanide Synthesis - Commercial Prebaked
Block Cathode

SPECIMEN IDENTITY	RUN NO.	TEMPERATURE (°C)	SODIUM CHARGE BASED ON CARBON wt (wt.%)	FREE CYANIDE CONTENT BASED ON SAMPLE wt (wt.% CN ⁻)
Showa Savoie	1	500	10.0	0.088
	2	550	9.99	0.18
	3	600	10.0	1.6
Nippon	1	500	10.0	<0.01
	2	550	9.99	0.053
	3	600	10.0	1.4

Table 9(iii): Cyanide Synthesis - Graphite AGSX

RUN NO.	TEMPERATURE	SODIUM CHARGE BASED ON CARBON wt	FREE CYANIDE CONTENT BASED ON SAMPLE wt
	(°C)	(wt.%)	(wt.% CN^-)
1	500	9.99	0.74×10^{-3}
2	550	10.0	1.3×10^{-3}
3	600	10.0	2.9×10^{-3}

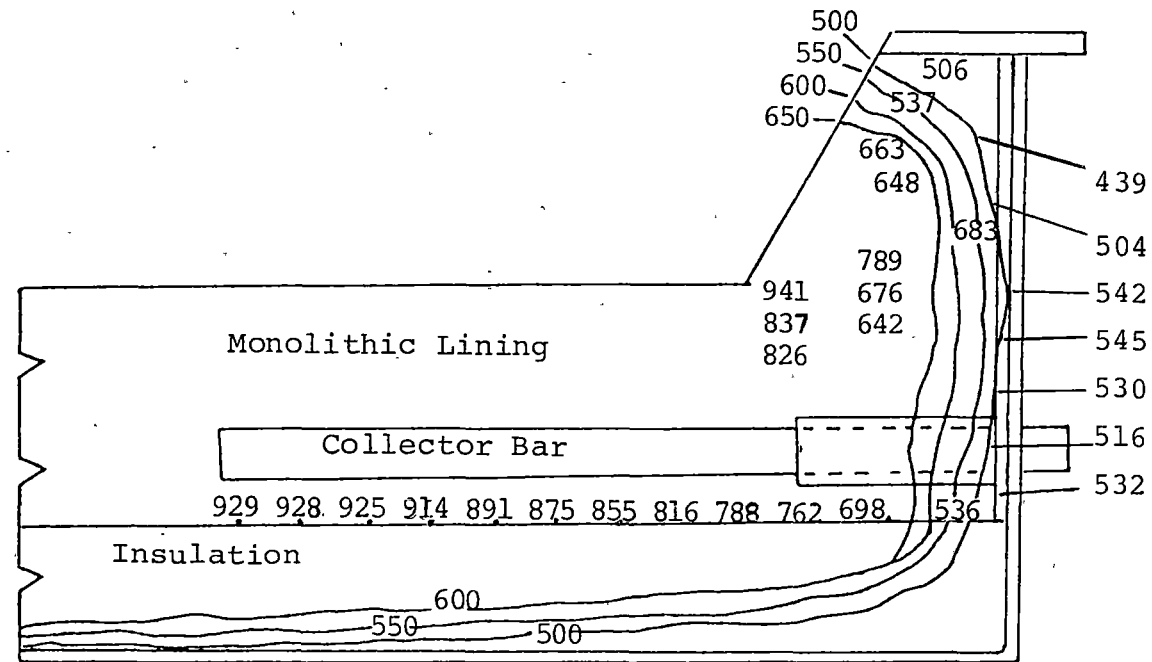


Figure 26: Typical Isotherms in Transverse Centre
Half-Section of an Aluminium Reduction Cell⁽³⁰⁾

3.3.3 Effect of Graphite Content

Evaluation of the cyanide distribution profiles in the potlinings suggests that preformed cathode carbon is less prone to cyanide formation compared to monolithic sidewall carbon. Furthermore, XRD scans⁽¹⁾ of unused potlining samples for graphite content reveal that commercial preformed cathode carbon has a significant graphitic nature, while monolithic carbon is non-graphitic (Table 10). Therefore, to ascertain whether the graphitic nature of carbon has any significant influence on cyanide formation, laboratory trials using different carbon types were conducted. The data obtained are tabulated in Table 11 and plotted in Figures 27(i) and 27(ii).

The investigations show that highly graphitised carbon is least susceptible to cyanide formation. For instance, commercial preformed cathode carbon and high purity graphite offer greater resistance to cyanide formation within their structures, while monolithic carbon-mix is the most vulnerable. As graphitisation increases, the carbon tends to a more ordered structure with subsequent decrease in permeability to gas infusion. In fact, porosimetry measurements by the mercury intrusion technique confirm that the specific permeability decreases with increase in graphitic composition of the carbon specimen. Thus, as ingress of reactant nitrogen is partially inhibited by the ordered structure of the carbon, formation of cyanide will also be expected to decrease. Data in Table 11 reinforce the evaluation given above.

In general, the above findings are consistent with the cyanide profiles established in Section 2.5. Preformed cathode carbon has consistently been found

to contain low levels of cyanide compared to the monolithic carbon sidewall. Specimens derived from pot autopsies have similarly reflected the same trend in carbon susceptibility to cyanide generation. Plant measurements collected in Table 12 show that samples containing high levels of graphitised carbon tend to be less prone to cyanide formation. Although there is some uncertainty over the chronological order of graphitisation of the potlining during pot operation, the quantity of cyanide generated in highly graphitised carbon is significantly reduced.

Therefore, the introduction of semi-graphitised carbon as sidewall lining for the pot should significantly reduce the extent of cyanide formation, resultant environmental problems, and in the longer term the consequent detoxification processing of cyanide-contaminated effluents.

Table 10: Graphite Content in Prebaked Block Cathode and Monolithic Carbon⁽¹⁾

CARBON TYPE	GRAPHITE (wt.%)
UCAR PREBAKED BLOCK	30
SHOWA - SAVOIE PREBAKED BLOCK	15
SAVOIE (SERS) PREBAKED BLOCK	20
GREAT LAKES PREBAKED BLOCK	38
CARBONE - SAVOIE PREBAKED BLOCK	25
MONOLITHIC CARBON	0

Table 11: Effect of Graphite Content on Cyanide Formation

CARBON TYPES	GRAPHITE CONTENT (wt.%)	SPECIFIC PERMEABILITY (D'Arcy)	REACTION TEMPERATURE (°C)	FREE CYANIDE CONTENT (wt.% CN ⁻)
Showa Savoie (preformed cathode carbon)	14	5.47	500	0.088
			550	0.18
			600	1.6
Nippon (preformed cathode carbon)	19	3.00	500	<0.01
			550	0.053
			600	1.4
High purity graphite (extruded rod)	100	1.04	500	0.74×10^{-3}
			550	1.3×10^{-3}
			600	2.9×10^{-3}
Monolithic Carbon (plant manufactured)	0	6.41	500	0.17
			550	0.82
			600	1.9

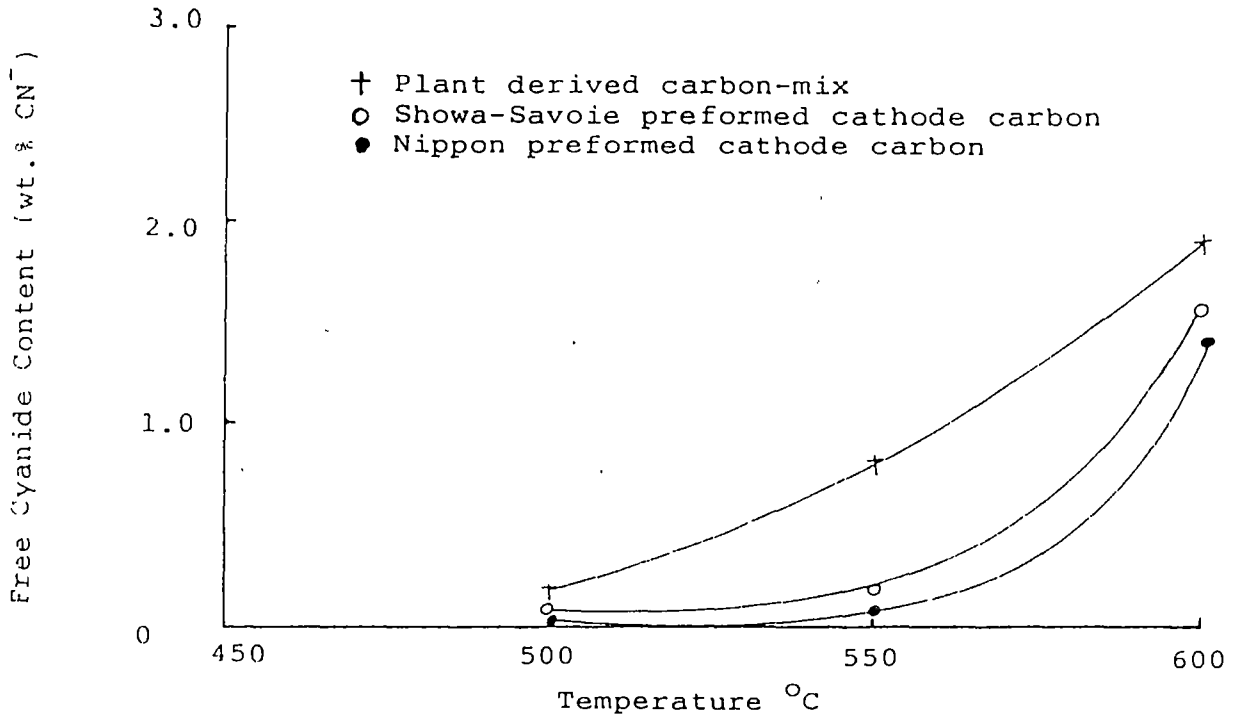


Figure 27 (i): Cyanide Formation in Different Carbon Types

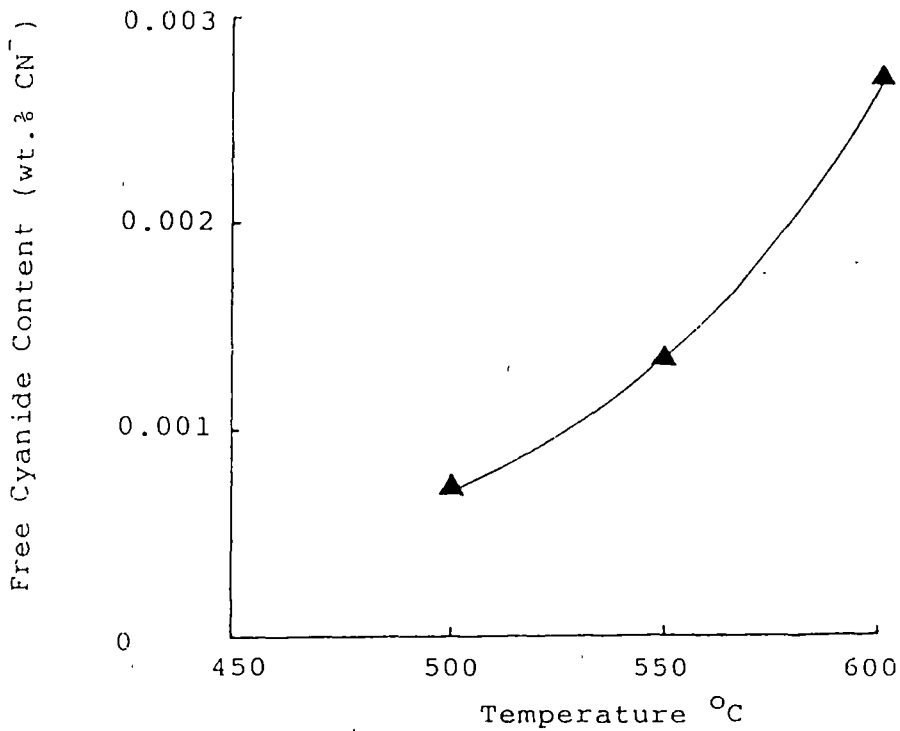


Figure 27 (ii): Cyanide Formation in Graphite

Table 12: Effect of Graphite Content of Spent Potlinings on
Total Cyanide concentration

SAMPLE IDENTITY	GRAPHITISED CARBON ESTIMATED wt.% (XRD)	TOTAL CYANIDE (wt.% CN^-)
<u>Pot 2/65. Age: 823 Days</u> <u>Sers Block Cathode</u>		
Block 1; from sidewall - block inteface adjacent to collector bar	30 ± 0.5	7.1
Block 2; from centre of block cathode	50 ± 0.5	<0.1
Block 2; from sidewall region above collector bar	10 ± 0.5	9.4
Block 3; from block - consolidated alumina interface	55 ± 0.5	0.3
Block 4; from sidewall region above collector bar	20 ± 0.5	7.9

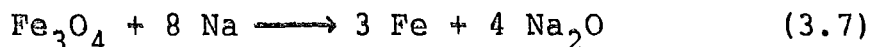
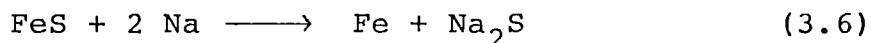
3.3.4 Effect of Iron (as Fe₂O₃) Impurity

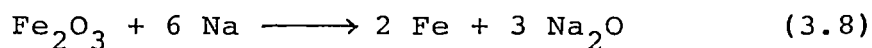
To measure the effect of small amounts of iron impurity on cyanide generation, an attempt was made to determine the amount of cyanide produced at various Fe₂O₃ additions to plant derived carbon-mix. The reaction was carried out over a range of temperatures (500-600°C) using sodium-impregnated carbon specimens previously doped with Fe₂O₃.

The results obtained show that small amounts of iron contamination can accelerate cyanide formation at low temperatures. At 500°C, an increase in iron addition from 0.5 to 1.0 wt.% approximately doubles the degree of sodium conversion to sodium cyanide. However, a similar effect is not observed for iron additions at the higher temperature range. Analysis of the data in Table 13 shows that the amount of cyanide generated is increased by as much as a factor of three as a consequence of the iron addition. The role of iron impurity as a catalyst in cyanide formation is also reflected in Figure 28.

In the industrial situation, a certain amount of iron contamination can be expected to occur during the processing of carbon used in the manufacture of pot-sidewalls and cathode-slot mix. In addition, some of the iron impurities originate in the anthracite, pitch and pitch oil used in the process. The common impurities include ferrous sulphide (FeS) and iron oxides (Fe₂O₃ and Fe₃O₄)⁽¹⁴⁾.

In the thermal environment of the pot, the above chemical impurities may react with metallic sodium to form metallic iron via the interactions⁽¹⁴⁾:





Moreover, metallic Fe can also form from the step-wise reduction of Fe_2O_3 and Fe_3O_4 by carbon at pot operating temperatures.

Although the initial level of iron impurity in the carbon-mix is relatively low (Table 4), the total iron content in the potlining may increase as a result of gradual bath-erosion of the collector bars during pot operation. According to Mitchell⁽⁸⁾ the iron level can increase threefold during the life of the cathode, although no supporting data were provided in his report.

The high levels of metallic iron that can be generated from the above processes in the potlining are expected to significantly accelerate cyanide formation in regions accessible to air ingress. For instance, previous investigations^(18,19) have demonstrated that massive amounts of particulate iron can catalyse cyanide formation at temperatures above 850°C. Therefore, it appears that pot-cathode regions, near the collector bars and in the range of 850-930°C (Figure 26), are also potential reactive sites for cyanide formation. Data obtained from pot-autopsy examinations (Section 2.5) confirm the presence of cyanide in the above described regions, although it seems that mass transfer of reacting nitrogen diffusing into the cathode via the collector bars limits the amount of cyanide formed.

Table 13: Effect of Iron (as Fe_2O_3) Addition on Cyanide Production in Plant Derived Carbon-Mix

Iron Addition based on carbon wt. (wt.% Fe)	Reaction Temperature (°C)	Sodium based on carbon wt. (wt.% Na)	Free Cyanide Content (wt.% CN^-)
0.0	500	10.0	0.17
0.5	500	9.99	0.22
1.0	500	10.0	0.47
0.0	550	10.0	0.82
0.5	550	9.99	1.1
1.0	550	10.0	1.3
0.0	600	9.99	1.9
0.5	600	10.0	2.3
1.0	600	10.0	2.9

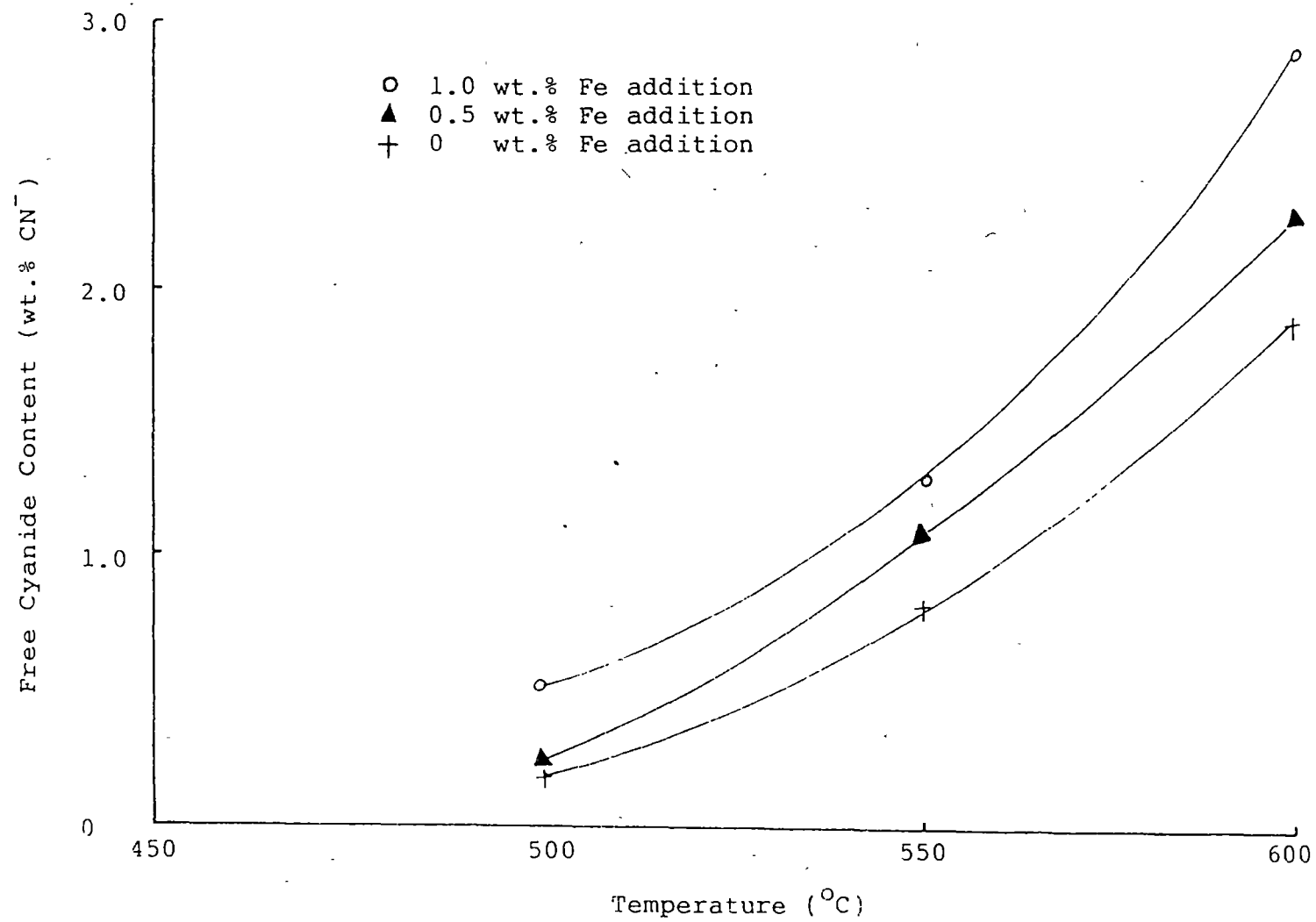


Figure 28 : Effect of Iron Impurity on Cyanide Formation in Carbon-Mix

3.3.5 Predominant Cyanide - Containing Species

It has been suggested in several reports^(8,11,31) that the cyanide species in potlinings exist as two forms - free and complex iron cyanides. However, there has been no conclusive evidence pinpointing the predominant species that exists.

Because solid ferri- and ferro-cyanides are unstable at temperatures above 400°C⁽³²⁾, they would be expected to originate in the cooler zones of the potlining. As the thermal environment in the sidewalls is usually above 500°C and there is considerable amount of sodium intercalated with the carbon, the formation of uncomplexed sodium cyanide is more likely.

If complex iron cyanides are the major species produced, the amount of free cyanide will be significantly lower compared to the total cyanide concentration in the sample. So that a comparison of the total and free cyanide content could be made, specimens extracted from failed potlinings were subjected to chemical analyses.

A solution of acidic cuprous chloride was used to decompose any complex iron cyanide in the determination of the total cyanide content, while only hydrochloric acid was used for extracting free cyanide from the samples. Results of the analyses, tabulated in Table 14, clearly show that the total cyanide content is almost identical to the free cyanide concentration.

Laboratory tests (XRD scans using Rigaku DMAS 2 XRD unit)⁽³³⁾, where the formation of cyanide was carried out under conditions that favoured formation of iron

cyanide (via doping with Fe_2O_3), also indicate the absence of complex iron cyanides. This lends further support for the existence of sodium cyanide as a major cyanide-containing species in the potlinings.

Table 14: Comparison of Total and Free Cyanide
Content in Spent Potlining Specimens

Specimen No./ (Identity) *	Total Cyanide (wt.% CN ⁻)	Free Cyanide (wt.% CN ⁻)
1/ (Pot 4/57)	2.3	2.3
2/ (Pot 4/57)	4.4	4.2
3/ (Pot 4/57)	3.4	3.5
4/ (Pot 3/1)	0.60	0.60

* Specimens extracted from carbon sidewalls.

Chapter 4

4.

Conclusion

Throughout the course of this investigation, efforts were made to apply the findings obtained from both plant measurements and laboratory studies, to the industrial situation. An attempt to relate the implications of the overall results in Chapters 2 and 3 to the complex situation in the plant is carried out in the following discussion.

During normal pot operation the thermal and chemical environment creates a situation favouring the formation of a host of sodium-containing compounds within the carbon lining. From pot autopsy data and laboratory results in Sections 2.5 and 3.3.2 respectively, it becomes evident that transfer of metallic sodium from the bath and ingress of gaseous nitrogen from the atmosphere to chemically reactive regions are two essential factors leading to the generation of sodium cyanide in the potlining. Based on the cyanide distribution profiles illustrated in Figures 8-13 of Chapter 2, it is also clear that direct air ingress into the carbon mass via the collector bar seals provides a continuous supply of reactant nitrogen for cyanide formation.

As thermal isotherms vary in the cathode, chemical precursors for cyanide formation can be generated in higher temperature zones and migrate towards cooler regions in the sidewalls. According to the data in Section 3.3.1, intermediate sodium carbide formed in regions at high temperatures is expected to diffuse towards relatively cooler pot sidewall regions and react directly with nitrogen to form sodium cyanide. Similarly, as sodium cyanide can also exist in the gaseous phase at pot operating temperatures^(18,19),

diffusion to the cooler sidewalls will also contribute to the higher concentrations of cyanide in these locations.

Furthermore, results derived from fundamental rate studies in Section 3.3.1 imply that the formation of sodium cyanide will be rapid during the initial stages of pot operation when the potlining is permeated by metallic sodium. In particular, a new pot commissioned on the process-line can be expected to commence generating sodium cyanide at a fast rate, with the initial "waves" of sodium advancing through the cathode and towards the sidewalls.

Therefore, on the basis of the evaluation above it is clear that metallic sodium is particularly an efficient reactant for cyanide formation. Its continuous accumulation in the carbon lining of the pot soon leads to the creation of a highly reactive chemical "sink" favouring cyanide generation during normal operation.

Another situation commonly experienced is the slow build-up of iron in the potlining as the pot ages. In some instances, the total iron content of the cathode can increase threefold during the pot life as a consequence of chemical erosion of the collector bars by infiltration or bath components⁽⁸⁾. The confirmation of this effect through laboratory studies has been reported in Section 3.3.4. The results clearly show that the presence of metallic iron will significantly accelerate cyanide generation in the thermal environment of the pot. These findings are also in general agreement with results from previous work involving large quantities of particulate iron under different operating conditions^(18,19). Thus, based on the findings above, significant concentrations of cyanide are

expected to form in the sidewall regions around the collector bars and in other sections of the carbon lining contaminated with high levels of iron impurities.

Although complete elimination of cyanide in potlinings may not be possible, the findings in this thesis suggest that measures for reducing the extent of cyanide formation could be adopted as a practical alternative. In this instance, laboratory results in Section 3.3.3 imply that the introduction of carbon with an ordered structure, such as graphite, as potlining material may inhibit the formation of cyanide. Accordingly, from the aspect of future chemical treatment of spent potlinings, high purity graphite or semi-graphitised carbon may be used as potlining if it is compatible with the pot technology or pot design from heat balance considerations.

Subsequent to this research, results from a recent paper⁽³⁴⁾ showed much agreement in regard to the distribution of cyanide in the pots. The authors reported that there was a similar trend of high cyanide concentrations in the sidewalls and moderate to low cyanide levels in the block cathodes. On the other hand, there was a disparity regarding the effect of graphitic carbon on cyanide formation. Laboratory results in the paper indicated that highly graphitised carbon was more susceptible to cyanide formation compared to anthracitic carbon. However, these findings are in contrast to the laboratory results in Section 3.3.3 in this thesis which shows that highly ordered carbon such as graphite is consistently more resistant to cyanide formation.

In the experiments reported in the above paper, metallic sodium was placed in a slot on top of the carbon specimen and the system reacted in a stainless

steel reactor at 800°C. At this temperature, loss of sodium from the top of the specimen may be significant and can lead to reduced sodium penetration of the specimen. Contrasting with this, the technique reported in this thesis involved the insertion of metallic sodium in a cylindrical slot in the centre of the carbon specimen which was subsequently inverted in a reaction crucible. This system facilitated sodium-impregnation of the carbon and minimised sodium loss during reaction at 500-600°C (refer Section 3.2.5).

It would appear that the different techniques used in sodium-impregnation of the carbon may have affected the rate of sodium cyanide formation under varying reaction conditions. However, the underlying factors causing the disparity are still not very clear as data on the porosity, graphite content and purity of the carbon specimens used were not documented in the above publication for evaluation.

Although sodium intercalation can occur in both graphitisable and non-graphitisable carbons, the amount of sodium uptake is strongly affected by the heat treatment temperature (HTT) of the carbon; the degree of sodium insertion is found to decrease significantly in carbon that is originally prepared at 2500°C⁽³⁵⁾. At this temperature, graphitisation of carbon occurs and a highly ordered structure is consequently formed. Accordingly, graphite is expected to be more resistant to sodium intercalation compared to ungraphitised carbon. In fact, earlier documentation of the composition of sodium - carbon reaction products as a function of different grades of carbons based on their HTT, confirms that the amount of sodium insertion diminishes significantly in carbons originally prepared at HTT around 2500°C⁽¹⁾.

Clearly, as carbon becomes more graphitic it tends to be less susceptible to sodium intercalation and the formation of stable sodium-containing compounds within its highly ordered and compact structure. On the basis of the information above, it is evident that carbon possessing a significant graphitic structure such as graphite, tends to be more resistant to sodium cyanide formation compared to ungraphitised carbon. Presently, this reasoning is consistent with both laboratory and autopsy measurements presented in Sections 3.3.3 and 2.5 respectively.

However, the findings reported in the above paper⁽³⁴⁾ suggest that there may be other more complex operating factors controlling the magnitude of cyanide formation in graphitic carbon under different reaction conditions outside the scope of the present investigation. For example, it appears that further research related to the structural transformation of both graphitisable and non-graphitisable carbons during the formation of sodium cyanide, may be needed to elucidate other variables likely to influence cyanide formation in different carbon types. For instance, systems incorporating the addition of lithium fluoride or lithium carbonate as an electrolyte modifier in the baths of industrial cells are also used in some smelters⁽³⁶⁾. Metallic lithium that is chemically generated in the bath can react easily with carbon lining at high temperatures to yield a mixture of intercalation compounds and lithium carbide (Li_2C_2)⁽³⁷⁾. However, the practical implication in the direction of cyanide formation has not been reported.

In general, the model developed in this thesis makes it possible to explain the presence of cyanide and some of the variation in the cyanide distribution

profiles in industrial cells. However, this model is limited to the effect that sodium penetration of potlining contributes in the formation of sodium cyanide during pot operation.

In this research, the consistency in measurements derived from parallel laboratory and plant investigations implies that valid comparisons may be confidently drawn between the results obtained here and industrial operating cells.

The results in this thesis have been published recently (refer Appendix 3).

References

1. Houston, G.J.; Ph.D Thesis, Uni. New South Wales, Australia (1980)
2. Lu, B-F and Shelly, T.R.; J. Metals, 9, 21 (1978)
3. Lu, B-F and Shelly, T.R.; Light Metals, 2, 539 (1978)
4. Bacon, L.E.; Extractive Met. of Aluminium, 2, Aluminium, ed. G. Gerard, Interscience, (1963) p.461
5. Ecological Analysts, Inc.; "Cyanide : An Overview and Analysis of the Literature on Chemistry, Fate, Toxicity and Detection in Surface Waters", Maryland, U.S.A. (1979)
6. Farrier, P.M. and Patterson, N.R.; "Cathode Leaching Experiment", presented at Technical Exchange Committee Meeting, 24-26th March, Bluff, New Zealand (1976)
7. Development Services Section; "Ferrous Sulphate Treatment of Iron and Cyanide in Spent Cathode Leachate", Report No. 3, Comalco Aluminium (Bell Bay) Limited (1982)
8. Mitchell, R.E.; "Cyanide Chemistry in a Recovery Process", presented at the Meeting of the EPAA Pollution Abatement Committee, Dec., Dusseldorf (1978)
9. Holo, H.; "Recovery from Solid Wastes and Dumping", presented at the International Symposium on the Fluoride Problem in the Aluminium Smelting Industry, Trondheim, Norway, 24-26th May (1972)

10. Wacha, E.; German Patent No. 2628192 (1977)
11. Dolbey, D.H. and Harrison, D.A.; "Development of a Method for Detoxification of Spent Cathode Leachate", T.M.S. Paper Selection, A-79-17 (1979) pp.1-12
12. Snow, R.J. and Welch, B.J.; J. Electrochem. Soc., 115 (1968) p.1170
13. Waddington, J.; Extractive Met. of Aluminium, 2, Aluminium, ed. G. Gerard, Interscience (1963) p.435
14. Hess, J.B. and Strahl, E.O.; Research Report (CFT RR 79-6), Kaiser Aluminium and Chemical Corporation, Feb. 2nd (1979)
15. Grjotheim, K. and Welch, B.J.; Aluminium Smelter Technology, Aluminium-Verlag GmbH, Dusseldorf, (1980) p.5
16. Mineralight Lamp (Model UVSL-15) - Multiband UV-254/366 nm, Ultra-Violet Products, Inc. California, U.S.A.
17. Sittig, M.; Sodium, Its Manufacture, Properties and Uses, New York (1956) p.222
18. Bucher, J.E.; J. Ind. and Eng. Chem., 9, (1917) p.233
19. Guernsey, E.W. and Sherman, M.S.; J. Am. Chem. Soc., 47, (1925) p.1932
20. Thompson, M.; Chem. Met. Eng., 26, (1922) p.124
21. Stull, D.R. and Prophet, H., et. al.; Janaf Thermochemical Tables, NSRDS-NBS 37, U.S. Dept. of Commerce Washington D.C. (1971)

22. Cathode Batch Worksheet, Green Carbon, Comalco Aluminium (Bell Bay) Limited (1982)
23. Union Carbide Pty Ltd., Melbourne, Australia (1982)
24. Instruction Manual - Cahn RH Automatic Electrobalance
Cahn Instrument Company, California, U.S.A.
25. Szekely, J., Evans, W.J., Sohn, Y.H.; Gas - Solid Reactions, Academic Press Inc. (Lond.) Ltd. (1976)
p.3
26. Thorpe's Dictionary of Applied Chemistry, fourth edition, 10, Longmans, Green and Co., London (1939)
p.810
27. Comprehensive Inorganic Chemistry, 1, Pergamon Press Ltd., Great Britain (1973) p.439
28. Johnson, K.G., et. al.; J. Chem. Thermodynamics, 5, 1 (1973)
29. Comprehensive Inorganic Chemistry, 1, Pergamon Press Ltd., Great Britain (1973) p.1205
30. Jones, S.S.; "Cathode Carbon - Failure Mechanisms", presented at Kaiser Aluminium and Chemical Corporation Carbon Seminar, Palo Alto, California, U.S.A. (1978)
31. Trachtenberg, J.J. and Murphy, M.A.; Light Metals, 2, (1979) p.861
32. Thorpe's Dictionary of Applied Chemistry, fourth edition, 3, Longmans, Green and Co., London (1939)
p.965

33. X-Ray Diffraction Analyses of Carbon Specimens; Courtesy of Comalco Research Centre, Comalco Ltd, Melbourne, Australia (1982)
34. Peterson, R.W., Blayden, L.C., Martin, E.S.; Light Metals, Proc. Met. Soc. AIME (1985) p.1411
35. Robert, M.C., Oberlin, M. and Mering, J.; Chemistry and Physics of Carbon, 10, editors P.L. Walker and P.A. Thrower, New York (1973) p.141
36. Grjotheim, K. and Welch, B.J.; Aluminium Smelter Technology, Aluminium - Verlag GmbH, Dusseldorf (1980) p.22
37. Guerard, D. and Harold, A.; Proc. Fourth Conf. Ind. Carbon (1974) p.325

APPENDIX 1

Autopsy Examination of Potlinings

Table 1.1: Cyanide Profile - Bell Bay Pot 1/92

Upstream Side - Mid-section of Cathode

POT DESCRIPTION	SPECIMEN		TOTAL CYANIDE (WT.% CN ⁻)
	LOCATION NUMBER	DESCRIPTION	
Monolithic construction Pot Life: 1 920 days Pot cut-out due to phasing out of Line 1	1	From collector bar slot; mainly carbon matrix, hard and difficult to break	3.6
	2	From outer sidewall carbon is brittle; surface covered with thin layer of alumina	4.9
	3	From inner sidewall; carbon is brittle and impregnated with bath	3.6

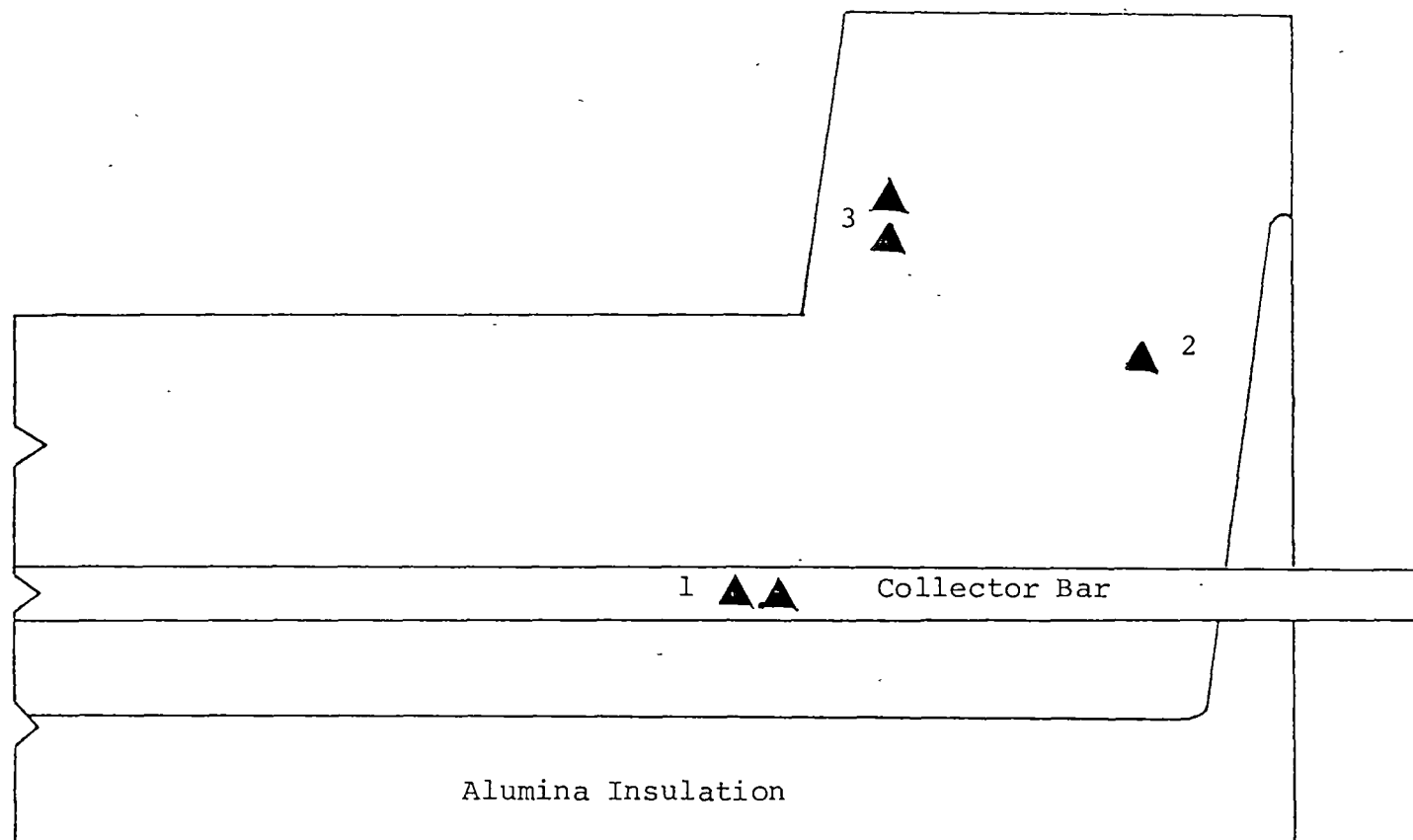


Figure 1.1: Bell Bay Pot 1/92

Transverse Half-Section - Monolithic Cathode (Mid-Section of Pot)

Legend: ▲ Sampling Area

Table 1.2: Cyanide Profile - Bell Bay Pot 1/92

Downstream Side - Mid-section of Cathode

POT DESCRIPTION	SPECIMEN		TOTAL CYANIDE (WT.% CN ⁻)
	LOCATION NUMBER	DESCRIPTION	
As in Table 1.1	4	From isotherm region; brittle and impregnated with bath	2.6
	5	Adjacent to collector bar and base insul- ation; brittle and covered with thin layer of powdery alumina	3.5

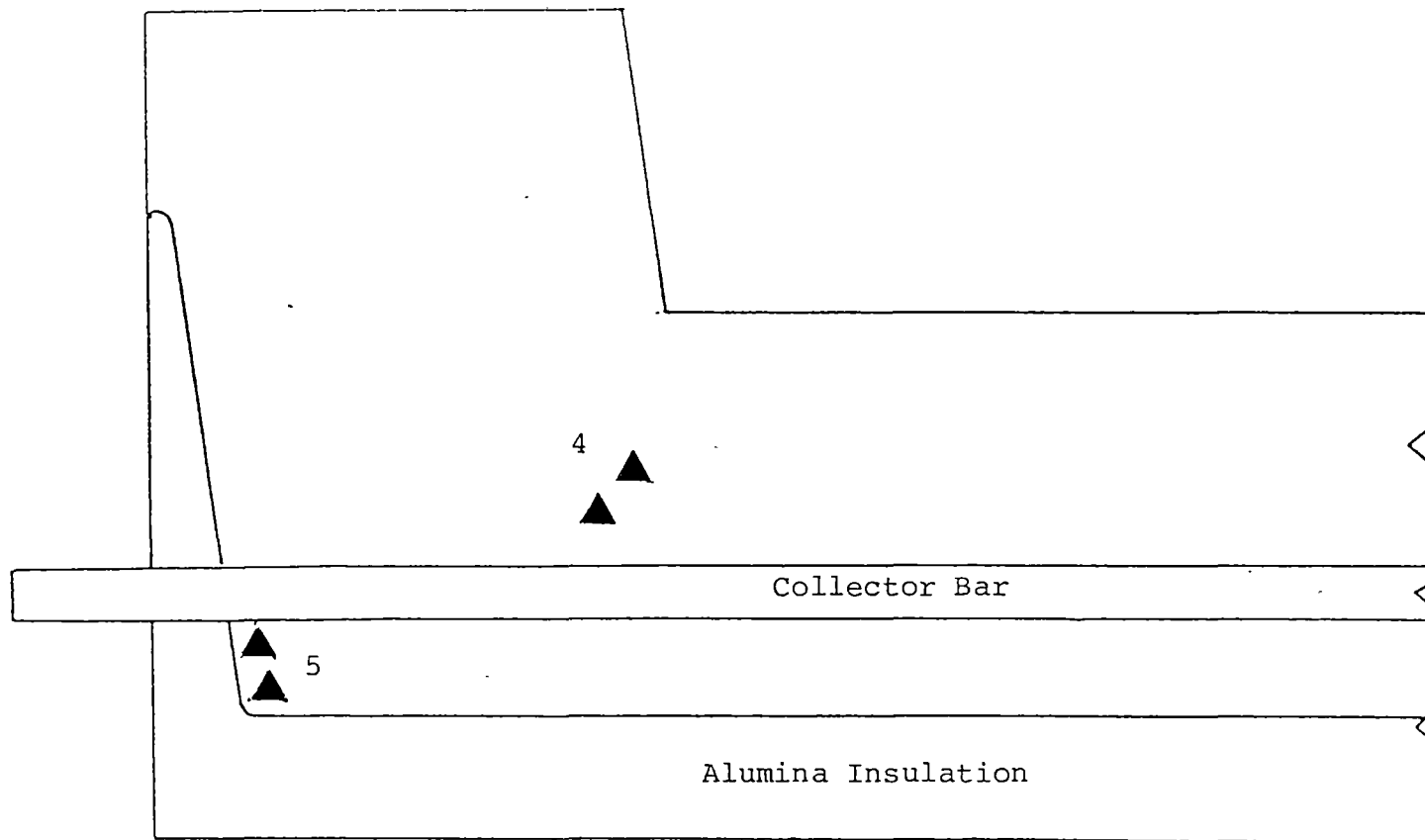


Figure 1.2: Bell Bay Pot 1/92

Transverse Half-Section - Monolithic Cathode (Mid-Section of Pot)

Legend: ▲ Sampling Area

Table 1.3: Cyanide Profile - Bell Bay Pot 2/137

Upstream Side - Block No. 5 from Duct End

POT DESCRIPTION	SPECIMEN		TOTAL CYANIDE (WT.% CN ⁻)
	LOCATION NUMBER	DESCRIPTION	
<p>GLCC Block Cathode</p> <p>Construction: SiC Type III</p> <p>Pot Life: 1 060 days</p> <p>Failure Mode: Corner Tap-out</p>	1	Below collector bar; very hard with mixture of consoli- dated alumina and carbon	2.2
	2	From block-slot interface; near upper surface of collector bar; brittle carbon containing flaky, columnar greyish- white crystals	0.24

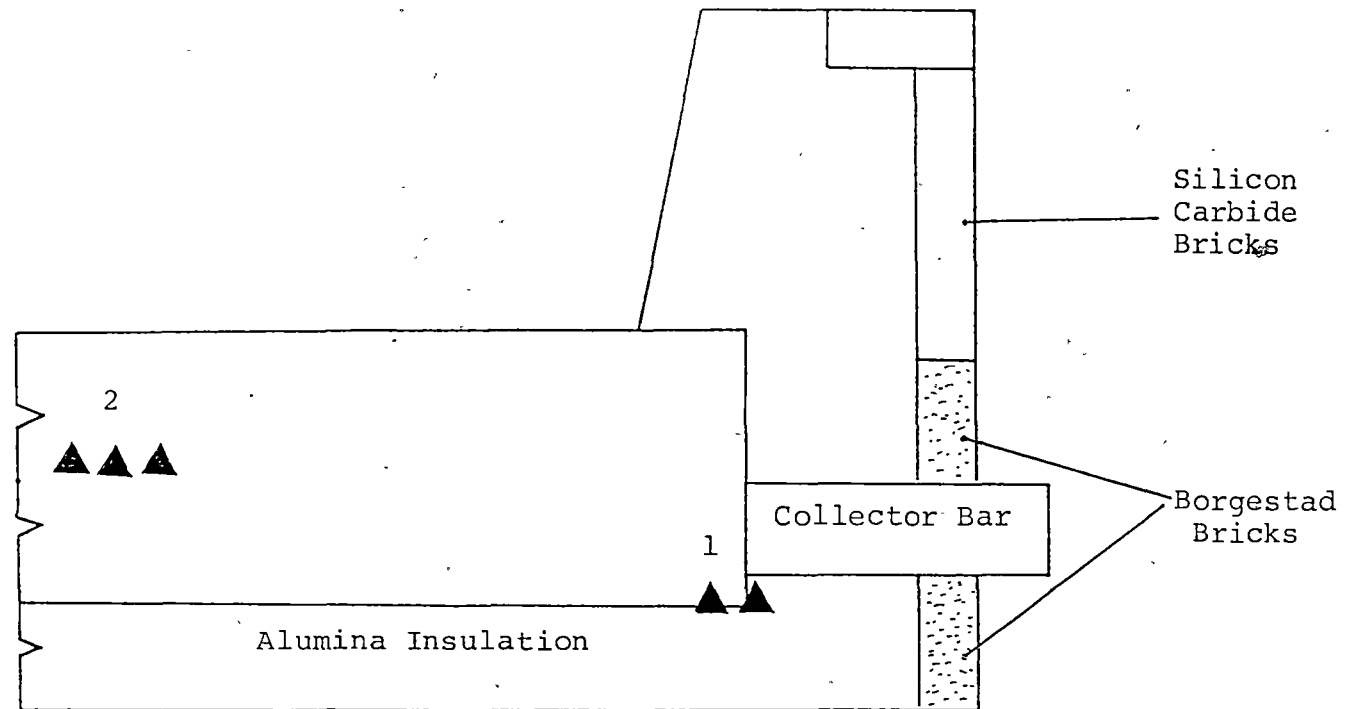


Figure 1.3: Bell Bay Pot 2/137

Transverse Half-Section of Block Cathode No. 5 from Duct End

Legend: ▲ Sampling Area

Table 1.4: Cyanide Profile - Bell Bay Pot 2/137

Block No. 2 from Tap End

POT DESCRIPTION	SPECIMEN		TOTAL CYANIDE (WT.% CN ⁻)
	LOCATION NUMBER	DESCRIPTION	
As in Table 1.3	3 (Fig. 1.4(a))	Upstream side from sidewall; adjacent to SiC bricks; very hard	2.9
	4 (Fig. 1.4(b))	Downstream side: from sidewall; near upper surface of block; flaky carbon impreg- nated with sodium	4.9

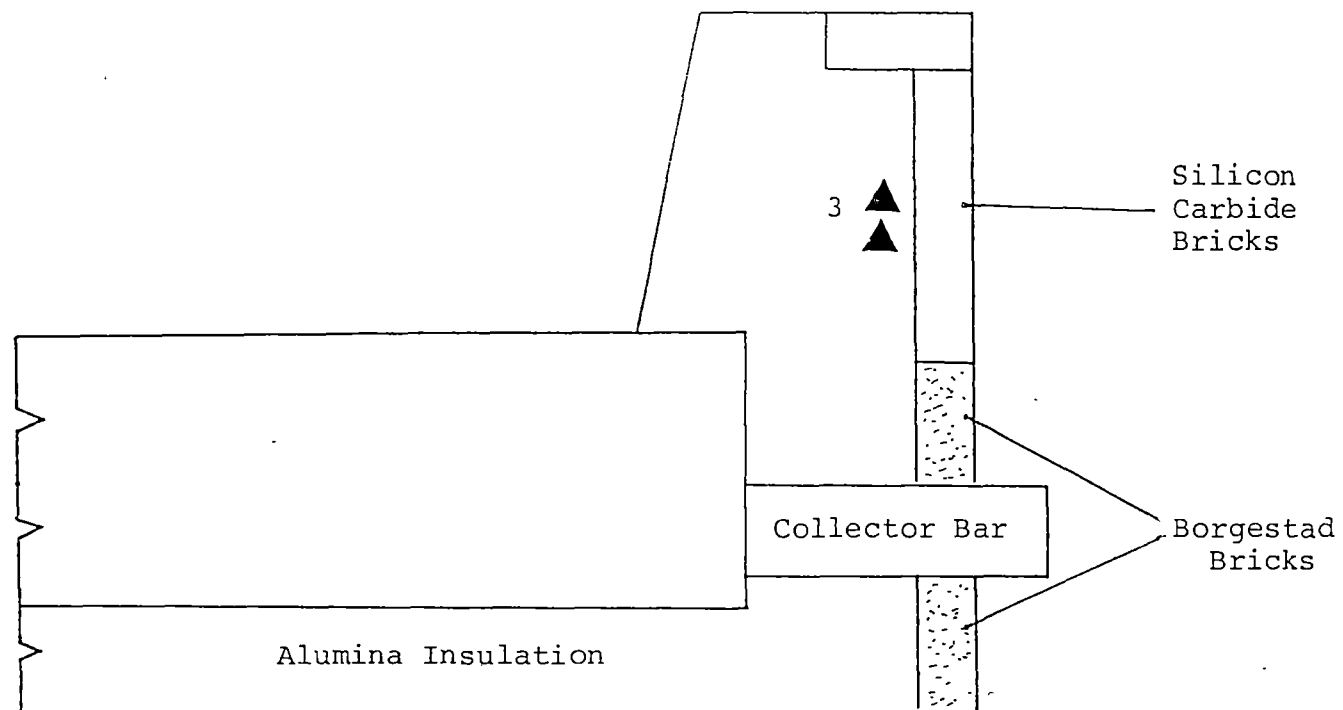


Figure 1.4 (a): Bell Bay Pot 2/137

Transverse Half-Section of Block Cathode No. 2 from Tap End

Legend: ▲ Sampling Area

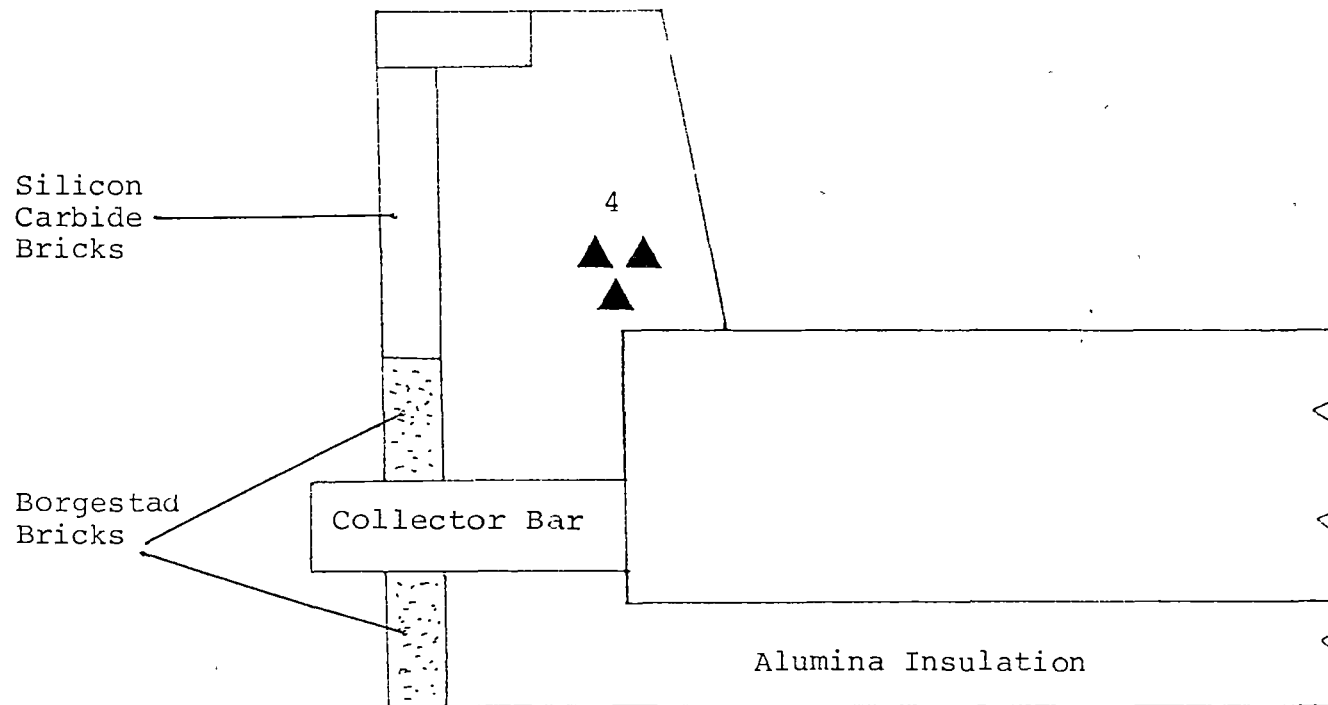


Figure 1.4(b): Bell Bay Pot 2/137

Transverse Half-Section of Block Cathode No. 2 from Tap End

Legend: ▲ Sampling Area

Table 1.5: Cyanide Profile - Bell Bay Pot 2/137

Block No. 4 from Duct End

POT DESCRIPTION	SPECIMEN		TOTAL CYANIDE (WT.% CN ⁻)
	LOCATION NUMBER	DESCRIPTION	
As in Table 1.3	5 (Fig. (1.5(a)))	Downstream side: from sidewall along sidewall-block interface; brittle and covered with thin layer of bath.	2.6
	6 (Fig. (1.5(b)))	Upstream side; from sidewall near SiC bricks; brittle carbon	2.9

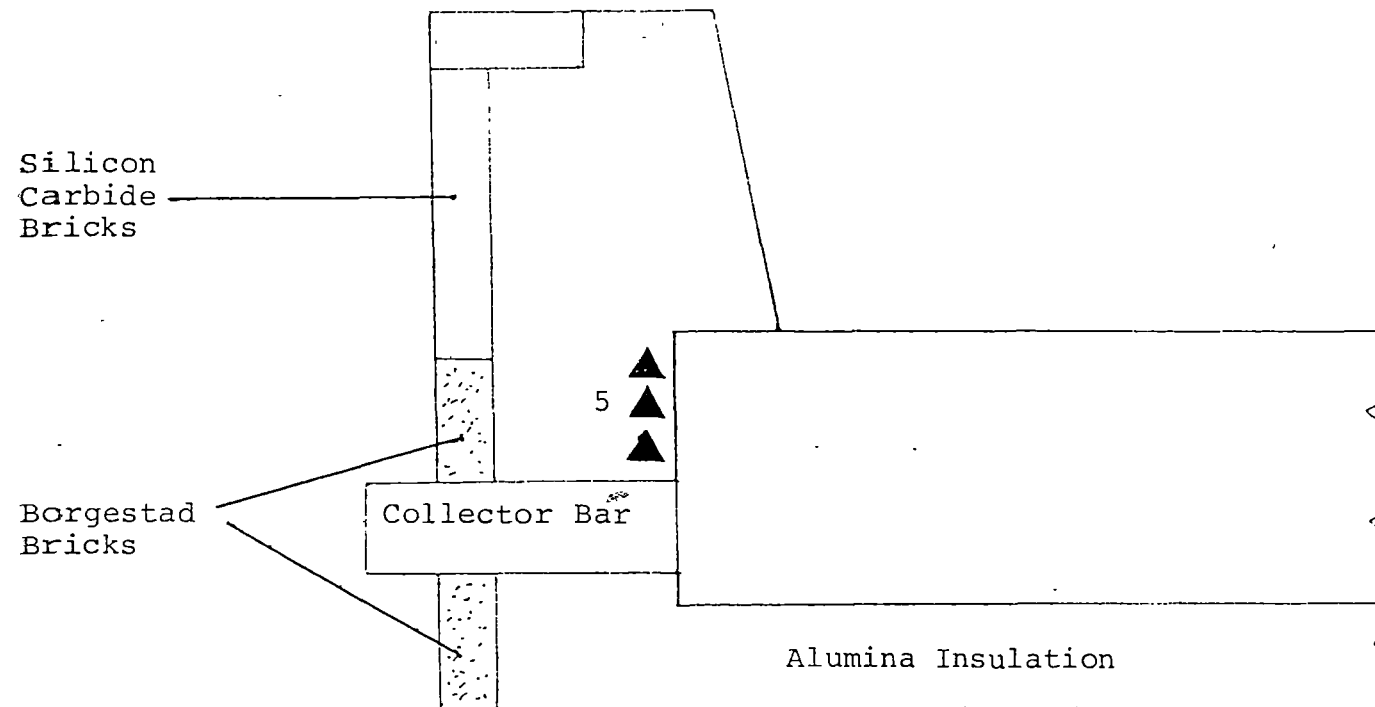


Figure 1.5(a): Bell Bay Pot 2/437

Transverse Half-Section of Block Cathode No. 4 from Duct End

Legend: ▲ Sampling Areas

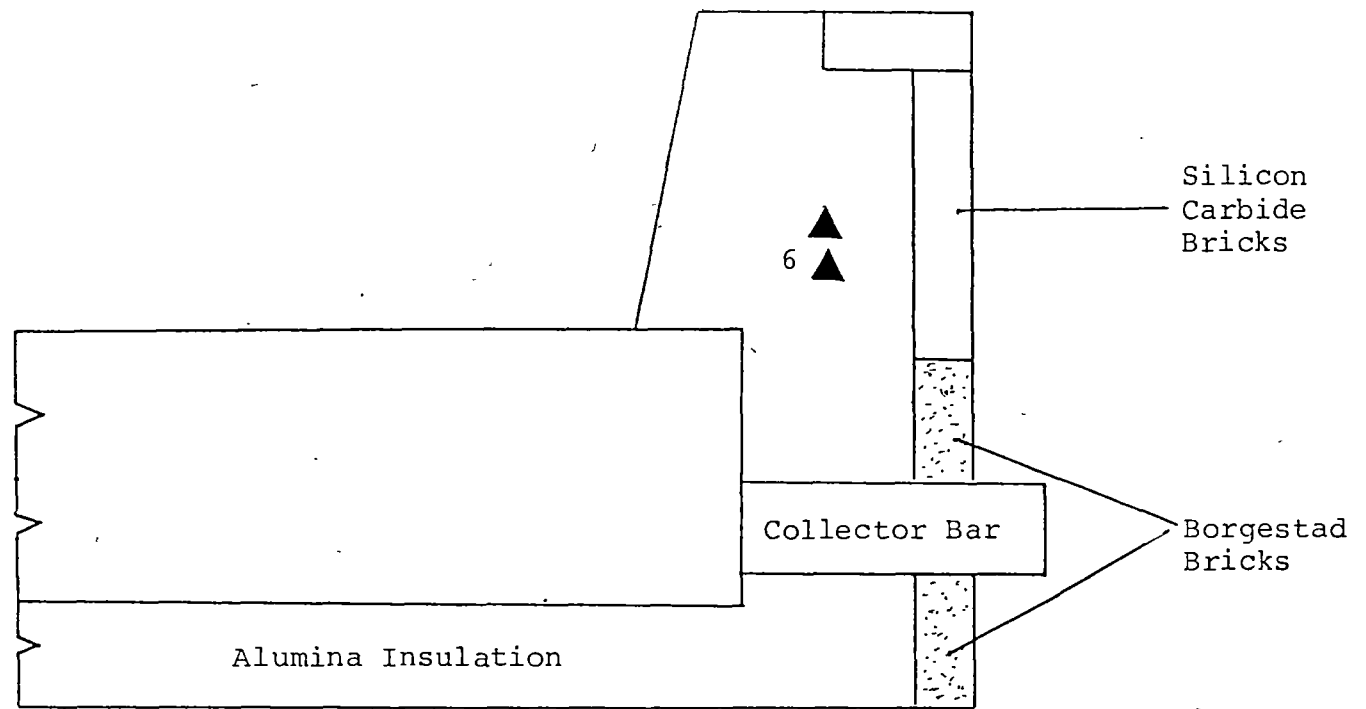


Figure 1.5(b): Bell Bay Pot 2/137

Transverse Half-Section of Block Cathode No. 4 from Duct End

Legend: ▲ Sampling Area

Table 1.6: Cyanide Profile - Bell Bay Pot 2/65

Downstream Side - Block No. 1 from Tap End

POT DESCRIPTION	SPECIMEN		TOTAL CYANIDE (WT.% CN ⁻)
	LOCATION NUMBER	DESCRIPTION	
<p>Sers Block Cathode</p> <p>Construction: SiC Type III</p> <p>Pot Life: 823 days</p> <p>Failure Mode: Tap-out through collector bar between stall no. 4 & no. 8</p>	1	From sidewall-block interface immediately adjacent to collector bar; brittle and impregnated with bath; adjacent to sodium-condensation zone along sidewall	7.1
	2	From block-slot interface; brittle carbon	0.1
	3	From block-slot interface; hard carbon	<0.1
	4	Near block-base insulation interface; hard carbon with mixture of consolidated alumina	<0.1

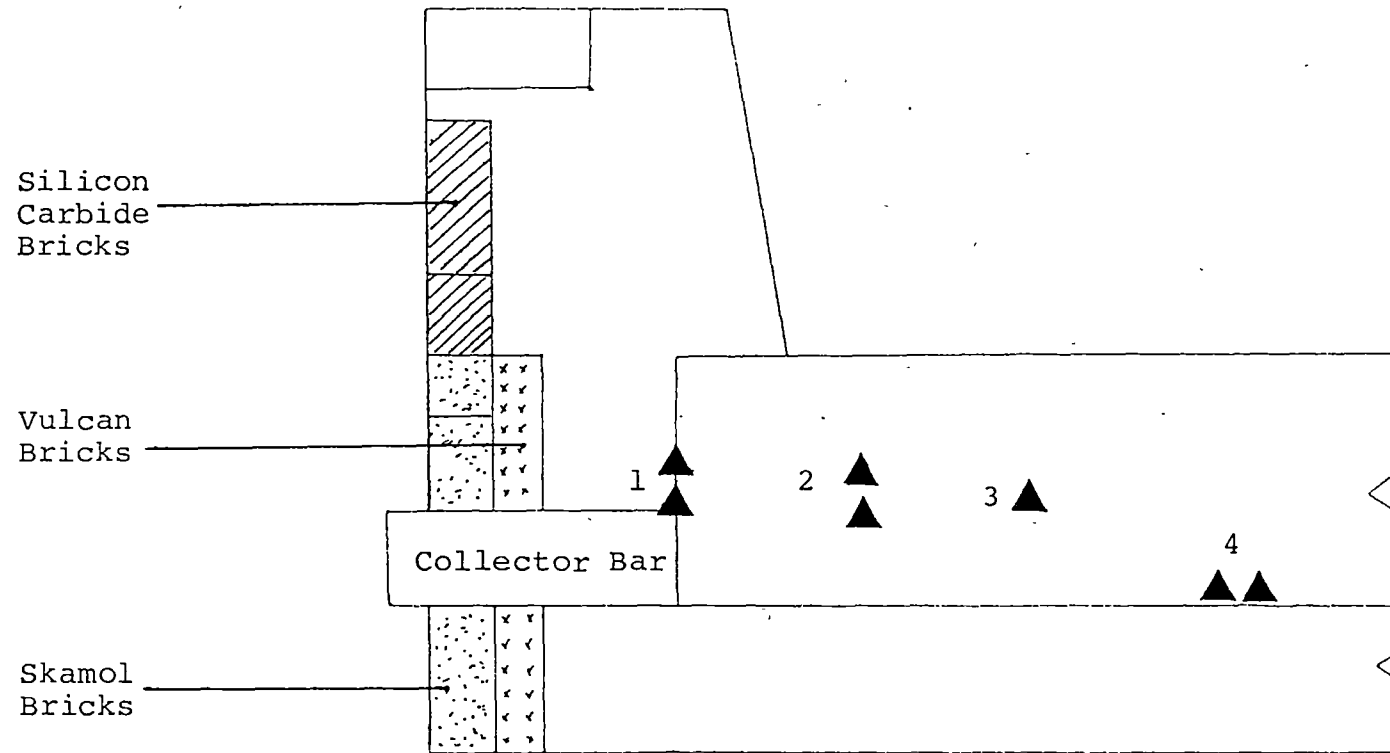


Figure 1.6: Bell Bay Pot 2/65

Transverse Half-Section of Block Cathode No. 1 from Tap End

Legend: ▲ Sampling Area

Table 1.7: Cyanide Profile - Bell Bay Pot 2/65

Block No. 2 from Tap End

POT DESCRIPTION	SPECIMEN		TOTAL CYANIDE (WT.% CN ⁻)
	LOCATION NUMBER	DESCRIPTION	
As in Table 1.6	1	From sidewall above collector bar; friable carbon containing bath particles, impregnated with sodium	9.4
	2	From block-slot interface; flaky and hard	0.50
	3	Near critical isotherm; at junction between cathode block and consolidated alumina layer; hard material	4.3
	4	Towards centre of cathode block; hard carbon	<0.1
	5	Centre of cathode block; hard carbon	<0.1

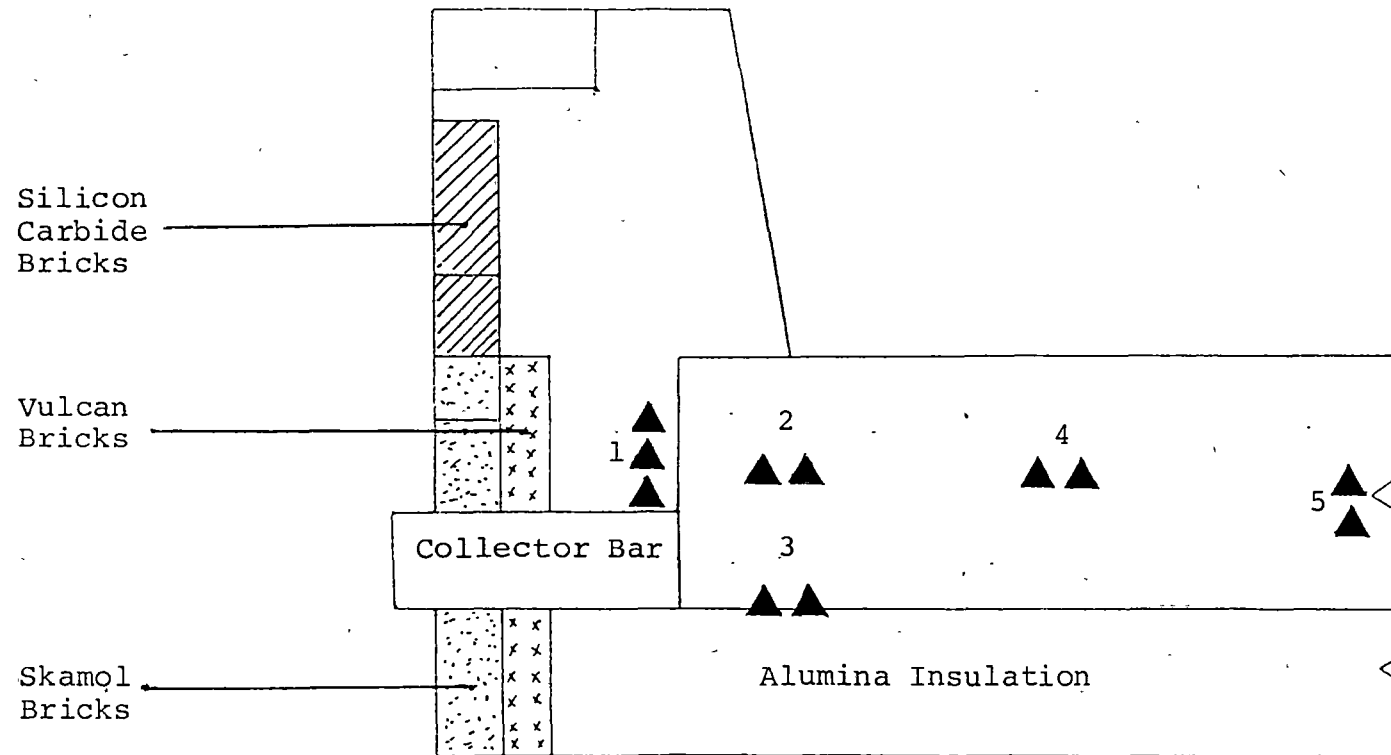


Figure 1.7: Bell Bay Pot 2/65

Transverse Half-Section of Block Cathode No. 2 from Tap End

Legend: ▲ Sampling Area

Table 1.8: Cyanide Profile - Bell Bay Pot 2/65.

Block No. 3 from Tap End

POT DESCRIPTION	SPECIMEN		TOTAL CYANIDE (WT.% CN ⁻)
	LOCATION NUMBER	DESCRIPTION	
As in Table 1.6	1	From block-slot interface; centre of cathode, hard carbon	<0.1
	2	Above collector bar; hard carbon	<0.1
	3	Adjacent to upper surface of collector bar; hard carbon	<0.1
	4	From block-consoli- dated alumina inter- face, hard mixture of carbon and alumina	0.30
	5	From sidewall, adjacent to block- end; friable carbon containing a layer of bath material	2.1

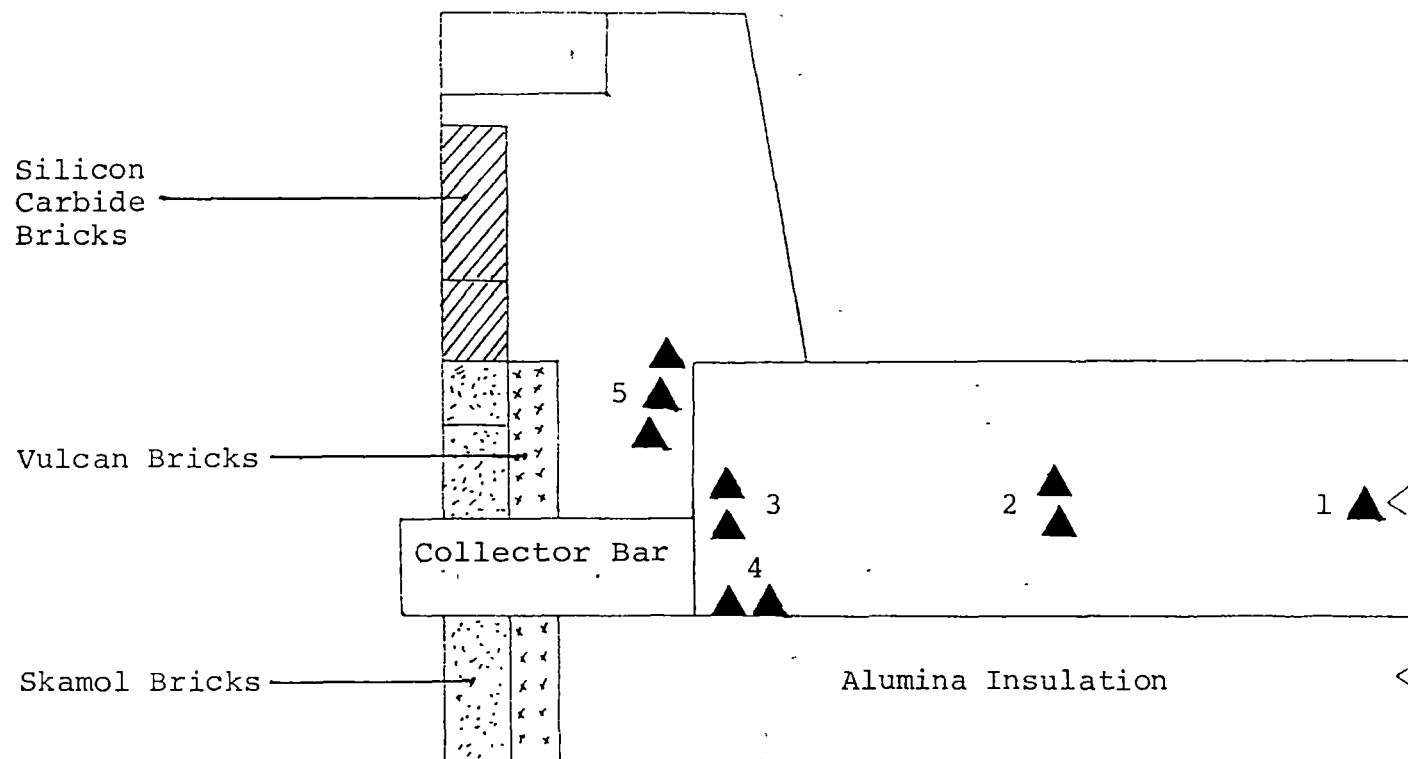


Figure 1.8: Bell Bay Pot 2/65

Transverse half-Section of Block Cathode No.3 from Tap End

Legend: ▲ Sampling Area

Table 1.9: Cyanide Profile - Bell Bay Pot 2/65

Block No. 4 from Tap End

POT DESCRIPTION	SPECIMEN		TOTAL CYANIDE (WT.% CN ⁻)
	LOCATION NUMBER	DESCRIPTION	
As in Table 1.6	1	From sidewall; impregnated with sodium, above collector bars; friable carbon	7.9
	2	From block-slot interface; hard carbon	<0.1
	3	Near block-alumina interface; hard carbon	<0.1
	4	Centre section of block; hard carbon	<0.1

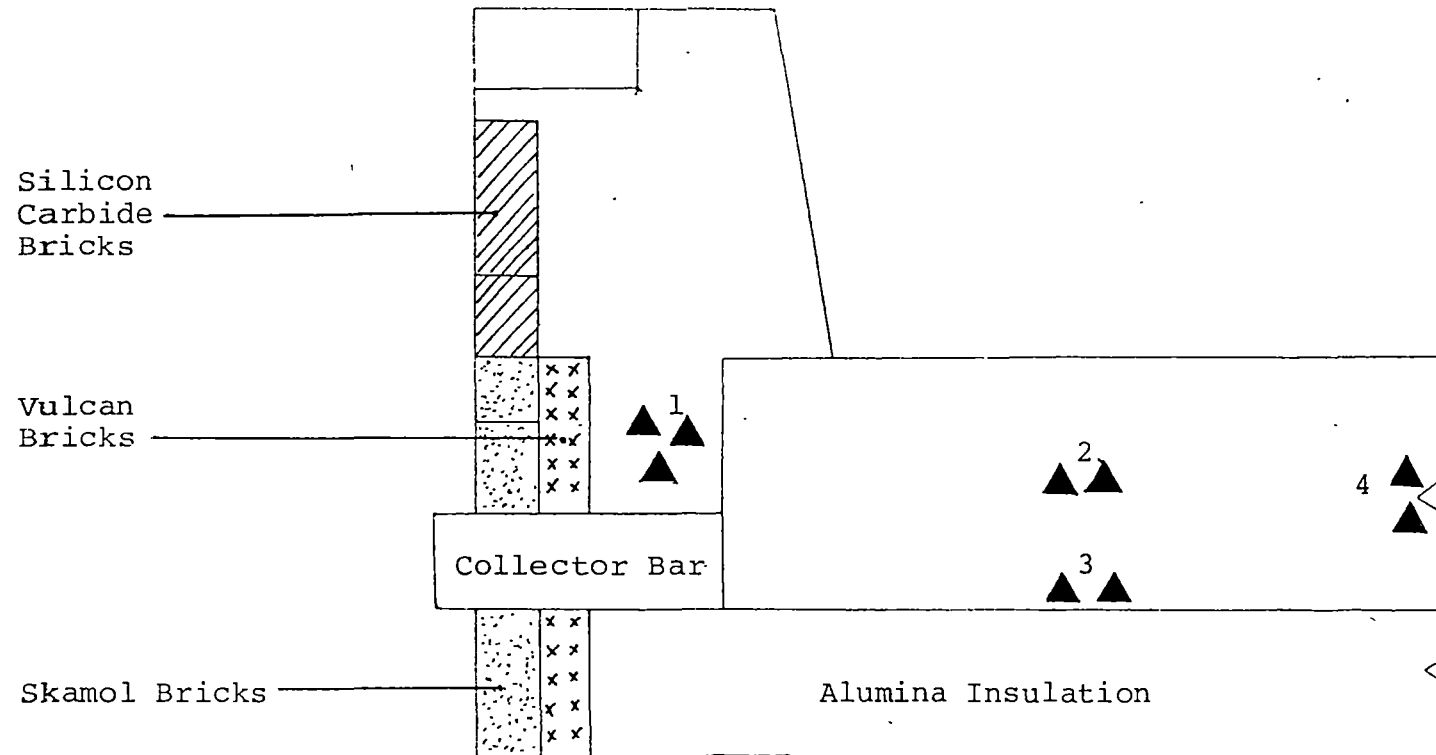


Figure 1.9: Bell Bay Pot 2/65

Transverse Half-Section of Block Cathode No. 4 from Tap End

Legend: ▲ Sampling Area

Table 1.10: Cyanide Profile - Bell Bay Pot 4/201

Block No. 3 from Tap End

POT DESCRIPTION	SPECIMEN		TOTAL CYANIDE (WT.% CN ⁻)
	LOCATION NUMBER	DESCRIPTION	
Nippon Cathode Block Construction: SiC Type IV Pot Life: 432 days Failure Mode: Tap-out through collector bar no. 3 from tap-end	1	From sidewall immediately above collector bar; soft, friable carbon impregnated with sodium and bath	2.6
	2	From block-slot interface; near carbon-alumina interface; flaky carbon containing sintered alumina	0.23
	3	Near tap out region; friable carbon containing aluminium carbide matrix; saturated with sodium	7.7
	4	From bath saturated alumina layer; hard and flaky; saturated with sodium	5.9

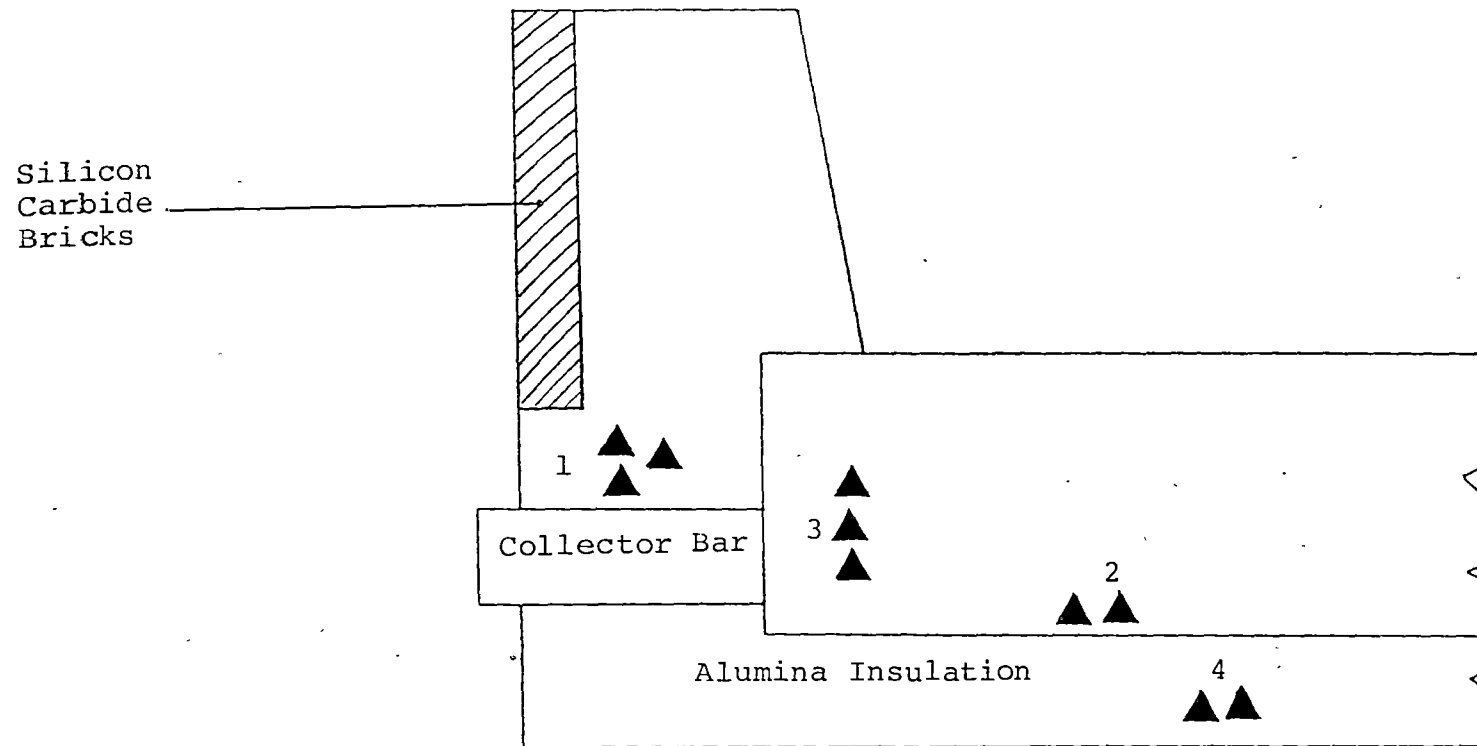


Figure 1.10: Bell Bay Pot 4/201

Transverse Half-Section of Block Cathode No. 3 from Tap End

Legend: ▲ Sampling Area

Table 1.11: Cyanide Profile - Bell Bay Pot 4/201

Block No. 2 from Duct End

POT DESCRIPTION	SPECIMEN		TOTAL CYANIDE (WT.% CN ⁻)
	LOCATION NUMBER	DESCRIPTION	
As in Table 1.10	1	From block-slot interface; soft, friable carbon containing mixture of aluminium carbide and bath; near dish- cracks in block; saturated with sodium	6.7

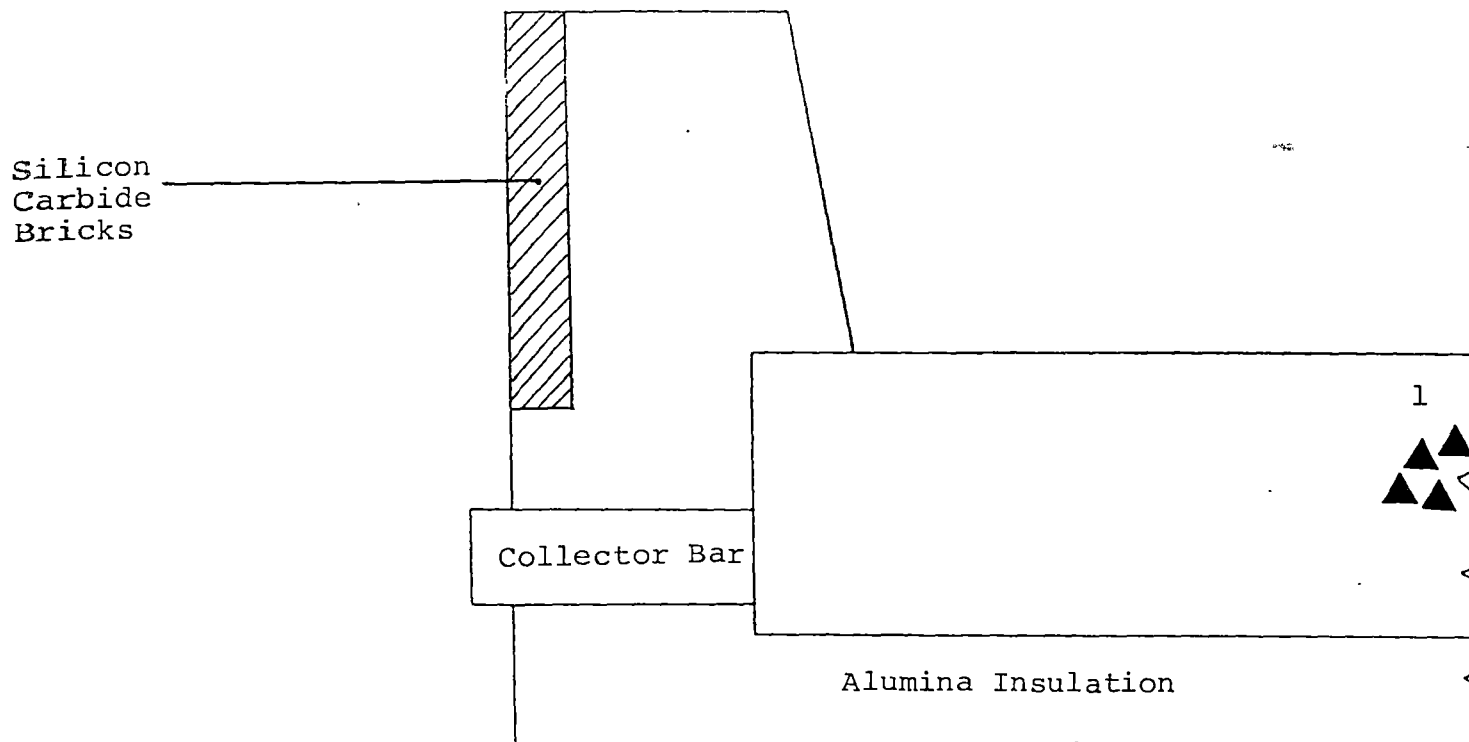


Figure 1.11: Bell Bay Pot 4/201

Transverse Half-Section of Block Cathode No. 2 from Duct End

Legend: ▲ Sampling Area

Table 1.12: Cyanide Profile - Bell Bay Pot 4/201

Block No. 3 from Duct End

POT DESCRIPTION	SPECIMEN		TOTAL CYANIDE (WT.% CN ⁻)
	LOCATION NUMBER	DESCRIPTION	
As in Table 1.10	1	From block-slot interface; adjacent to dish-crack; flaky carbon containing mixture of bath and aluminium carbide, saturated with sodium	5.5
	2	Near to dish-crack; hard and flaky carbon impregnated with bath	0.94

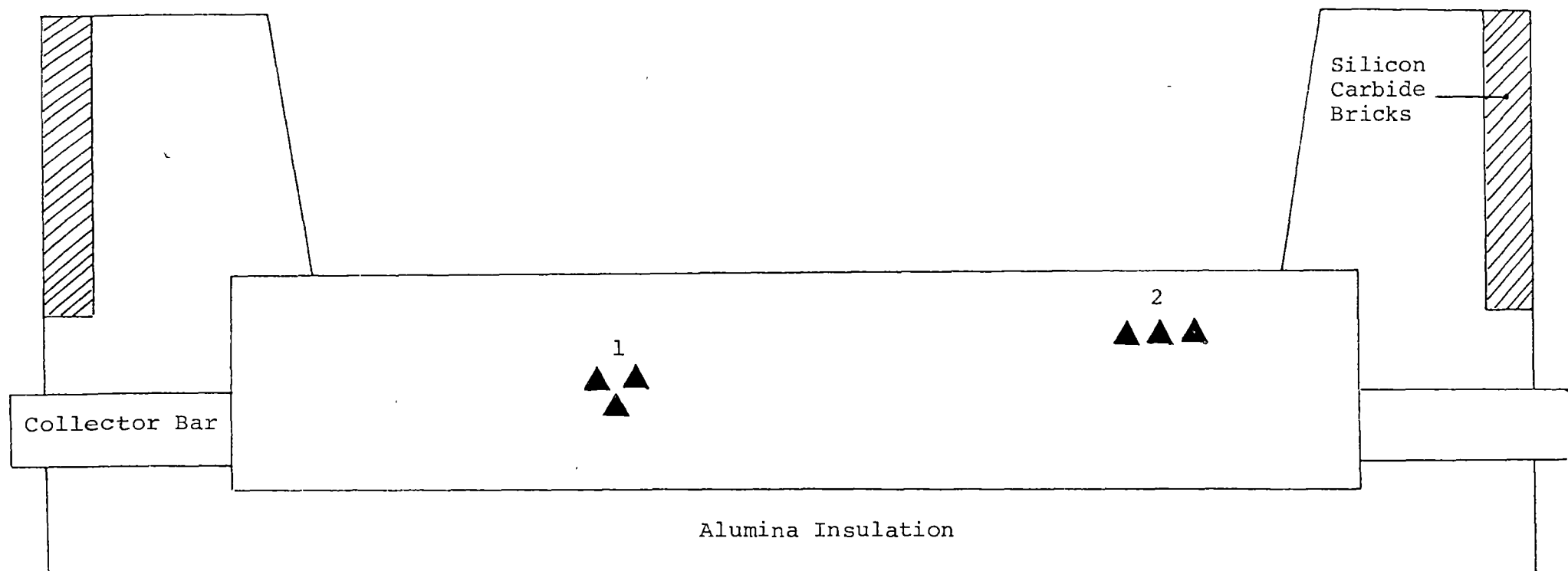


Figure 1.12: Bell Bay Pot 4/201

Transverse Section of Block Cathode No. 3 from Duct End

Legend: ▲ Sampling Area

Table 1.13: Cyanide Profile - Bell Bay Pot 4/201

Block No. 4 from Tap End

POT DESCRIPTION	SPECIMEN		TOTAL CYANIDE (WT.% CN ⁻)
	LOCATION NUMBER	DESCRIPTION	
As in Table 1.10	1	From block-slot interface; near bath saturated alumina, hard, flaky carbon	<0.1
	2	Friable carbon impregnated with sodium	1.5
	3	Near sidewall section; hard and flaky carbon	0.15

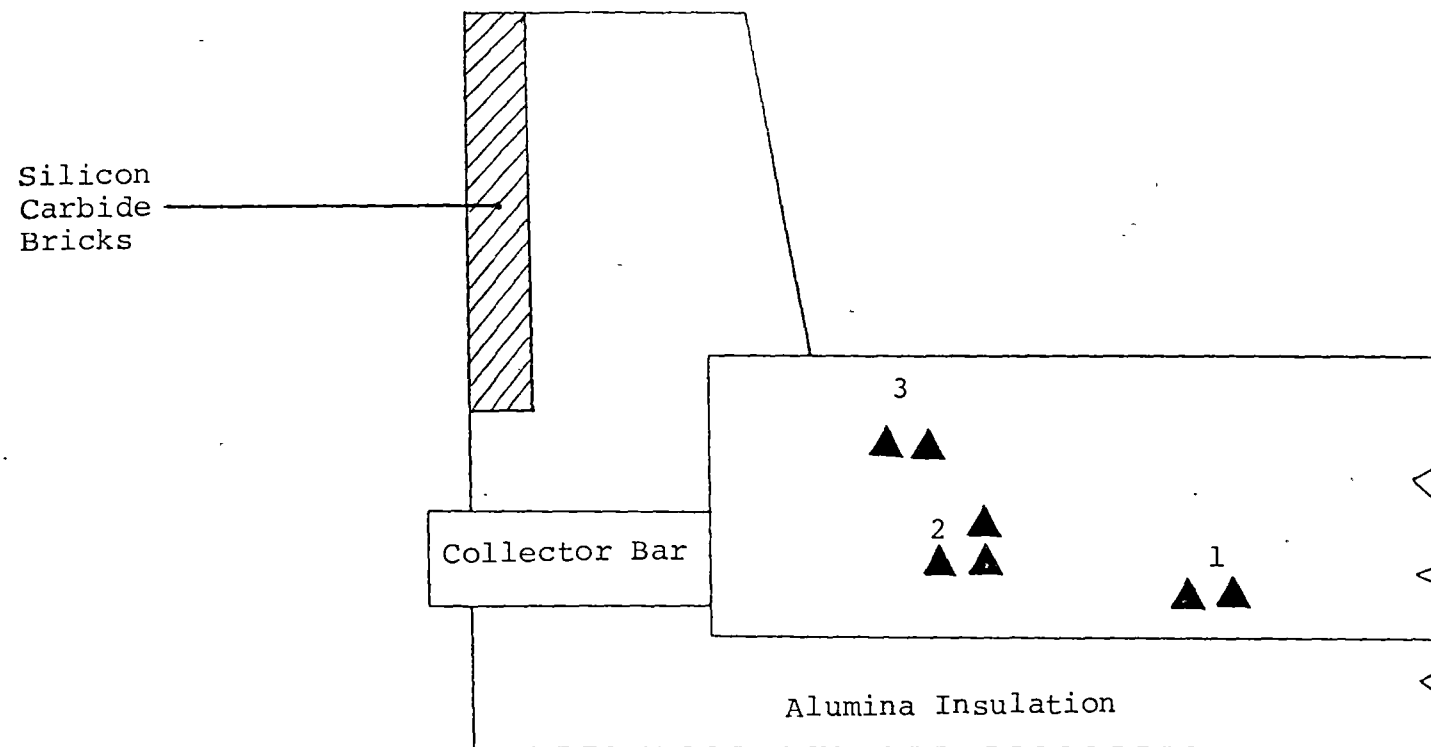


Figure 1.13: Bell Bay Pot 4/201

Transverse Half-Section of Block Cathode No. 4 from Tap End

Legend: ▲ Sampling Area

Table 1.14: Cyanide Profile - Bell Bay Pot 4/ 57

Block No. 2 from Tap End

POT DESCRIPTION	SPECIMEN		TOTAL CYANIDE (WT.% CN ⁻)
	LOCATION NUMBER	DESCRIPTION	
<p>Nippon Cathode Block</p> <p>Construction: SiC Type IV</p> <p>Pot Life: Approx. 850 days</p> <p>Failure Mode: Tap-out through collector bar at stall no. 4</p>	1	Near sidewall adjacent to tap-out region; brittle and flaky	2.3
	2	From collector bar surface and adjoining areas; soft and flaky contaminated with bath and alumina	4.6
	3	Above collector bar slot, near to dish crack area; flaky with some Al ₄ C ₃ matrix and bath	<0.1
	4	From underside of heaved carbon, near dish crack region; flaky with layer of bath	<0.1
	5	Above collector bar; flaky carbon, adjacent to bath isothermal freeze zone	4.4
	6	Adjacent to tap-out region; brittle and saturated with sodium	3.3

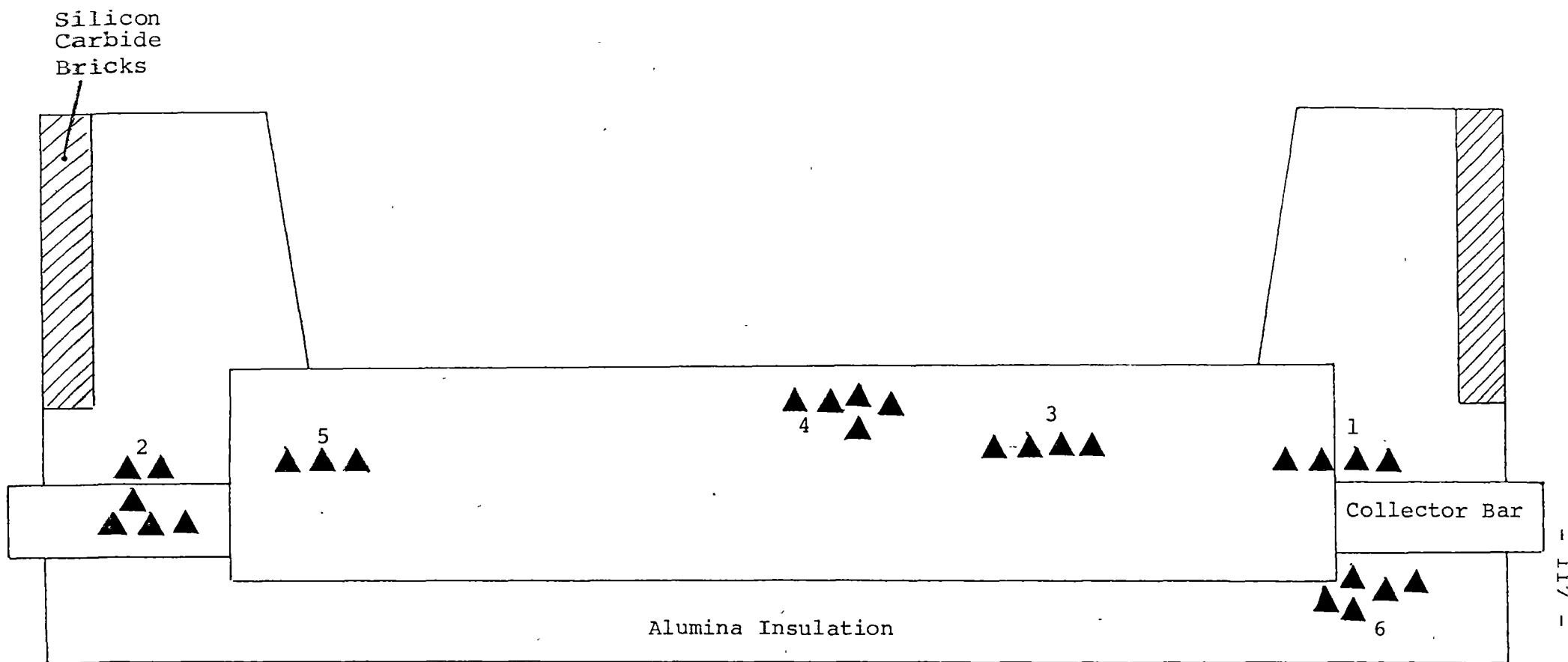


Figure 1.14: Bell Bay Pot 4/57

Transverse Section of Cathode Block No. 2 from Tap End

Legend: ▲ Sampling Area

Table 1.15: Cyanide Profile - 150 kA Pot

Block No. 7 from Duct End

POT DESCRIPTION	SPECIMEN		TOTAL CYANIDE (WT.% CN ⁻)
	LOCATION NUMBER	DESCRIPTION	
Great Lakes Cathode Block Construction Pot Life: 1347 days Pot cut out for reconstruction	1	From sidewall near cathode-sidewall interface; hard carbon impregnated with cathodic bath	1.9
	2	Bath saturated alumina immediately below collector bar; hard consolidated alumina saturated with sodium; contains opaque columna crystals.	2.5
	3	Near mid-section of block cathode; hard carbon containing cathodic bath.	0.6

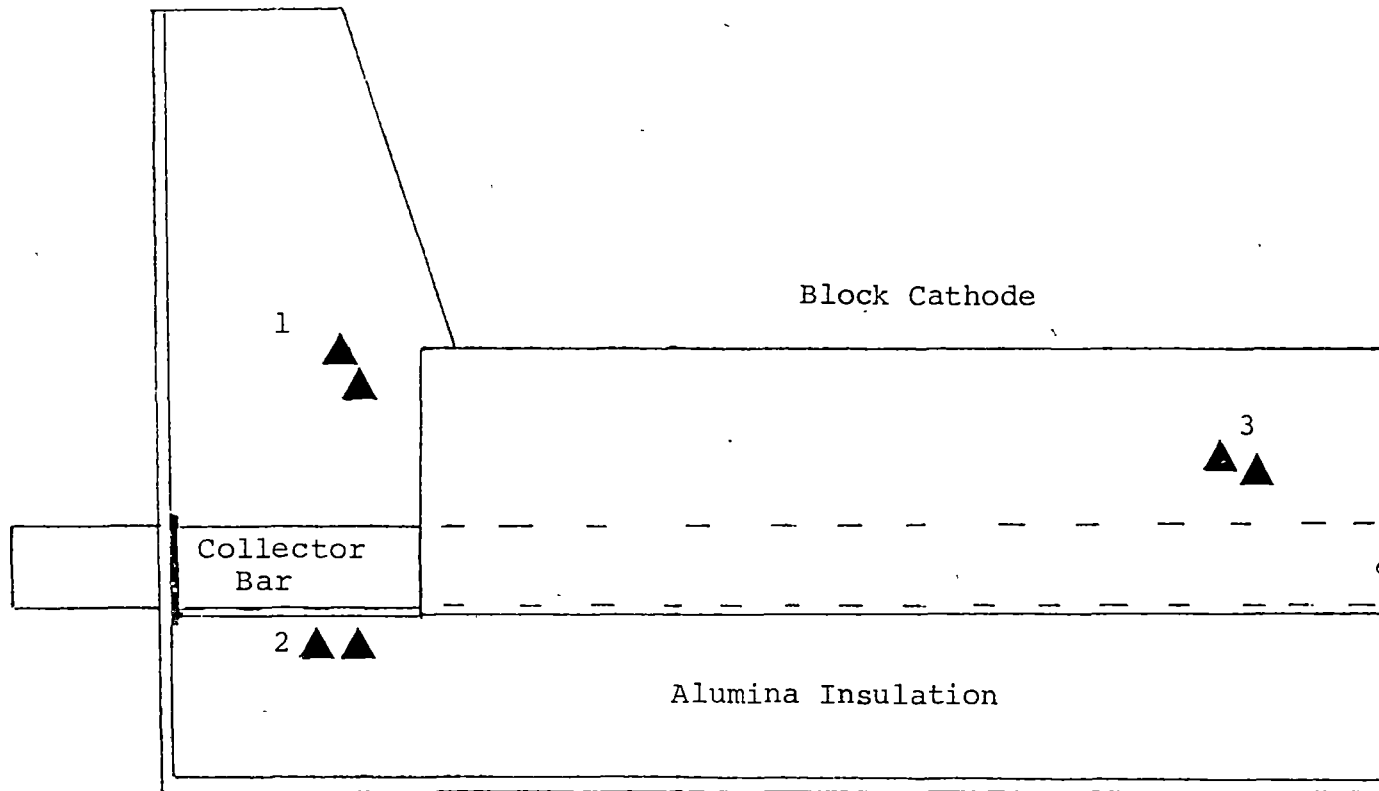


Figure 1.15: 150 kA Pot

Transverse Half-Section of Block Cathode No. 7 from Duct End

Legend: ▲ Sampling Area - Total Cyanide Concentration

Table 1.16: Cyanide Profile - 150 kA Pot

Block No. 7 from Duct End

POT DESCRIPTION	SPECIMEN		TOTAL CYANIDE (WT.% CN ⁻)
	LOCATION NUMBER	DESCRIPTION	
<p>Great Lakes Cathode Block Construction</p> <p>Pot Life: 2382 days</p> <p>Failure Mode: Tap-out through collector bar no. 7 from tap-end</p>	1	From sidewall region; hard carbon with Al ₄ C ₃ matrix on surface; impregnated with bands of cathodic bath	3.8
	2	Near mid-section of block cathode; hard, flaky carbon contaminated with bath particles; impregnated with bands of cathodic bath.	<0.1

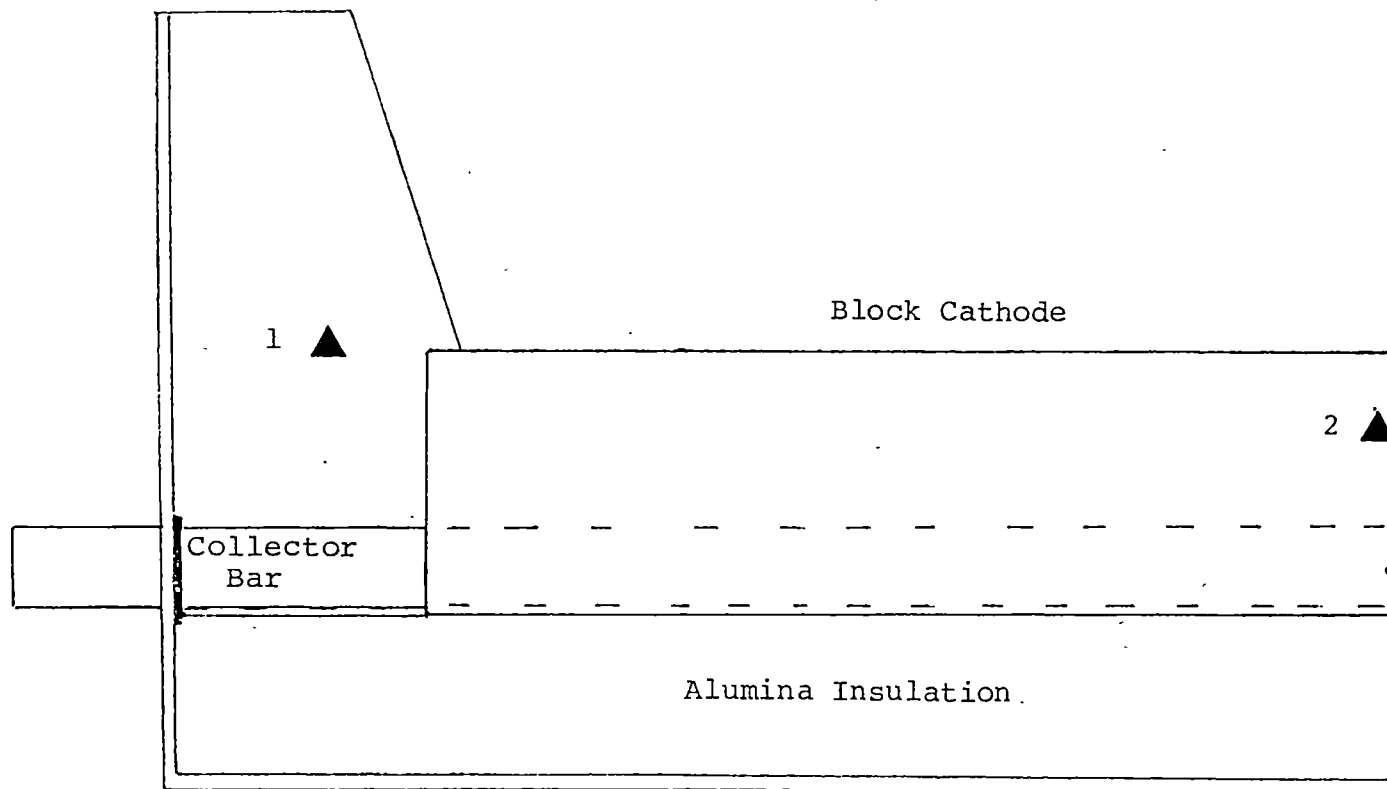


Figure 1.16: 150 kA Pot

Transverse Half-Section of Block Cathode No. 7 from Duct End

Legend: ▲ Sampling Area - Total Cyanide Concentration

APPENDIX 2

Procedure for Determining Total Cyanide

Content in Spent Cathode

Procedure

Transfer approximately 1.0 - 2.0g of crushed sample into a round bottomed distillation flask.

Add 50 mls of acid cuprous chloride solution (2% w/v solution in 5N HCl), a few glass beads and assemble the apparatus for distillation.

Place a conical flask containing approximately 30 mls of 2.5N NaOH solution under the condensor so that the end dips beneath the surface.

Distill the mixture until approximately 250 mls of distillate has been collected.

Pipette 100 mls of distillate into a 200 ml plastic beaker and add 1 ml 10N NaOH solution.

Measure the cyanide content directly with a Cyanide Ion Selective Electrode.

APPENDIX 3

Publication in Light Metals, Proc. Met. Soc. AIME (1985)

A STUDY OF CYANIDE DISTRIBUTION AND FORMATION IN
ALUMINIUM REDUCTION CELL LININGS

B.K. Yap

Comalco Aluminium (Bell Bay) Limited
P.O. Box 290, George Town, Tasmania
Australia 7253

Abstract

From autopsies of failed cells, the cyanide distribution profiles within the linings were extensively mapped, as part of an investigation into factors likely to influence cyanide formation. A parallel laboratory study^{carbon to} was conducted to determine the susceptibility of different forms of ^{carbon to} cyanide generation, the carbon ranging from plant derived sidewall-mix through commercial prebaked cathode material to high purity graphite.

In the laboratory study, sodium cyanide was synthesized by impregnating the carbon specimens with metallic sodium followed by chemical reaction with pure nitrogen. Whilst cyanide formation was found to readily occur in the temperature range of 500-600°C in all carbons tested, the less ordered sidewall mix was significantly more vulnerable. The reaction was accelerated by the presence of iron impurities, and the amount of cyanide generated in a given reaction time can vary by a factor of three.

Autopsy examination of the potlinings revealed that major amounts of cyanide were generally concentrated in the carbon sidewall and in regions near the collector bars. These observations would not be inconsistent with laboratory measurements. The cyanide profiles suggest that air ingress through the collector bar seals into and sodium saturation of the carbon also influence the favoured region for cyanide formation.

Introduction

The presence of cyanide compounds in potlinings of failed aluminium reduction cells has stimulated much interest in and discussion on the strategies and methods of disposing cyanide-contaminated water from the smelter (1-3). While efforts have been directed towards the development of various treatment processes, information related to the distribution and formation of cyanide in potlinings is very limited.

A survey of the literature reveals that most of the information is of a general nature related to the detection of cyanide in potlining samples. Although earlier reports (4,5) suggest that cyanide may be distributed near the collector bars and zoned according to temperature gradients in the cathode, no specific evidence has been presented to support this assumption. As the need for improved management of cyanide-bearing wastes in aluminium smelters still exists, a greater understanding of the formation of cyanide and its distribution profile in the pot is desirable.

Experimental

The experimental method comprised two stages:

- (i) cyanide profile mapping
- (ii) cyanide formation studies

A. Cyanide Mapping

Several failed cells of various types (47kA and 88kA) and construction were selected for autopsy. Essentially, each cathode was systematically trenched, with the pot in an upright position and the shell intact, after cleaning of the cathode cavity. Specimens from various selected areas of the trenched sidewall and cathode regions were extracted to enable mapping of the cyanide distribution profile in the pot.

A weighed portion of the specimen, ground to -200 mesh size, was taken for determination of cyanide using acidic cuprous chloride distillation and Cyanide Ion-Selective Electrode.

B. Cyanide Formation Synthesis

A fundamental approach was adopted using small moulded carbon specimens. Carbon types ranging from specimens prepared by baking a typical plant formulation for the monolithic sidewall carbon-mix through commercial preformed cathode material to high purity graphite were used. As the structural form of some of these carbon types is relevant to the industry, laboratory data obtained from this investigation have the real advantage of being closely related to plant measurements.

The test cell used comprised a recrystallised alumina crucible suspended in a silica reaction tube attached to a Cahn RH Electrobalance. This apparatus was positioned in an electrical resistance furnace, and temperature control of the system was effected via the set-point control facility of a Trendtrak unit connected to the furnace. Operational temperatures ranging from 500 to 600°C were used in the reaction.

The carbon specimen in the form of a 20 mm diameter rod, with a 9 mm diameter hole in the centre packed with metallic sodium, was placed in an inverted position in the crucible to facilitate sodium-impregnation of the carbon during heating. Initially, an argon atmosphere was introduced in the test cell. When the reaction temperature was attained, pure, dry nitrogen was introduced to replace the argon atmosphere and the reaction maintained for a period of three hours. At the end of this period, the nitrogen atmosphere was replaced with argon gas and the reaction cell disconnected. The crucible containing the reacted sample was immediately removed and allowed to cool to room temperature over silica gel in a desiccator under vacuum.

The sample was subsequently ground to -200 mesh size for cyanide analysis as described above.

Results and Discussion

(1) Autopsy Examination of Potlinings

While a generalised picture of all the results and cyanide distribution profiles in potlinings is illustrated in Figures 1 to 3, a fuller attempt to explain the presence of cyanide in the pot is made in this section. Typical cyanide distribution profiles in a monolithic and preformed block cathode pot are presented in Figure 1 and Figure 2 respectively, while Figure 3 shows the features encountered in an abnormal cyanide profile.

Autopsy examination of the trenched potlinings show that high to moderate concentrations of cyanide are generally located in the sidewalls and adjoining areas. Carbon which is impregnated with sodium appears to be more susceptible to cyanide formation in regions which are easily accessible to air ingress. This is particularly evident in sidewall regions near the collector bar seals.

However, relatively low cyanide concentrations are found in cathode regions near the mid-section of the pot. A number of factors may limit the generation of cyanide in these regions, but it seems that restricted access to air may have been a major contributor. Accordingly, severe crack formation in cathode blocks would also facilitate direct entry of air into the sodium-impregnated carbon and subsequently enhance cyanide formation. The abnormalities in cyanide distribution that can occur when a cathode block has a major crack, is illustrated in Figure 3, where some pockets of high cyanide concentration were present in the mid-section of the block and in the alumina insulation. Whilst direct entry of air via the cracks into the carbon mass most likely contributed to the high cyanide level in the carbon, downward permeation or flow of molten salt containing cyanide into the base insulation was largely responsible for the presence of cyanide in the alumina.

Autopsy examinations of spent potlining specimens from two failed 150 kA cells with average age at failure of 1865 days also reveal cyanide distribution profiles similar to those illustrated in Figure 2. Whilst medium to high concentrations of cyanide are located in the sidewall regions, small amounts of cyanide are distributed in the cathode carbon.

In general, cyanide formation in potlinings will increase with potlife. As sodium penetration and deterioration of the lining progresses, air ingress into the carbon mass is expected to increase. Eventually, this will lead to a gradual build-up of cyanide in the potlining.

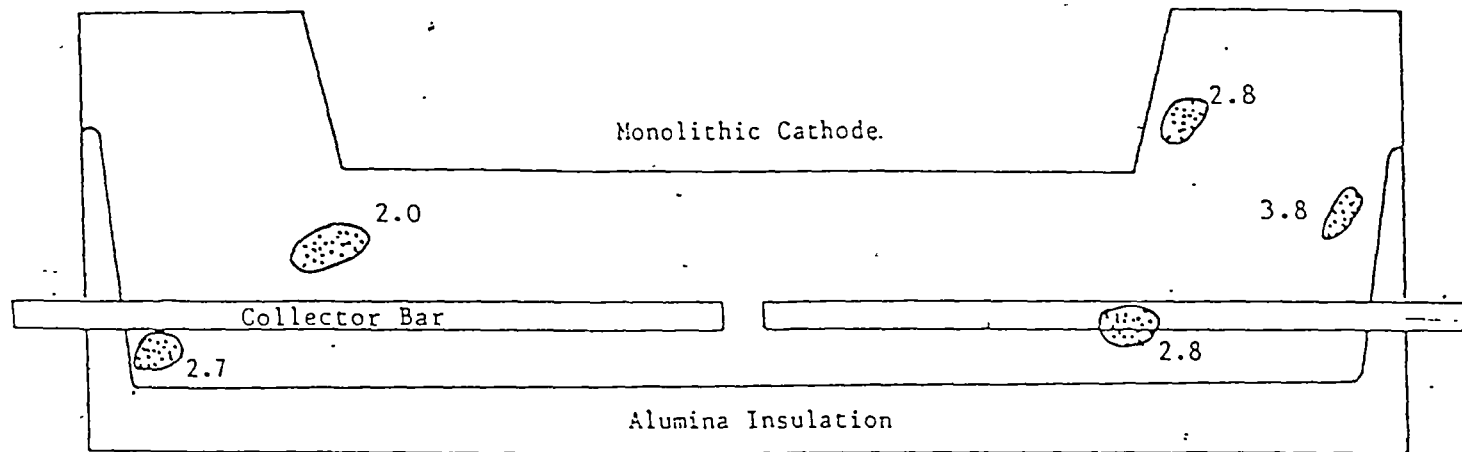



Figure 1 Generalised Cyanide Distribution Profile

47 kA Pot 1920 days at failure

Transverse Section - Monolithic Construction

Legend:  Location of Cyanide Species -
concentration (mmol. cm^{-3})

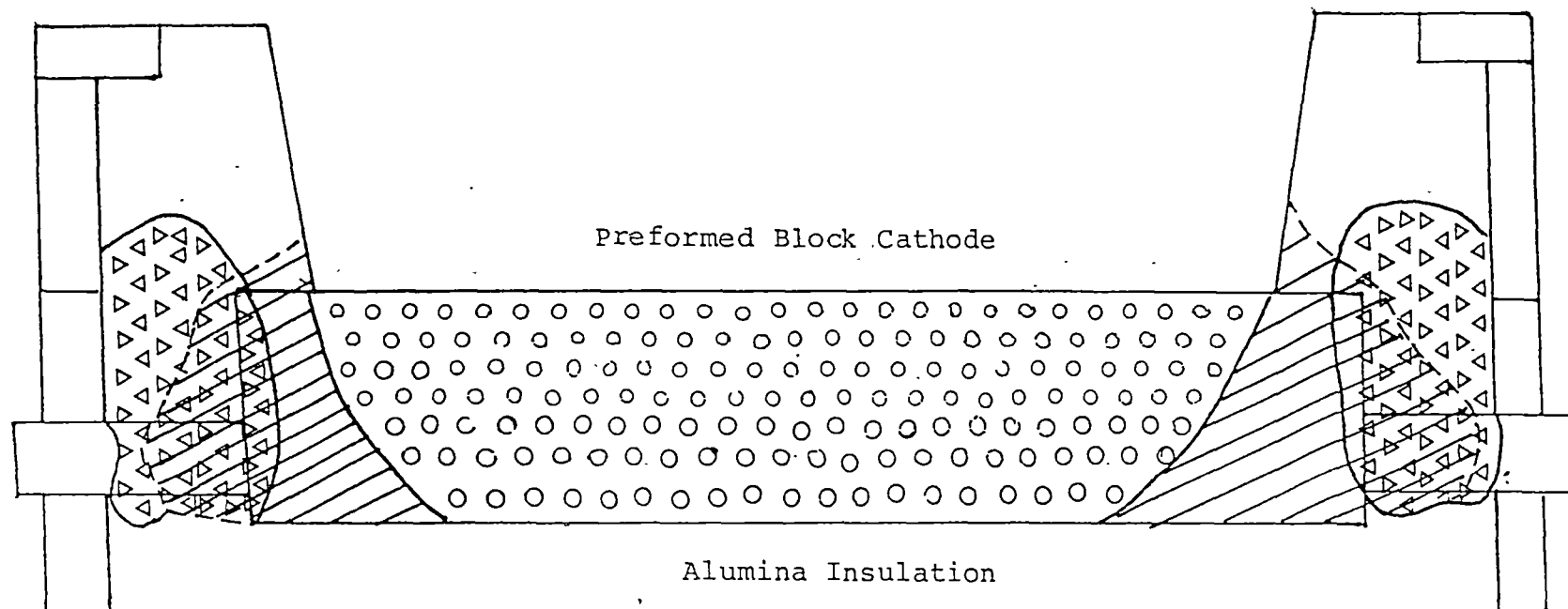
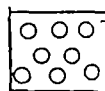


Figure 2 Typical Cyanide Distribution Profile

Transverse Section - Block Cathode Construction

Legend:



Low Cyanide Concentration Range: $< 0.1 - 0.5 \text{ mmol.cm}^{-3}$



Medium Cyanide Concentration Range: $0.5 - 2.0 \text{ mmol.cm}^{-3}$



High Cyanide Concentration Range: $> 2.0 \text{ mmol.cm}^{-3}$

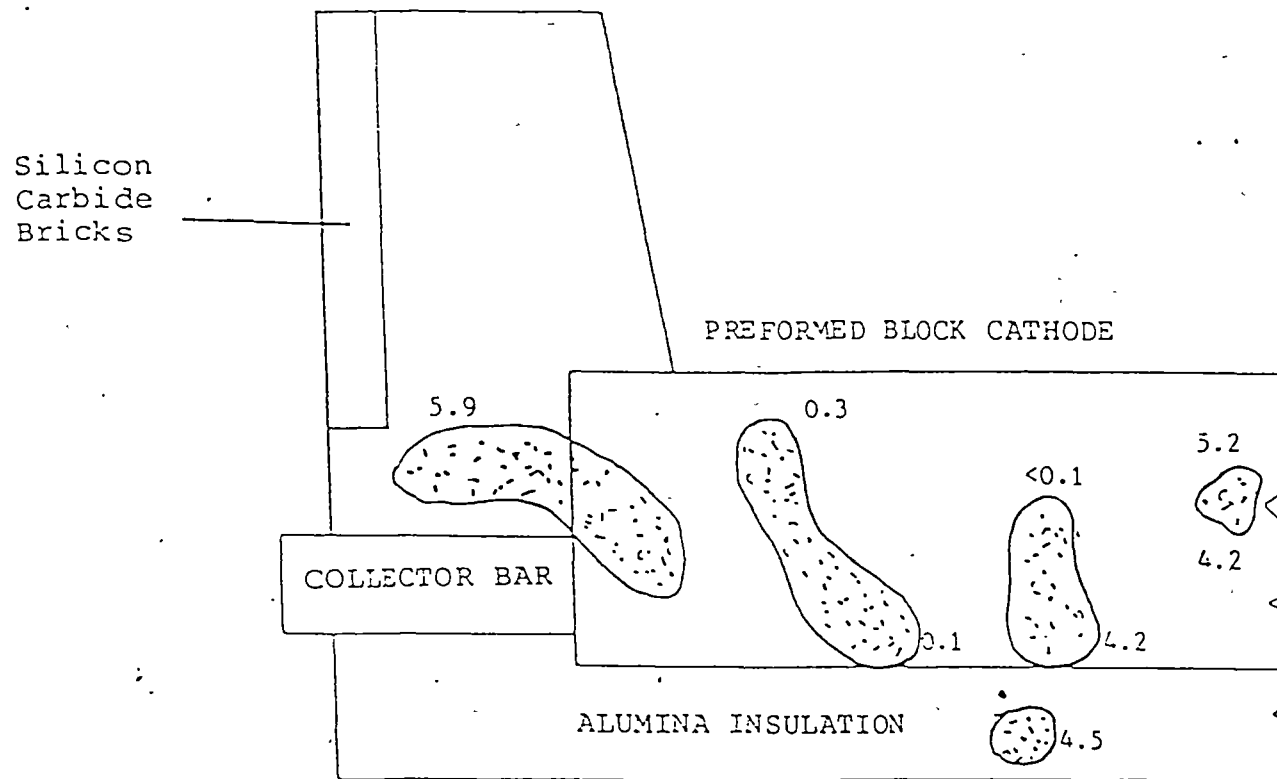
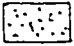


Figure 3 Generalised Cyanide Distribution Profile -
Special Features

88 kA Pot - Age at failure 432 days

Abnormal Cyanide Profile

Transverse Half-Section - Block Cathode
Construction

Legend:  Location of Cyanide Species -
Concentration Range ($\text{mmol} \cdot \text{cm}^{-3}$)

Cyanide Formation Studies

Effect of Temperatures

The effects of temperature ranging from 500-600°C on cyanide formation in the three carbon types were investigated. The results reveal that formation of cyanide in plant derived carbon-mix, preformed cathode material and graphite is feasible in the temperature range studied. There is also a consistent trend of greater cyanide generation with increase in temperature irrespective of the type of carbonaceous material used. A summary of the effect of temperature on cyanide generation in carbon used in pot-sidewall construction is listed in Table I.

Accordingly, formation of the cyanide species must occur in the sidewall carbon during normal pot operation. Existing information clearly indicates that the temperature in the sidewalls can range from 450-700°C, while recent autopsy data confirm that significant amounts of sodium and cyanide are located in these regions of the pot. Therefore, it is now evident that reactive sites for the production of cyanide are continuously generated in the thermal environment of the sidewalls and adjoining regions during pot operation.

Moreover, cyanide species originating from higher temperature zones are also likely to condense in the sidewalls. Earlier experiments (6) have demonstrated that the formation of gaseous cyanide species can occur at 850-950°C. Seemingly, cathode regions at these temperatures may also serve as potential reactive sites for cyanide generation.

Table I - Effect of Temperature on Cyanide Formation
in Carbon prepared from Sidewall Mix

Reaction Temperature (°C)	Sodium charge based on unreacted specimen wt. (%)	Free cyanide content based on reacted specimen wt. (% CN ⁻)
500	10.0	0.17
550	10.0	0.82
600	9.99	1.9

Nature of Cyanide Species

It has been suggested in several reports (1,4) that the cyanide species in potlinings exist as two forms, free and complex iron cyanides. However, to date there has been no conclusive evidence pinpointing the predominant species in the pot.

Because solid ferri- and ferrocyanides are unstable at temperatures above 400°C (7), they would be expected to originate in the cooler zones of the potlinings. As the thermal environment in the sidewalls is usually above 500°C and large amounts of sodium are embedded in the carbon; the formation of cyanide as sodium cyanide seems more likely.

Chemical analysis for free and total cyanide in spent potlining samples show no significant difference between the free and total cyanide content (Table II). XRD scans of experimental specimens doped with Fe_2O_3 and reacted at temperatures in the range of 500-600°C also indicate the absence of complex iron cyanides, lending further support for the existence of sodium cyanide as the major cyanide species in potlinings at pot-operating temperatures.

Table II - Comparison of Free and Total Cyanide Content in Spent Potlining Specimens

Specimen No/(Identity)*	Free Cyanide content based on specimen wt. (% CN^-)	Total Cyanide content based on specimen wt. (% CN^-)
1/(Pot 4/57)	2.3	2.3
2/(Pot 4/57)	4.2	4.4
3/(Pot 4/57)	3.5	3.6
4/(Pot 3/2)	0.60	0.60

* Samples all located in sidewall region of cells.

Effect of Graphite Content

Evaluation of the cyanide distribution profiles in the potlinings suggest that preformed cathode carbon is less vulnerable to cyanide formation compared to the monolithic carbon-mix. XRD scans (5) of unused potlining samples for graphite content reveal that commercial preformed cathode carbon has a significant graphitic nature while monolithic carbon is non-graphitic. Therefore, to ascertain whether the graphitic nature of the carbon has any influence on cyanide formation, laboratory trials using different carbon types were conducted.

The data obtained are compiled in Table III and graphed in Figures 4 (i) and 4 (ii). The results show that commercial preformed cathode carbon and high purity graphite offer greater resistance to cyanide formation within their structures, while plant manufactured monolithic carbon is the most vulnerable to cyanide generation. As graphitisation increases, the carbon structure becomes more ordered and permeability to gas ingress decreases. Porosimetry measurements confirm that the specific permeability decreases with increase in graphite content of the carbon specimen. Thus, the partial inhibition of nitrogen diffusion into carbon reduces the extent of cyanide generation.

Autopsy examinations of failed potlinings have similarly reflected the same trend in carbon susceptibility to cyanide formation. Table IV shows that specimens containing high levels of graphitised carbon are significantly less vulnerable to cyanide formation. Although there is some uncertainty over the chronological order of graphitisation of the potlining during pot operation, the quantity of cyanide produced in highly graphitised carbon is significantly reduced.

Table III - Effect of Graphite Content on Cyanide Generation

Carbon Type	Graphite Content (%)	Specific Permeability (D'Arcy)	Reaction Temperature (°C)	Free Cyanide Content (% CN ⁻)
Specimen A (preformed cathode carbon)	14	5.47	500	0.088
			550	0.18
			600	1.6
Specimen B (preformed cathode carbon)	19	3.00	500	<0.01
			550	0.053
			600	1.4
High Purity Graphite (extruded rod)	100	1.04	500	0.74×10^{-3}
			550	1.3×10^{-3}
			600	2.9×10^{-3}
Monolithic Carbon (plant manufactured)	0	6.41	500	0.17
			550	0.82
			600	1.9

Table IV - Effect of Graphite Content of Spent Potlining Samples on Cyanide Generation

Sample Identity	Graphite Content (%)	Total Cyanide Content (% CN ⁻)
Pot age : 832 days Block cathode construction		
Block 1; from sidewall - block interface adjacent to collector bar	30	7.1
Block 2; from centre of block cathode	50	<0.1
Block 2; from sidewall above collector bar	10	9.4
Block 3; from block- consolidated alumina interface	55	0.3
Block 4; from sidewall above collector bar	20	7.9

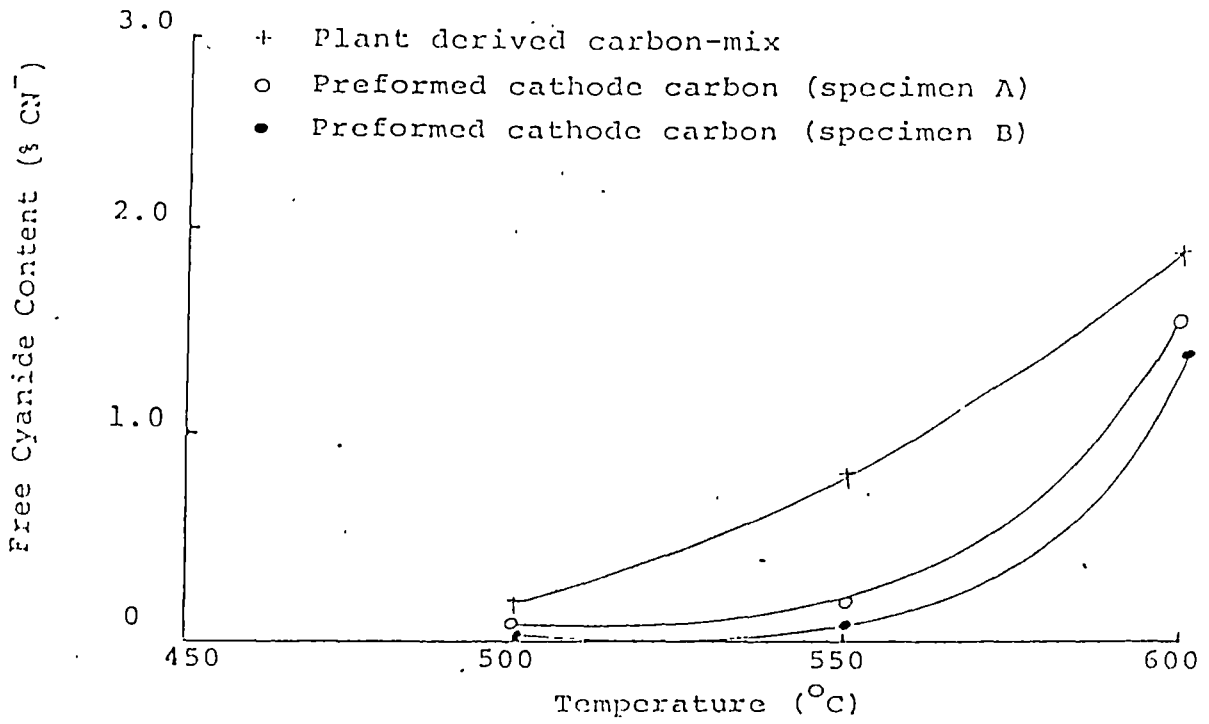


Figure 4 (i) Cyanide Formation in Different Carbon Types

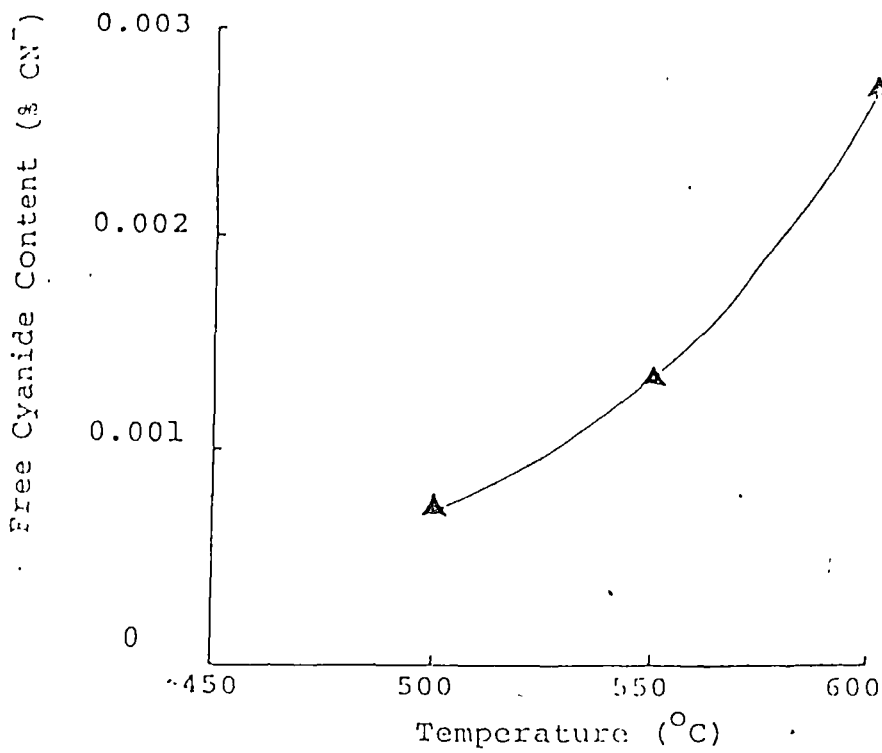
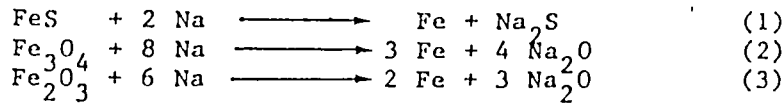


Figure 4 (ii) Cyanide Formation in Graphite

Effect of Fe (as Fe₂O₃) Impurity

Some of the common iron impurities in anthracite used in the manufacture of pot-sidewalls and cathode-slot mix include FeS, Fe₃O₄ and Fe₂O₃. In the environment of the pot, these compounds may react with metallic sodium to form metallic Fe via the interactions:



Metallc Fe can also form from the step-wise reduction of Fe₂O₃ and Fe₃O₄ by carbon at pot-operating temperatures.

Although large amounts of particulate Fe have been found to accelerate cyanide formation at high temperatures, (7,8) it appears that small amounts of metallic Fe which are chemically generated with the potlinings may also produce a similar catalytic effect on the rate of cyanide formation at lower temperatures. Laboratory trials using carbon specimens containing additions of iron as Fe₂O₃ confirm that even low levels of iron impurities can promote cyanide formation in potlinings. Table V shows that the amount of cyanide generated in a given reaction time can vary by as much as a factor of three, while the role of Fe impurity as a catalyst is reflected in Figure 5.

Table V - Effect of Fe Content on Cyanide Formation
in Carbons prepared from Sidewall Mix

Fe Addition based on specimen wt. (% Fe)	Reaction Temperature (°C)	Free Cyanide based on sample wt. (% CN ⁻)
0	500	0.17
0.5	500	0.22
1.0	500	0.47
0	550	0.82
0.5	550	1.1
1.0	550	1.3
0	600	1.9
0.5	600	2.3
1.0	600	2.9

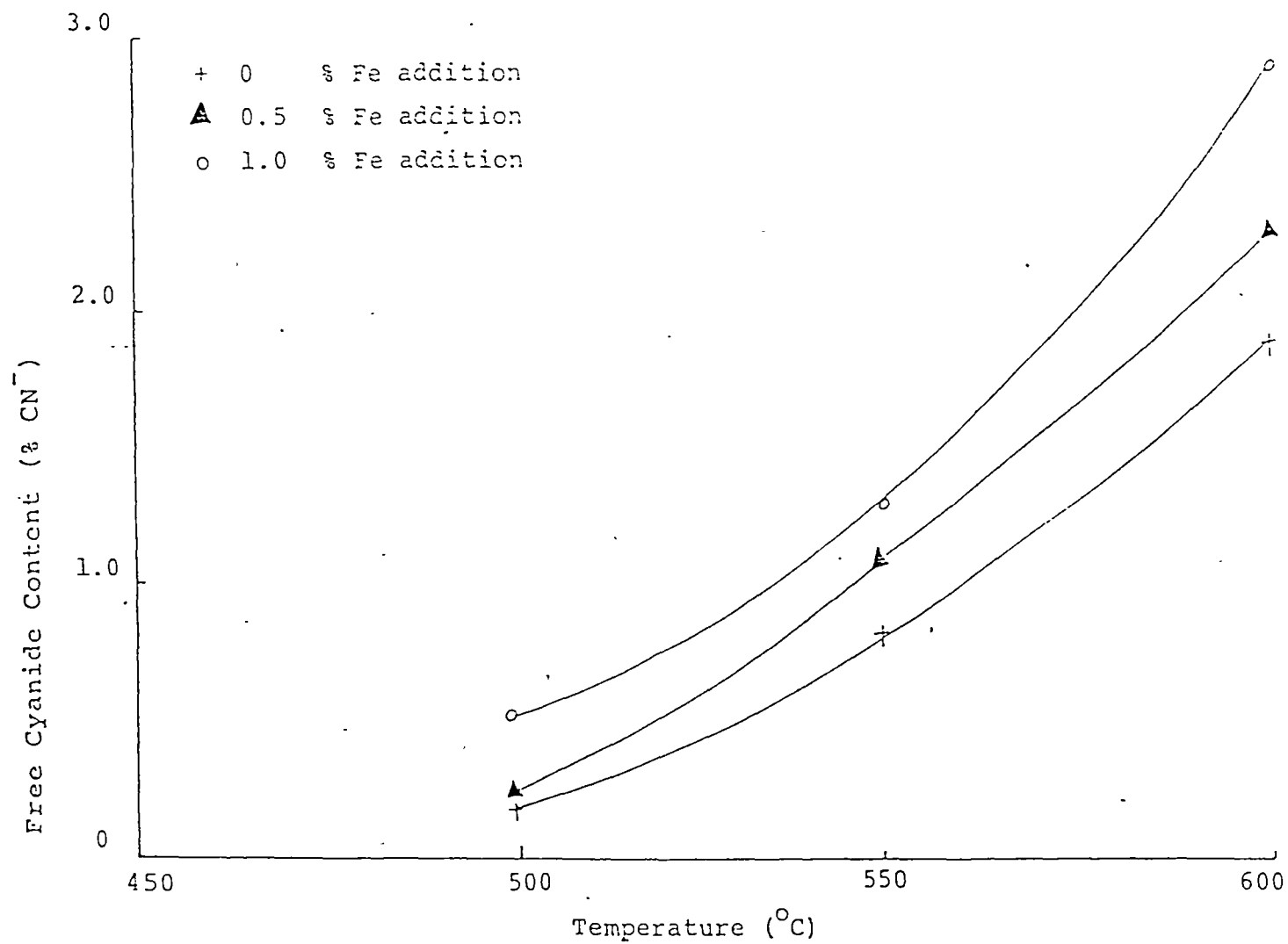


Figure 5 Effect of Iron Impurity on Cyanide Formation
in Carbon Prepared from Sidewall-Mix

Rate of Sodium Cyanide Formation

Examination of the kinetics of the reaction of metallic sodium with nitrogen to form cyanide was accomplished using a combination of thermogravimetric and integral analysis techniques. Attention was focussed on the effect of sodium content (5% and 10% based on specimen wt.) on the rate of cyanide formation in plant derived carbon-mix. The amount of cyanide generated at a particular sodium concentration and temperature has been measured against time, and an estimate of the pseudo rate constant relative to reactant sodium evaluated using approximations to the standard rate equation (9). It has been found that the overall reaction rate is faster at the lower sodium concentration, suggesting that when the carbon sidewalls are gradually impregnated with metallic sodium in the early stages of pot operation, a parallel production of cyanide at an accelerating rate is occurring in the potlining. As the carbon lining is penetrated with increasing amounts of sodium, the rate of cyanide generated is reduced.

Conclusion

Generally from the cyanide distribution profiles in the pots, it is evident that major concentrations of cyanide are located in the sidewall carbon region around the collector bars and to a lesser extent in the preformed block cathodes. The formation of sodium cyanide is controlled by a combination of air ingress around the collector bars and sodium penetration into the potlining. Whilst monolithic carbon-mix is more susceptible to cyanide generation compared to preformed cathode carbon, high purity graphite is even more resistant to cyanide formation within its structure. Although the presence of small amounts of iron impurity will accelerate cyanide formation at typical sidewall temperatures, iron is not necessary for the production of cyanide in the potlinings.

Thus, the introduction of high purity semi-graphitised carbon as sidewall lining for the pot should significantly reduce the extent of cyanide generation, resultant environmental problems, and in the longer term the consequent detoxification processing of cyanide-contaminated plant effluents.

References

1. Trachtenberg, J.J., Murphy, M.A.; Light Metals, 2, (1979) p.861
2. Wacha, E.; German Patent No. 2628192 (1977)
3. Holo, H.; "Recovery from Solid Wastes and Dumping", presented at International Symposium on the Fluoride Problem in the Aluminium Industry, Trondheim, Norway (1972)
4. Mitchell, R.E.; "Cyanide Chemistry in a Recovery Process", presented at Meeting of the EPAA Pollution Abatement Committee, Dec., Dusseldorf (1978)
5. Houston, G.J.; Ph.D Thesis, University of New South Wales, Australia (1980)
6. Guernsey, E.W., Sharman, M.S.; J.Am. Chem. Soc., 47, (1925) p.1932
7. Thorpe's Dictionary of Applied Chemistry, 3, 4th edition (1939) p.965
8. Bucher, J.E.; J. Ind. Eng. Chem., 9, (1979) p.233
9. Atkins, P.W.; Physical Chemistry, Oxford University Press, (1978) p.859

APPENDIX 4

Integral and Thermogravimetric Analysis Procedures

Calculation and Experimental Data

Thermogravimetric Analysis Procedure

1. Calibrate the Thermobalance according to the specifications listed in the manufacturer's operating manual. Select a 100 mg recording range for the XY chart recorder.
2. Purge the apparatus above with ultra high purity argon gas for at least 30 minutes before commencing the experiment.
3. Weigh approximately 5 grams of predried, -200 mesh carbon into the sample container which has been purged with argon gas initially.
4. Weigh out some freshly-cut metallic sodium pieces (analytical grade) approximately equal to the selected weight ratio (5 or 10 wt.%) of the carbon specimen weight. Gently immerse the sodium pieces into the soft carbon mass so that they are completely covered by carbon.
5. Immediately assemble the sample arrangement in the hangdown tube according to the layout in Figure 15.
6. Continue purging the system with argon gas at 0.2 litres/min. for at least 15 minutes at ambient temperature.
7. Apply gradual heating (approximately $5^{\circ}\text{C}/\text{min}$) to the reaction cell until the selected temperature is reached.
8. Allow the system to stabilise and facilitate sodium-saturation of the carbon for another 10 minutes. Then replace the argon atmosphere with high purity nitrogen gas.

9. Monitor the weight change over the selected reaction period with the chart recorder.
10. Calculate the amount of sodium converted to sodium cyanide from measurements derived from the plot of weight change over reaction time recorded .

Integral Analysis Procedure

1. Follow the steps (number 2 to 8) described in the Thermogravimetric Procedure.
2. At the end of the reaction period, switch on the argon gas to replace the nitrogen atmosphere. Then transfer the sample to a desiccator. Allow the sample to cool over granulated silica gel in the desiccator under vacuum.
3. Determine the free cyanide content in the sample according to the procedure described in Section 3.2.6.
4. Calculate the cyanide content as metallic sodium concentration and express the result as a percentage of the reacted sample weight.

Data used in Thermogravimetric Analysis
with 5 wt.% Initial Sodium Charge.

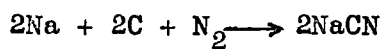
Time t (min,)	Wt. gain w (mg)	Sodium converted at time, t (wt.%)
6	8.3	0.26
12	8.9	0.28
18	10.5	0.33
24	11.1	0.35
30	13.1	0.59
36	14.4	0.45
42	16.0	0.50
48	16.6	0.52
54	17.3	0.54
60	17.9	0.56
66	18.9	0.59
72	19.5	0.61
78	20.2	0.63
84	20.8	0.65
90	20.8	0.65
96	21.5	0.67
102	21.5	0.67
108	22.8	0.71
114	22.8	0.71
120	22.8	0.71

Data used in Thermogravimetric Analysis
with 10wt.% Initial Sodium Charge

Time t (min.)	Wt. gain w (mg)	Sodium converted at time, t (wt.%)
6	32.0	0.99
12	39.7	1.23
18	44.6	1.38
24	49.6	1.53
30	51.9	1.60
36	54.2	1.67
42	56.4	1.74
48	58.5	1.80
54	60.8	1.87
60	60.8	1.87
66	63.1	1.94
72	63.1	1.94
78	65.1	2.00
84	65.1	2.00
90	67.1	2.06
96	67.1	2.06
102	67.1	2.06
108	69.5	2.13
114	69.5	2.13

Calculations used in rate studies

Basis: Reaction equation for NaCN



$$\begin{array}{l} \text{Na converted} \\ \text{in reaction} \end{array} = \frac{w}{m} \times \frac{2 K}{s} \times 100 \%$$

w = wt. gain recorded

m = mol. wt. N_2

s = total sample wt. at time t

K = mol. wt. Na